63-2-3

RADC-TDR-62-484
ASTIA Document No. AD-

September 1962

INTERFERENCE ANALYSIS OF NEW COMPONENTS AND CIRCUIT TECHNIQUES

S. Becker, L. M. Orloff, P. Kalisiak,
J. W. Lyons, and M. L. Wright

Airborne Instruments Laboratory
A Division of Cutler-Hammer, Inc.
Deer Park, New York

Report No. 1760-TN-1

Contract AF 30(602)-2690

Prepared for

Rome Air Development Center
Air Force Systems Command
United States Air Force

Griffiss Air Force Base
New York

20

RADC-TDR-62-484
ASTIA Document No. AD-

September 1962

INTERFERENCE ANALYSIS OF NEW COMPONENTS AND CIRCUIT TECHNIQUES

S. Becker, L. M. Orloff, P. Kalisiak,
J. W. Lyons, and M. L. Wright

Airborne Instruments Laboratory
A Division of Cutler-Hammer, Inc.
Deer Park, New York

Report No. 1760-TN-1

Contract AF 30(602)-2690

Project 4540

Task 454002

Prepared for

Rome Air Development Center
Air Force Systems Command
United States Air Force

Griffiss Air Force Base
New York

FOREWORD

The authors of this technical note, S. Becker, L. M. Orloff, P. Kalisiak, J. W. Lyons, and M. L. Wright, wish to acknowledge the assistance rendered to them by Captain R. E. Fitts, RAUMA, of the Rome Air Development Center. In addition, several people at AIL contributed materially to this report. These consultants include E. W. Sard and S. Okwit. This document is AIL No. 1760-TN-1.

ABSTRACT

A theoretical analysis was performed to better understand the nonlinear behavior and spurious responses of such solid-state devices as masers, parametric amplifiers, tunnel diodes, transistors, ferrite devices, and crystal mixers. The results were used to estimate the extent of interference effects such as saturation, desensitization, cross modulation, intermodulation, and gain recovery time. Predicted interference effects are also compared with measured data. This report is a continuation of the work described in RADC-TDR-62-221, entitled "Final Report on Interference Analysis of New Components and Circuit Techniques" [Contract AF 30(602)-2384].

TABLE OF CONTENTS

LIST OF ILLUSTRATIONS

LIST OF TABLES

I. INTRODUCTION

The work presented in this technical note was performed under Contract AF 30(602)-2690 for the Electromagnetic Vulnerability Laboratory at Rome Air Development Center and is a continuation of the work that was begun under Contract AF 30(602)-2384. The purpose of this investigation was to analyze new solid-state components and advanced circuit techniques for receivers and amplifiers. The components and devices that were investigated include masers, parametric amplifiers, transistors, tunnel diodes, ferrite devices, and crystal mixers. Throughout the investigation our primary concern was the relationship of operational characteristics to electromagnetic interference and the susceptibility of the components and devices to this interference.

The interference parameters of several solid-state electronic devices are presented in this technical note. All of these devices, except the maser and the ferrite limiter, have a transfer characteristic that is determined by the voltage-current curve of the device. Since this basic similarity exists among all the types of solid-state devices, certain generalizations can be made about them. These generalizations are true of every voltage-controlled device studied and, though no proof is presented, are believed true of all similar devices.

A. SATURATION

Saturation occurs when an input signal drives a device, such as an amplifier, to a point where the transfer function becomes nonlinear. This condition is the voltage (or current) limitation of the device. The point at which

saturation occurs depends upon the device. In transistors, the power-supply voltage determines the maximum limitation. In negative-resistance devices, the region over which the negative resistance is relatively constant is the fundamental factor. In mixers, the maximum signal voltage that maintains the small signal approximation determines the saturation level.

The shape of the saturation characteristic is similar in all devices. The gain versus input power curve has a negative slope that increases gradually as the input power increases. In devices with isolation between input and output, a maximum output level causes the gain versus input power curve to have a slope of -1 for large inputs. For reflection-type devices and others with low isolation between input and output, the gain curve levels off to a small loss for large input power levels.

B. DESENSITIZATION

In the voltage- or current-controlled devices studied, desensitization is another form of saturation. When a large signal produces a loss of gain because the device is saturated, there is also a loss of gain for every other signal present. Thus, these two interference parameters would be expected to follow similar curves. The curves, however, are not the same.

For example, two signals entering a device that has a transfer function with a gain G to the point of saturation, A_s, and a constant output for inputs greater than A_s can be considered. One signal has large amplitude, A_1, that exceeds the saturation level, and the other signal is of small amplitude. Representative waveforms of the two signals are shown in Figure 1-1. The reduction in gain due to saturation of the large signal can be found by taking the fundamental term of the Fourier Series of the saturated waveform:

$$C_1 = \frac{1}{\pi} \int_{-\pi}^{\pi} f(\theta) \sin \theta d\theta \qquad (1\text{-}1)$$

where

$$f(\theta) = \begin{cases} A_i \sin \theta \begin{cases} -\pi < \theta < -\pi + X \\ -X < \theta < X \\ \pi - X < \theta < \pi \end{cases} \\ -A_s \qquad -\pi + X < \theta < -X \\ A_s \qquad X < \theta < \pi - X \end{cases}$$

and

$$X = \sin^{-1}\left(\frac{A_s}{A_i}\right)$$

Integrating and solving for the appropriate limits gives the relative gains: $G_{sat} = \frac{C_1}{A_i} G$

or

$$G_{sat} = \frac{2X + \sin 2X}{\pi} G \qquad (1\text{-}2)$$

The gain for the small signal in the desensitized device is just the fractional amount of time that the device has gain G. This is easily found to be:

$$G_d = \frac{2}{\pi} XG \qquad (1\text{-}3)$$

Thus, though saturation and desensitization are functions of the same variables, the expressions are somewhat different.

In this simplified case, the expressions are relatively easy to determine. In most of the actual devices under test, however, the saturation phenomenon is quite complex and the

relationship between saturation and desensitization cannot be found by analytic means. Only in certain instances, when simple expressions exist describing saturation, can the relationship be found exactly.

C. CROSS MODULATION

Cross modulation has sometimes been described as time-varying desensitization. The cross modulation between a large, modulated, interfering signal and a small CW signal is caused by changes in desensitization as the amplitude of the interfering signal changes with time. Thus, by measuring desensitization, cross modulation can be accurately determined.

A device with a large input signal 100-percent square-wave modulated is shown in Figure 1-2A. The gain of the device for a small signal (Figure 1-2B) is desensitized during the on-time of the square wave and returns to its normal gain, G, when the interfering signal is off--this analysis assumes no appreciable gain recovery time. Letting the desensitized gain equal G_d, a desensitization factor $D = \frac{G_d}{G}$ can be defined. Using the common definition of modulation index,

$$m = \frac{V_p - \overline{V}}{\overline{V}} \tag{1-4}$$

where

m = modulation index,

V_p = peak voltage of modulated waveform,

$\overline{V}$ = average voltage of modulated waveform.

The relationship between desensitization and the modulation index of the small signal caused by modulation in the large signal is:

$$m = \frac{1 - D}{1 + D} \tag{1-5}$$

From this expression, it can be seen that there is no reason for measuring both cross modulation and desensitization. Once one of these quantities has been determined, the other can be found by using equation 1-5.

D. INTERMODULATION

The three interference parameters mentioned previously, saturation, desensitization, and cross modulation, occur only at large signal levels. When all signals into a device are small these interference parameters can not be detected. Intermodulation, however, occurs at both small- and large-signal levels. Small-signal analysis of intermodulation is the main area of interest. It is often necessary to predict the power of the intermodulation products for input signals up to the saturation level.

The general form of intermodulation voltages can be found from equation 7-12 of reference 1. Using this equation and letting

$$E_{sb} = A_{sb} \left[\cos\,(s\omega_1 + b\omega_2)t + \cos\,(s\omega_1 - b\omega_2)t \right]$$

where

ω_1 = frequency of first input signal,
ω_2 = frequency of second input signal,

s = harmonic of ω_1,

b = harmonic of ω_2,

A_{sb} = peak voltage at the intermodulation frequency.

gives:

$$A_{sb} = 2R_o \sum_{c=o}^{\infty} \sum_{d=o}^{\infty} \frac{(2c + 2d + s + b)!\ A_1^{2c+s}\ A_2^{2d+b}\ g_{2c+2d+s+b}}{(c + s)!\ c!\ (d + b)!\ 2^{2c+2d+s+b}} \quad (1\text{-}6)$$

where

R_o = output resistance,

A_1 = peak input voltage at frequency ω_1,

A_2 = peak input voltage at frequency ω_2,

g_k = k^{th} coefficient of power series expansion for current.

For small input signals, $A_1 \ll 1$ and $A_2 \ll 1$, all terms of the double summation except the first term, $c = o$, and $d = o$, are negligible. Thus, for small input signals:

$$A_{sb} = 2R_o \frac{(s+b)!\ A_1^s\ A_2^b\ g_{s+b}}{s!\ b!\ 2^{s+b}} \quad (1\text{-}7)$$

The output powers, P_1 and P_2, can be expressed as

$$P_1 = \frac{GA_1^2}{2R_o}$$

$$P_2 = \frac{GA_2^2}{2R_o}$$

where G is the gain of the device. The factor 2 appears in

these expressions because the voltages given are peak values. The output power, P_{sb} is expressed as:

$$P_{sb} = \frac{A_{sb}^2}{2R_o}$$

Substituting the expressions for power into equation 1-7 results in:

$$P_{sb} = \left[\frac{R_o \ (s+b)! \ g_{s+b}}{s! \ b!}\right]^2 \left(\frac{R_o}{2}\right)^{s+b-1} \left(\frac{1}{G}\right)^{s+b} P_1^s \ P_2^b \qquad (1\text{-}8)$$

or more simply,

$$P_{sb} = C_{sb} \ P_1^s \ P_2^b \qquad (1\text{-}9)$$

If the powers are expressed in dbw, equation 1-9 becomes:

$$P_{sb}(\text{dbw}) = 10 \log C_{sb} + sP_1(\text{dbw}) + bP_2(\text{dbw}) \qquad (1\text{-}10)$$

Letting $K_{sb} = 10 \log C_{sb}$ gives:

$$P_{sb}(\text{dbw}) = K_{sb} + sP_1(\text{dbw}) + bP_2 \ (\text{dbw}) \qquad (1\text{-}11)$$

Equation 1-11 states that the intermodulation output power in dbw is a linear function of the signal output powers in dbw. The constant K_{sb} can be derived analytically from the characteristic of the device or found experimentally at any levels of P_1 and P_2 below saturation. Once the value of K_{sb} has been found, the level of the intermodulation product at all output signal powers below saturation can be found from equation 1-11.

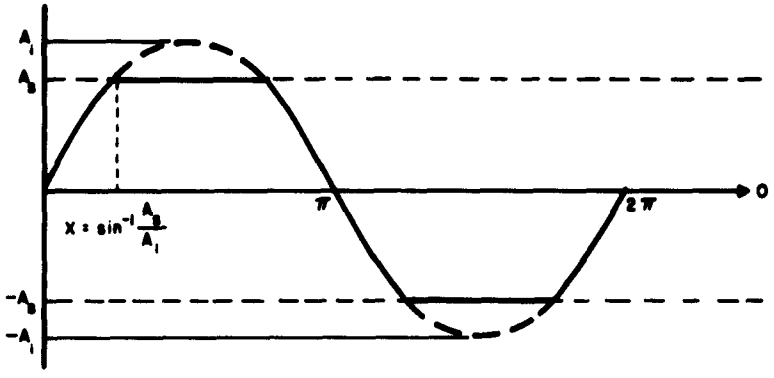

A. LARGE SIGNAL

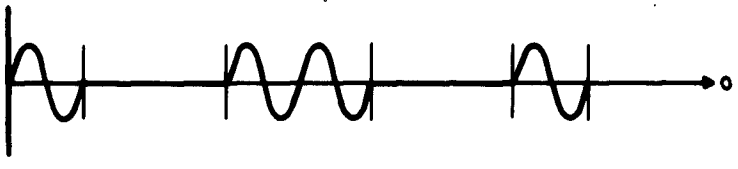

B. SMALL SIGNAL

FIGURE 1-1. LARGE-SIGNAL AND SMALL-SIGNAL WAVEFORMS IN A SATURATING DEVICE

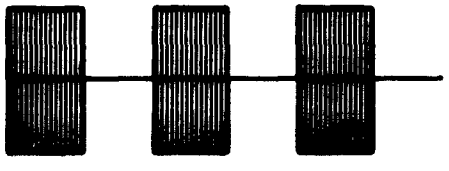

A. INTERFERING SIGNAL

B. SMALL SIGNAL

FIGURE 1-2. LARGE-SIGNAL AND SMALL-SIGNAL WAVEFORMS FOR CROSS MODULATION

II. MASERS

The gain-recovery time of an S-band traveling-wave maser (TWM) was measured (reference 1). The gain-recovery-time curve was not the simple exponential function that would be predicted by recovery through a spin-lattice relaxation mechanism. Instead, the recovery showed three relaxation times, one of 270 msec, another of 90 msec, and a third estimated at about 5 msec. The multiple relaxation times were attributed to cross relaxation. However, the actual cross-relaxation mechanisms and how they affect recovery time were not discussed. Additional investigation has revealed more about the cross-relaxation mechanism, thereby permitting an explanation of its effects.

Cross relaxation is the term used to describe multiple spin-flip processes involving several energy levels, which conserve Zeeman energy (reference 2). That is, when the sum energy of one set of allowed transitions is equal to the sum energy of another set, there is a finite probability that the transitions will occur between neighboring atoms so that energy is conserved. For example, the four-state system shown in Figure 2-1 can be considered. If the transitions $(W_3 - W_2)$ and $(W_3 - W_4)$ have equal energy, then there is a probability that an electron will go from state 3 to state 4 while a neighboring electron is going from state 3 to state 2.

The process is a resonance phenomenon. These transitions have maximum probability when energy is exactly conserved. As the energy difference increases, the probability that a transition will occur lessens. Cross relaxation is relatively independent of temperature, but highly dependent upon the concentration of the material.

The cross-relaxation mechanism introduces an additional constraint on the spin system (reference 3). For the example given in Figure 2-1, the constraint is $n_3^2 = n_2 n_4$, where n_k is the number of electrons at the k energy level.

Using this four-energy level system as a maser with pump frequency $f_p = f_{13}$ and signal frequency $f_s = f_{21}$, the cross-relaxation effect can be shown to decrease the gain-recovery time of the maser to a short saturating pulse. For gain at a frequency corresponding to the transition $(W_2 - W_1)$, a population inversion must exist between states 2 and 1. The pump frequency indirectly inverts these populations by forcing n_3 to equal n_1. Using this equality in the cross-relaxation condition:

$$n_1^2 = n_2 n_4$$

When a saturating signal enters the system, it reduces the population inversion between states 2 and 1. If the signal is large enough, it will make the two populations almost equal, $n_2 = n_1$. Thus, during the presence of a saturating signal $n_1 = n_2 = n_3$. Considering the cross-relaxation condition $n_1^2 = n_2 n_4$, it is apparent that the final condition imposed on the system is $n_1 = n_2 = n_3 = n_4$. However, there is a time constant associated with the cross-relaxation process. This time constant is dependent upon the cross-relaxation transition probability. Thus, if the saturating pulse is short with respect to this time constant, the population of energy level 4, n_4, will never reach n_1. Instead, when the saturating pulse is removed, the relative populations will be $n_1 = n_2 = n_3 > n_4$.

The cross-relaxation condition, $n_1^2 = n_2 n_4$, will now tend to make $n_2 > n_1$. The rate at which this condition will

occur will be the cross-relaxation time constant, which can be orders of magnitude smaller than the spin-lattice relaxation time. Thus, at least part of the gain of the system will be quickly restored.

In the S-band TWM, cross relaxation was found to be a four-level spin-flip process (reference 4) as shown in Figure 2-2. Thus, the energy relationship $2(W_4 - W_3) = (W_3 - W_2) + (W_3 - W_1)$ exists. Using the method shown in reference 3, the restraint imposed upon the spin system by the cross relaxation is: $n_3^4 = n_1 n_2 n_4^2$. Since pumping occurs from level 1 to level 3, $n_1 = n_3$. Substituting this equation into the cross-relaxation constraint gives:

$$n_1^3 = n_2 n_4^2$$

Using the same logic as in the previous example, it can be shown that cross relaxation helps restore the gain of the maser amplifier after the saturating signal is removed.

Cross relaxation is only helpful in decreasing gain-recovery time when the duration of the saturating signal is small with respect to the cross-relaxation time constant. If the saturating signal were longer in duration than the time constant, the cross relaxation would occur while the saturating signal was on, and the gain-recovery time would be determined by the spin-lattice relaxation time constant.

Not much is known about the cross-relaxation time constant. Some experimental results show that it can range upward from microseconds (reference 5). The time constant is proportional to the cube of the concentration, highly dependent upon small differences in the energy levels, and dependent upon the cross-relaxation mechanism involved. In the S-band TWM, there is little doubt that the short time constant, about 5 msec, is caused by this cross-relaxation

mechanism. The 270-msec recovery time is probably the spin-lattice time constant. The reason for the 90-msec recovery time can be attributed only to another cross-relaxation process that is not readily apparent. A six-level spin-flip process, $5(W_2 - W_1) = (W_4 - W_3)$, seems most probable. The energy levels are in close agreement for this transition and the 90-msec time constant is plausible.

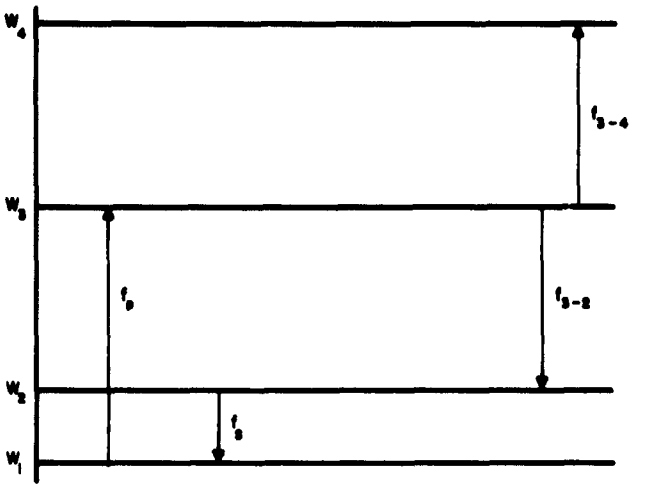

FIGURE 2-1. DIAGRAM OF ENERGY LEVELS FOR TWO-LEVEL CROSS-RELAXATION PROCESS

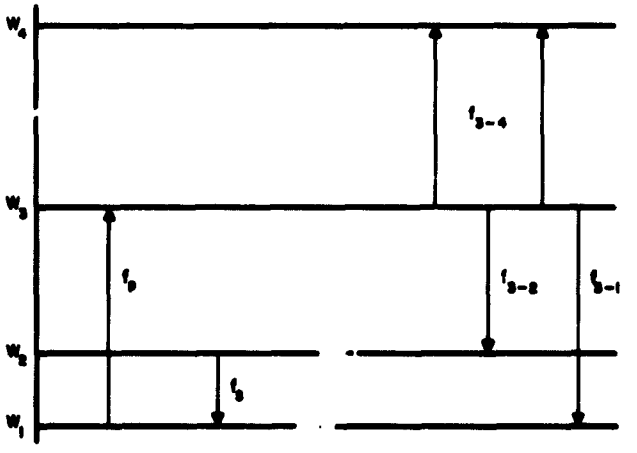

FIGURE 2-2. DIAGRAM OF ENERGY LEVELS FOR FOUR-LEVEL CROSS-RELAXATION PROCESS

III. PARAMETRIC AMPLIFIERS

An analysis of interference effects in parametric amplifiers was started to determine whether various modes of operation could reduce the interference effects. The two-port difference-frequency amplifier was analyzed using the nine frequencies (signal, pump, idler, and intermodulation) in Section III of reference 1 for a one-port amplifier. A two-port difference-frequency amplifier has different input and output frequencies, with the output taken at a point that corresponds to the idler frequency in a one-port amplifier.

Appendix I, an extension of the general analysis in reference 1, describes the basic operation of the two-port amplifier. The notations in both places are the same and are summarized in the list of symbols.

TABLE 3-I

LIST OF SYMBOLS

I_n = diode current at frequency n

I_{on} = input current at frequency n

$K_{m,n}$ = voltage gain between frequencies m and n

$Y_{t,n}$ = total of Y's at frequency n

$Y_{m,n}$ = transfer term for voltages and currents at frequencies m and n

v_n = diode voltage at frequency n

a = first coefficient of the power series of charge versus voltage for the varactor

b = second coefficient of the power series of charge versus voltage for the varactor

c = third coefficient of the power series of charge versus voltage for the varactor

ω_2 = first signal frequency

ω_3 = second signal frequency

ω_9 = pump frequency

ω_7 = idler frequency for signal v_2

ω_6 = idler frequency for signal v_3

$\omega_{11} = \omega_2 + \omega_9$

$\omega_{12} = \omega_3 + \omega_9$

ω_1 and ω_4 = intermodulation products in signal frequency pass band

ω_5 and ω_8 = intermodulation products in idler frequency pass band

ω_{10} and ω_{13} = intermodulation products in sum frequency pass band

A. GENERAL ANALYSIS

The analysis in reference 1 included only the idler or difference-frequency components caused by frequencies in the signal band. To investigate the effects of sum frequencies in amplifiers, additional components were included in the sum-frequency band. The 14 frequencies are shown in Figure 3-1; these include the signal, idler, pump, sum, and intermodulation product frequencies. The currents of interest in this spectrum are:

$$I_1 = j\omega_1\left[(a + c\,\overline{v}_t^{\,2})v_1 + b\,v_9\,v_8^* + b\,v_9^*\,v_{10} + c(v_2\,v_3^* + v_6\,v_7^*)v_2 + c(v_3^*\,v_7^* + v_2\,v_{12}^*)v_{11}\right] \tag{3-1}$$

$$= Y_{11}\,v_1 + Y_{18}\,v_8^* + Y_{1\,10}\,v_{10} + Y_{12}\,v_2 + Y_{1\,11}\,v_{11} \tag{3-2}$$

$$I_2 = j\omega_2\{(a + c\,\bar{v}_t^{\,2})v_2 + [b\,v_9 + c(v_3\,v_6 + v_3^*\,v_{12} + v_9^*\,v_{14} + v_2^*\,v_{11})]v_7^* + b\,v_9^* + c(v_3^*\,v_6^* + v_3\,v_{12}^* + v_9\,v_{14}^* + v_2^*\,v_7^*)v_{11}\} \tag{3-3}$$

$$= Y_{22}\,v_2 + Y_{27}\,v_7^* + Y_{2\,11}\,v_{11} \tag{3-4}$$

$$I_7^* = j\omega_7\{(a + c\,\bar{v}_t^{\,2})v_7^* + [b\,v_9^* + c(v_3^*\,v_6^* + v_3\,v_{12}^* + v_2\,v_{11}^* + v_9\,v_{14}^*)]v_2 + c(v_9^{*2} + v_6^*\,v_{12}^*)v_{11}\} \tag{3-5}$$

$$= Y_{77}^*\,v_7^* + Y_{72}^*\,v_2 + Y_{7\,11}^*\,v_{11} \tag{3-6}$$

$$I_8^* = -j\omega_8[(a + c\,\bar{v}_t^{\,2})v_8^* + b\,v_9^*\,v_1 + c(v_2\,v_3^* + v_6\,v_7^*)v_7^* + c(v_2^{\,2} + v_7^*\,v_{11})v_{12}^*] \tag{3-7}$$

$$= Y_{88}^*\,v_8 + Y_{81}^*\,v_1 + Y_{87}^*\,v_7^* + Y_{8\,12}^*\,v_{12}^* \tag{3-8}$$

$$I_{10} = j\omega_{10}[(a + c\,\bar{v}_t^{\,2})v_{10} + b\,v_9\,v_1 + c(v_2\,v_6 + v_3^*\,v_{11})v_2 + c(v_{11}\,v_{12}^* + v_6\,v_7^*)v_{11}] \tag{3-9}$$

$$= Y_{10\,10}\,v_{10} + Y_{10\,1}\,v_1 + Y_{10\,2}\,v_2 + Y_{10\,11}\,v_{11} \tag{3-10}$$

$$I_{11} = j\omega_{11}\{(a + c\,\bar{v}_t^{\,2})v_{11} + [b\,v_9 + c(v_3\,v_b + v_2\,v_7 + v_3^*\,v_{12} + v_9^*\,v_{14})]v_2 + c(v_9^{\,2} + v_6\,v_{12})v_7^*\} \tag{3-11}$$

$$= Y_{11\,11}\,v_{11} + Y_{11\,2}\,v_2 + Y_{11\,7}\,v_7^* \tag{3-12}$$

1. ONE-PORT AMPLIFIER

The one-port amplifier with sum- and difference-frequency components that exist simultaneously is somewhat more complicated than the simpler one- or two-port difference-frequency amplifier. The operation of the one-port amplifier can be determined from equations 3-4, 3-6, and 3-12. From equations 3-6 and 3-12:

$$v_7^* = -\frac{Y_{72}^* v_2 + Y_{7\,11}^* v_{11}}{Y_{t7}^*} \tag{3-13}$$

$$v_{11} = -\frac{Y_{11\,2} v_2 + Y_{11\,7} v_7^*}{Y_{t\,11}} \tag{3-14}$$

Substituting equations 3-13 and 3-14 into equation 3-4 and introducing an input generator v_{02}, the gain is:

$$K_{22} = \frac{v_2}{v_{02}} =$$

$$\frac{Y_{x\,2}}{Y_{t\,2} - \dfrac{Y_{2\,11} Y_{11\,2}}{Y_{t\,11}} + \dfrac{\left(Y_{27} - \dfrac{Y_{11\,7} Y_{2\,11}}{Y_{t\,11}}\right)\left(\dfrac{Y_{7\,11}^* Y_{11\,2}}{Y_{t\,7}^* Y_{t\,11}} - \dfrac{Y_{72}^*}{Y_{t\,7}^*}\right)}{1 - \dfrac{Y_{7\,11}^* Y_{11\,7}}{Y_{t\,7}^* Y_{t\,11}}}} \tag{3-15}$$

Substituting for the frequency and diode coefficients,

$$K_{22} = Y_{x\,2}\left[Y_{t\,2} + \frac{\omega_2\,\omega_{11}\,b^2\,\bar{v}_9^{\,2}}{Y_{t\,11}} + \frac{\frac{1}{Y_{t\,7}^*}\left(j\omega_2\,b\,v_9 + \frac{\omega_2\,\omega_{11}\,b\,c\,v_9^{\,3}}{Y_{t\,11}}\right)\left(j\omega_7\,b\,v_9^* + \frac{\omega_7\,\omega_{11}\,b\,c\,v_9^{\,3}}{Y_{t\,11}}\right)}{1 - \frac{\omega_7\,\omega_{11}\,c^2\,\bar{v}_9^{\,4}}{Y_{t\,7}^*\,Y_{t\,11}}}\right]^{-1} \tag{3-16}$$

2. <u>TWO-PORT AMPLIFIER</u>

The operation of the two-port difference-frequency amplifier, with an output at the idler frequency, can be determined by again using equations 3-4, 3-13, and 3-14.

$$K_{72} = \frac{Y_{x\,2}}{\dfrac{\left(Y_{t\,2} - \dfrac{Y_{2\,11}\,Y_{11\,2}}{Y_{t\,11}}\right)\left(1 - \dfrac{Y_{7\,11}\,Y_{11\,7}}{Y_{t\,7}^*\,Y_{t\,11}}\right)}{\dfrac{1}{Y_{t\,7}^*}\left(\dfrac{Y_{7\,11}\,Y_{11\,2}}{Y_{t\,11}} - Y_{72}^*\right)} + Y_{27} - \dfrac{Y_{2\,11}\,Y_{11\,7}}{Y_{t\,11}}} \tag{3-17}$$

The two-port sum-frequency amplifier operation can be obtained in a similar manner:

$$K_{11\,2} = Y_{x\,2}\,Y_{11\,2}\left(Y_{11\,2} - \frac{Y_{72}^*\,Y_{11\,7}}{Y_{t\,7}^*}\right)$$
$$\left[\left(Y_{2\,11}\,Y_{11\,2} - Y_{t\,2}\,Y_{t\,11}\right)\left(Y_{11\,2} - \frac{Y_{72}^*\,Y_{11\,7}}{Y_{t\,7}^*}\right) + \left(Y_{27}\,Y_{11\,2} - Y_{t\,2}\,Y_{11\,7}\right)\left(Y_{72}^*\,Y_{t\,11} - Y_{7\,11}^*\,Y_{11\,2}\right)\right]^{-1} \tag{3-18}$$

The relative complexity of the general expressions for the three modes of operation and the uncertainty of the values of the parameters make the use of such expressions not feasible, especially where interference effects are of primary interest.

3. INTERMODULATION IN DIFFERENCE-FREQUENCY AMPLIFIERS

From reference 1, the pertinent equations involving intermodulation products are:

$$Y_{t\ 8}^{*}\ v_8^{*} + Y_{81}^{*}\ v_1 = -Y_{87}^{*}\ v_7^{*} \tag{3-19}$$

$$Y_{t\ 1}\ v_1 + Y_{18}\ v_8^{*} = -Y_{12}\ v_2 \tag{3-20}$$

These equations express the relationships between signal and idler intermodulation voltages at the varactor diode and are independent of the mode of operation (one port or two port). Substituting equation 3-19 into equation 3-20 and for midband conditions when

$$\frac{v_7^{*}}{v_2} \approx \frac{v_8^{*}}{v_1} = R,$$

the two-port intermodulation voltage is

$$v_8 = \frac{K_{11}}{Y_{x\ 1}}\ v_2\left(\frac{Y_{12}\ Y_{81}^{*}}{Y_{t\ 8}^{*}} + \frac{Y_{t\ 1}\ Y_{87}^{*}\ Y_{72}^{*}}{Y_{t\ 7}^{*}\ Y_{t\ 8}^{*}}\right) \tag{3-21}$$

Under mid-band conditions with close frequency separation

$$K_{18} = \frac{-Y_{81}^{*}}{Y_{t\ 8}^{*}}\ K_{11} \approx \frac{-Y_{72}^{*}}{Y_{t\ 7}^{*}}\ K_{22}$$

because $K_{11} \approx K_{22}$.

and equation 3-21 becomes

$$v_8 = \frac{-K_{18}}{Y_{x\ 1}} v_2 \left(Y_{12} + \frac{Y_{t\ 1}\ Y_{87}^*}{Y_{t\ 8}^*} \right) \tag{3-22}$$

An equivalent intermodulation input generator I_{01} can be defined in a manner similar to that existing for one-port amplifiers. This equivalent intermodulation input generator is:

$$I_{01} = v_2 \left(Y_{12} + \frac{Y_{t\ 1}\ Y_{87}^*}{Y_{t\ 8}^*} \right) \tag{3-23}$$

From reference 1 the one-port equivalent intermodulation generator is:

$$I_{01} = \left(Y_{12} + \frac{Y_{18}\ Y_{87}^*\ Y_{72}^*}{Y_{t\ 7}^*\ Y_{t\ 8}^*} \right) v_2 \tag{3-24}$$

The equivalent intermodulation input generator for the one-port and two-port amplifiers would be equal if

$$Y_{t\ 1} = \frac{Y_{18}\ Y_{72}^*}{Y_{t\ 7}^*} \approx \frac{Y_{18}\ Y_{81}^*}{Y_{t\ 8}^*} \tag{3-25}$$

For example, if the signal-band intermodulation component and the idler-band intermodulation component are considered as small signals caused by an input generator I_0, the intermodulation currents are (reference 1):

$$I_1 = Y_{11} v_1 + Y_{18} v_8^* = I_0 - Y_{x\,1} v_1 \qquad (3\text{-}26)$$

$$I_8^* = Y_{81}^* v_1 + Y_{88}^* v_8^* = -Y_{x\,8}^* v_8^* \qquad (3\text{-}27)$$

when $I_0 = 0$, equations 3-26 and 3-27 become

$$Y_{t\,1} v_1 + Y_{18} v_8^* = 0 \qquad (3\text{-}28)$$

$$Y_{81}^* v_1 + Y_{t\,8}^* v_8^* = 0 \qquad (3\text{-}29)$$

To ensure that signal and idler currents will be present, the determinant of the coefficients of equations 3-28 and 3-29 must be zero. This condition is actually the condition for oscillation, but is approximately true for high gain. Solving this for determinant yields:

$$Y_{t\,1} = \frac{Y_{18}\, Y_{81}^*}{Y_{t\,8}^*} \qquad (3\text{-}30)$$

This condition is necessary for the one-port and two-port equivalent intermodulation input generators to be approximately equal and must be fulfilled to provide high gain in the amplifier. Therefore, the two-port amplifier has no apparent advantage over the one-port amplifier as far as intermodulation is concerned.

B. BALANCED PARAMETRIC AMPLIFIER

A balanced parametric amplifier is basically a one-port difference-frequency amplifier using two varactors in a push-pull arrangement. The basic diode arrangement for the applied signal and pump voltages is shown in Figure 3-2. Because the idler frequency is equal to the self-resonant

frequency of the diodes, each diode is a broad-band idler resonator for the other diode. This arrangement provides a wide-band idler circuit with a high degree of isolation between the signal and idler circuits.

1. THEORY

During the investigation of parametric amplifiers, it appeared that the balanced parametric amplifier might have a lower intermodulation output than the single-diode one-port amplifier. A simplified analysis concerned only with the intermodulation that was produced follows.

The equivalent input intermodulation generator for a single diode (as in the single-diode amplifier) is from reference 1:

$$I_{01} = Y_{12} + \left(\frac{Y_{18}\, Y_{87}^{*}\, Y_{72}^{*}}{Y_{t\,8}^{*}\, Y_{t\,7}^{*}}\right) v_2 \tag{3-31}$$

$$= j v_2 \left[\omega_1\, c \left(v_2^{*}\, v_3^{*} + v_6\, v_7 \right) - \frac{\omega_1\, \omega_8\, \omega_7\, b^2\, v_9\, c \left(v_2\, v_3^{*} + v_6\, v_7^{*} \right)}{Y_{t\,8}^{*}\, Y_{t\,7}^{*}} \right] \tag{3-32}$$

When phase shifts caused by reactive elements are neglected, v_n is written as V_n and

$$I_{01} = j V_2^{\,2}\, V_3\, \omega_1\, c \left[\left(e^{-\phi_3} + R^2 e^{-2\phi_9 + 2\phi_2 + \phi_3} \right) - \frac{\omega_7\, \omega_8\, b^2\, V_9 e^{\phi_9}}{Y_{t\,8}^{*}\, Y_{t\,7}^{*}} \left(e^{2\phi_2 - \phi_3} + R^2\, e^{\phi_3} \right) \right] \tag{3-33}$$

The second term in the brackets of equation 3-33 depends on the phase of the applied pump voltage (ϕ_9) and will not appear in the balanced amplifier because the pump voltages at the diode pumps differ in phase by 180 degrees. The relative magnitudes of the two components are not accurately predictable. Hence, the value of intermodulation can not be accurately determined. Therefore, a measurement program was started to examine the interference properties of a balanced parametric amplifier.

2. EXPERIMENT

a. OPERATION

Although the balanced amplifier is a broad-band device, it is not restricted to fixed broad-band operation. The operating frequency can be varied over a limited range by varying the bias voltage on the varactors. Generally, the pump power must also be adjusted to achieve the desired gain. The balanced amplifier used in this measurement program is a 4.55 to 4.71 Gc tunable amplifier. The amplifier gain is 20 db. Figure 3-3 shows the center frequency of the amplifier as a function of bias voltage and pump power required as a function of bias voltage to maintain a gain of 20 db.

b. SATURATION

The balanced amplifier has a higher saturation level than a single-diode amplifier, because, in the ideal case, each diode of the balanced amplifier will saturate at the same input power as for the single diode amplifier. Therefore, the balanced amplifier should saturate at a 3-db higher input power and provide a slightly greater dynamic range than the equivalent single-diode amplifier. Figure 3-4 shows the power output versus the power input for several values of bias voltage. The saturation characteristic is not very dependent on bias voltage.

c. DESENSITIZATION

The desensitization of this balanced amplifier was measured as a function of the frequency of an interfering CW signal. Figure 3-5 shows the interfering power required to reduce the amplifier gain by 1 db. The small-signal gain as a function of frequency is also shown for reference.

d. CROSS MODULATION

The cross-modulation characteristic of the balanced amplifier shows an unusual "null" not previously noticed on other amplifiers. These nulls occurred for interfering signals in the amplifier pass band. A representative curve of cross modulation versus interfering signal power is shown in Figure 3-6. There are two distinct regions of interest in this curve, A and B. Region A is below the null and region B is above the null.

A detailed investigation of the amplifier behavior shows that in region A the gain is increased by the interfering signal, and in region B the amplifier gain is decreased by the interfering signal. At the null point the gain is exactly equal to the gain with no signal present. This has been verified as accurately as possible with continuous-wave measurements; however, we believe that the cross-modulation measurement is a much more accurate determination of the point of equal gain.

The normal cross-modulation behavior is shown as a dotted line in Figure 3-6. In this situation, the amplifier gain is always decreasing. This situation occurs at most frequencies in the balanced amplifier. A plot of the cross-modulation behavior of the amplifier as a function of frequency is shown in Figure 3-7. The small-signal response is included for reference. The value of cross modulation indicated corresponds to the 1-db desensitization shown in Fig-

ure 3-5. The close correlation of the curves in Figures 3-5 and 3-7 indicates that the two effects are similar in nature.

e. INTERMODULATION

The intermodulation performance of the balanced amplifier was measured to determine if this type of amplifier provides any improvement over the single diode amplifier. Measurements were made at more than one point in the pass band to determine the validity of the general expression relating output signal powers and output intermodulation power--that is,

$$P_{IM} = P_1 + 2P_2 + K$$

where

P_{IM} = third order intermodulation output power

P_1 = output power at first signal frequency

P_2 = output power at second signal frequency

K = intermodulation figure of merit

Intermodulation was measured at 4607, 4612, and 4620 Mc with gains of 18, 20, and 17 db at the intermodulation products frequency. The intermodulation frequency and performance are summarized in Table 3-II.

TABLE 3-II

INTERMODULATION FREQUENCY AND PERFORMANCE

Intermodulation Frequency (Mc)	Gain (db)			K (dbw)
	f_{IM}	f_1	f_2	
4607	18	7	13	86
4612	20	8	10	95
4620	17	7	12	84

The value of K shown in the last column is relatively constant considering the complexity of these measurements and the measurement frequency. A larger sample of points would be needed to ensure that this concept is valid, but indications are that there is no large departure from the expected behavior.

f. TEMPERATURE EFFECTS

The effects of various temperature environments on the balanced amplifier were measured to determine the range over which the amplifier could operate. Some variation of frequency response was noticed; however, no attempt was made to compensate for this variation in the measurements. The gain change with temperature was corrected by varying the bias voltage until the room-temperature gain (20 db) was obtained. The pump power was held constant at 220 mw.

The results of the measurements of frequency and bias changes versus temperature are shown in Figure 3-8. The amplifier was easily adjusted to operate over the -180 to $0^{\circ}C$ range with 20 db gain.

g. GAIN-RECOVERY TIME

The gain-recovery time of a varactor is extremely short. In a parametric amplifier, however, the recovery time of the amplifier is highly dependent upon the design of the varactor DC bias circuit.

Figure 3-9 shows the measured gain-recovery characteristics of the parametric amplifier. For an input signal of -15 dbm, the recovery time is negligible. When the input is increased to 0 dbm the recovery time becomes about 10 μsec. This recovery time is attributed to the time constant of the DC bias circuit.

During a saturating pulse, the bias point of the varactor changes. When the pulse is removed, the signal DC bias is restored through the time constant of the bias circuit. Since the gain is highly dependent upon the bias voltage, the bias-circuit time constant will determine the gain-recovery time.

To demonstrate this effect, the time constant of the bias circuit was increased. The original circuit consisted of a 5-kilohm resistance and some stray capacitance. Another 5-kilohm resistor and a 1000-pf capacitor were added to the circuit (Figure 3-9A) and the gain-recovery time was measured again. The gain-recovery time increased to 30 μsec (Figure 3-9B).

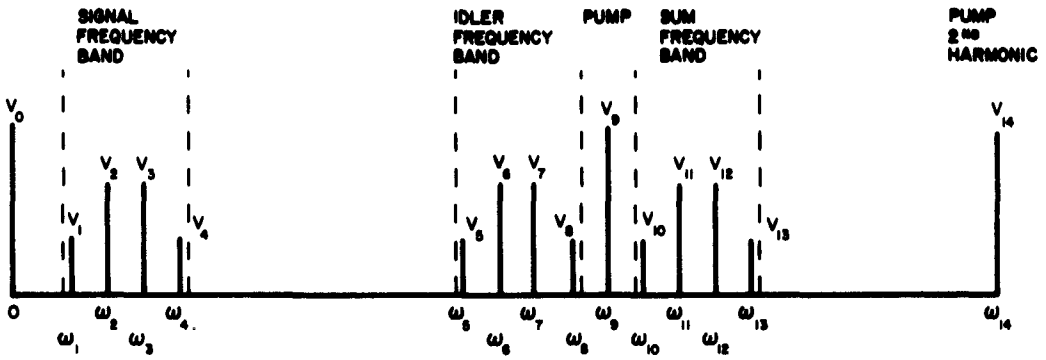

FIGURE 3-1. FREQUENCY SPECTRUM AT VARACTOR TERMINAL

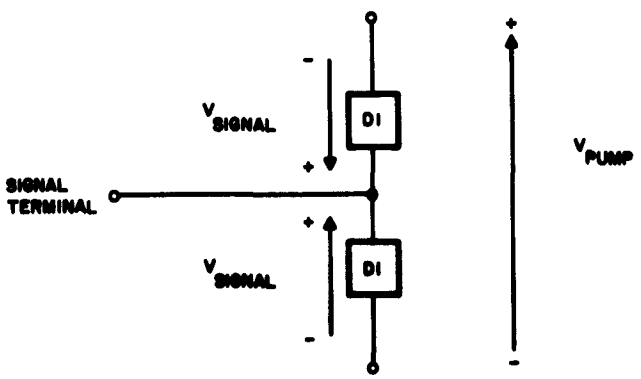

FIGURE 3-2. ARRANGEMENT OF DIODES IN BALANCED PARAMETRIC AMPLIFIER

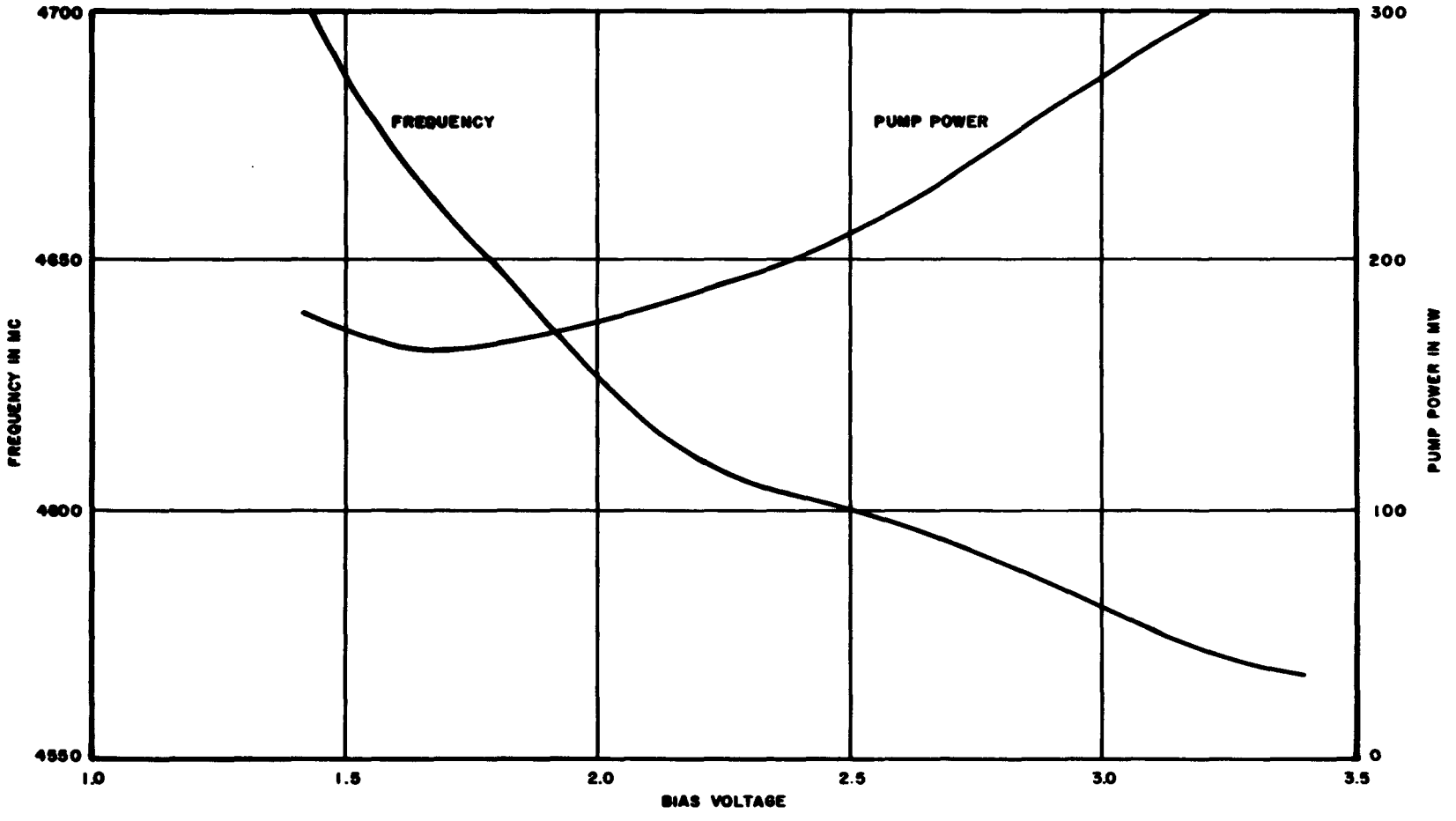

FIGURE 3-3. CENTER FREQUENCY AND PUMP POWER OF BALANCED PARAMETRIC AMPLIFIER AS A FUNCTION OF BIAS VOLTAGE

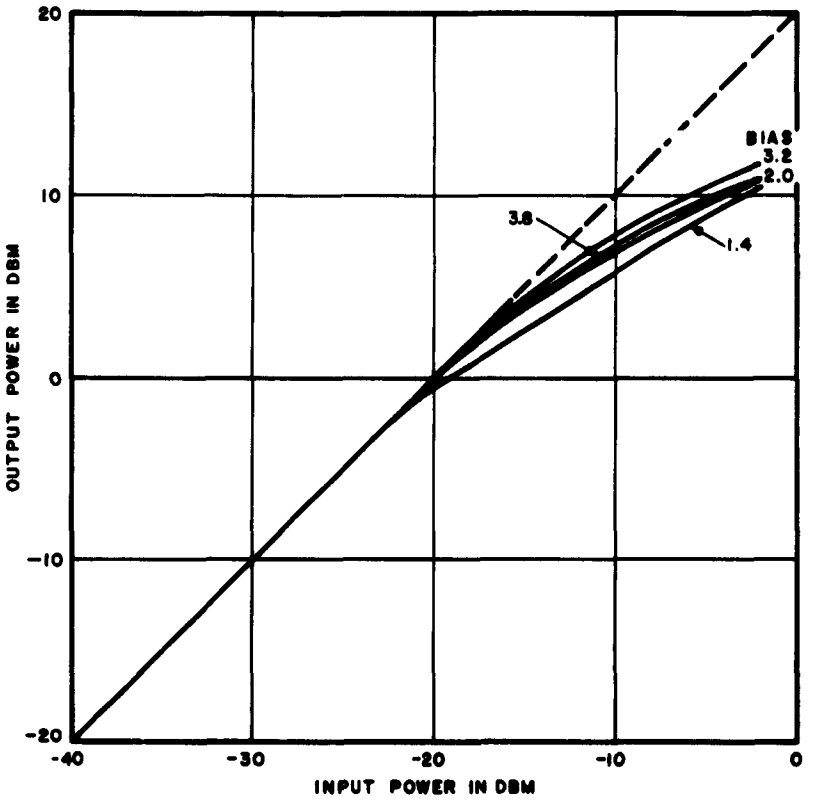

FIGURE 3-4. OUTPUT POWER VS INPUT POWER OF BALANCED PARAMETRIC AMPLIFIER AT DIFFERENT BIAS VOLTAGES

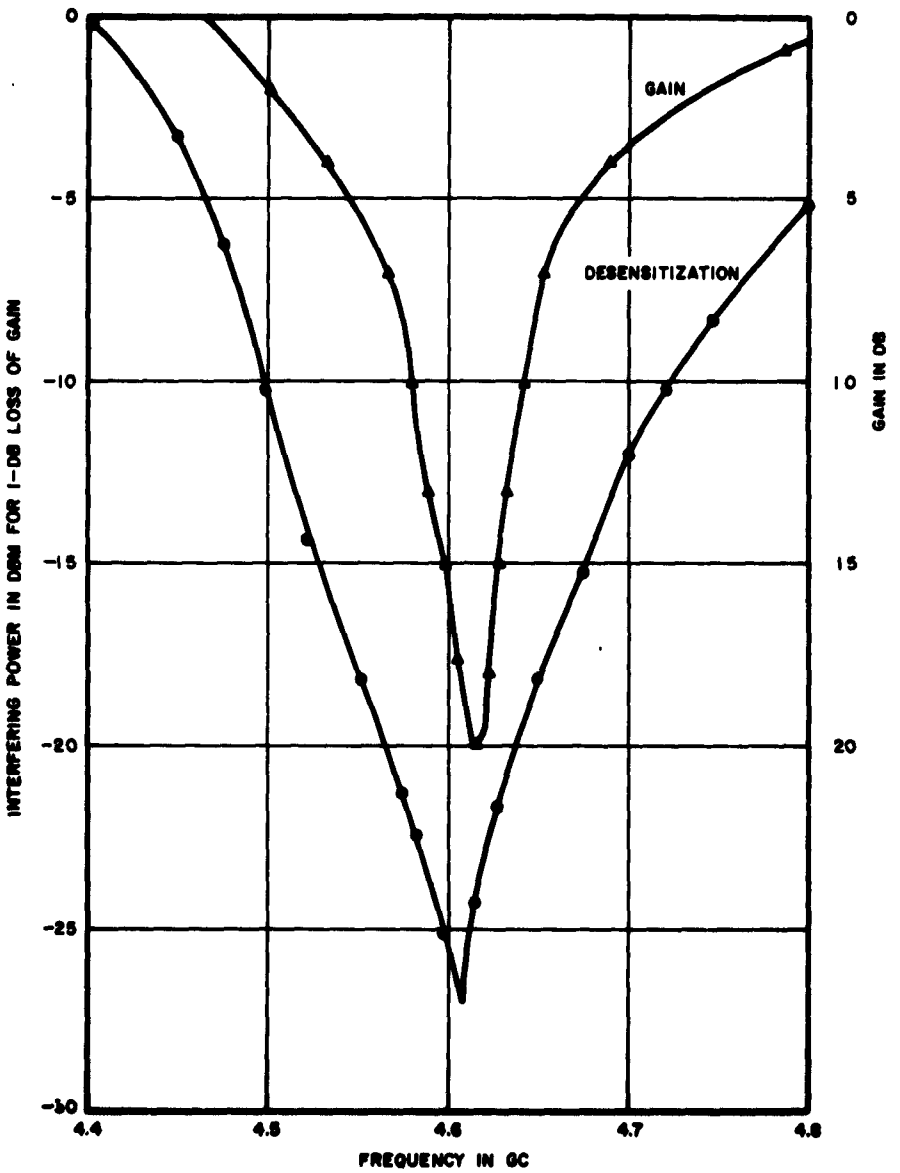

FIGURE 3-5. INTERFERING-SIGNAL POWER FOR CONSTANT DESENSITIZATION AND GAIN VS FREQUENCY FOR A BALANCED PARAMETRIC AMPLIFIER

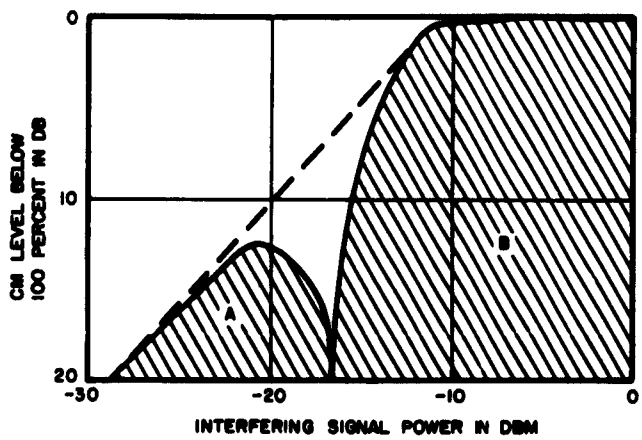

FIGURE 3-6. CROSS MODULATION VS INTERFERING-SIGNAL POWER FOR BALANCED PARAMETRIC AMPLIFIER

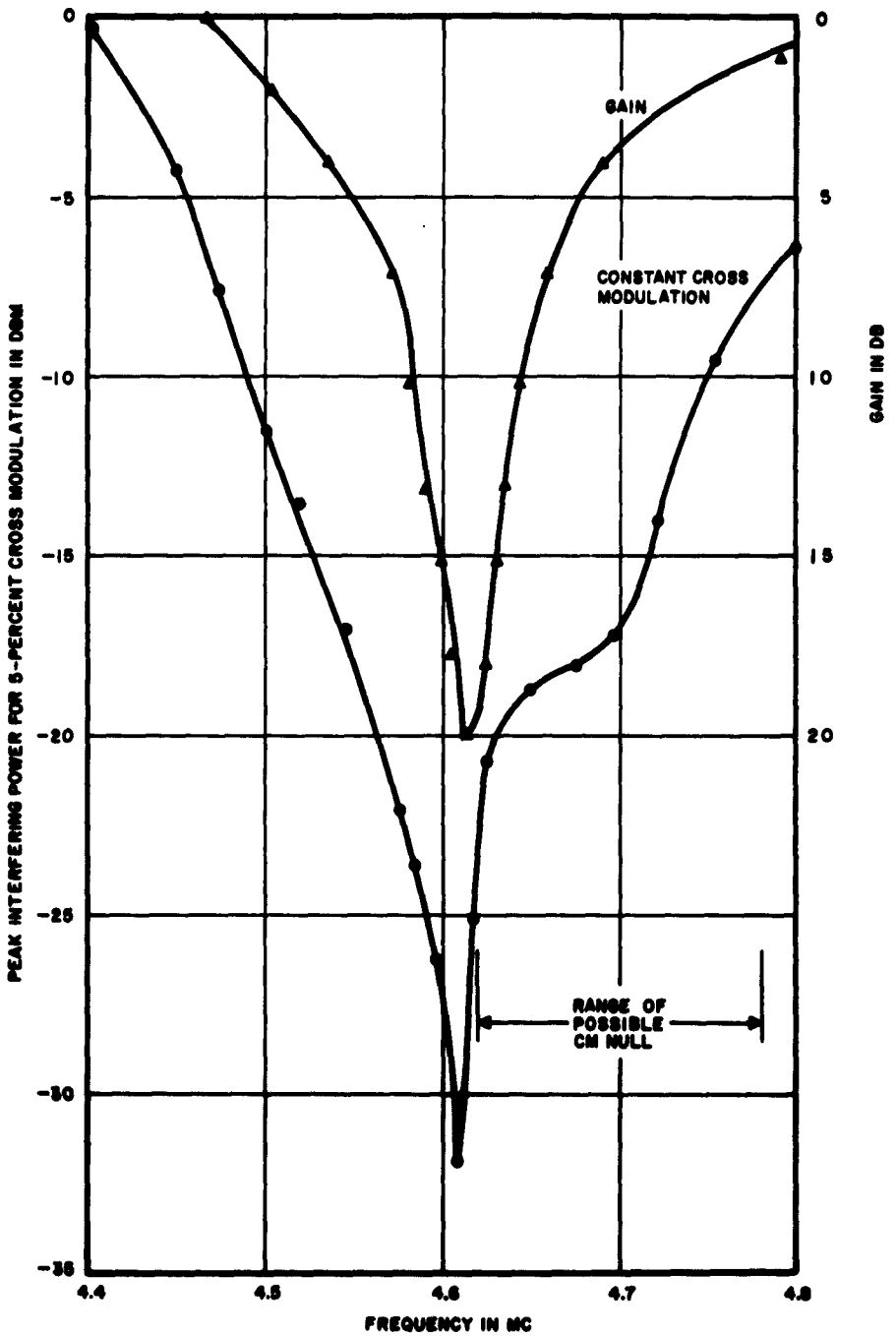

FIGURE 3-7. INTERFERING-SIGNAL POWER FOR CONSTANT CROSS MODULATION AND GAIN VS FREQUENCY FOR A BALANCED PARAMETRIC AMPLIFIER

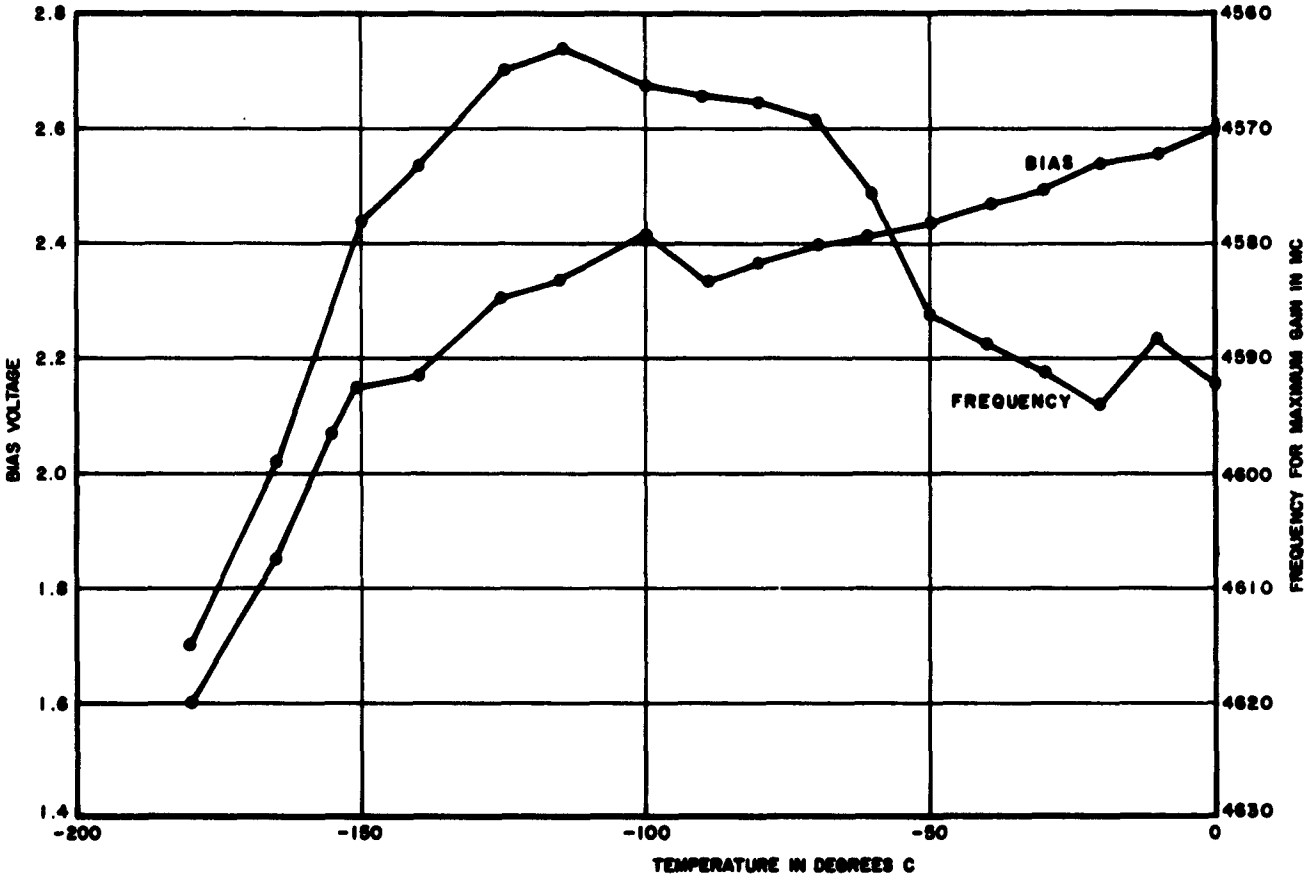

FIGURE 3-8. FREQUENCY OF OPERATION AND BIAS VOLTAGE VS OPERATING TEMPERATURE FOR BALANCED PARAMETRIC AMPLIFIER

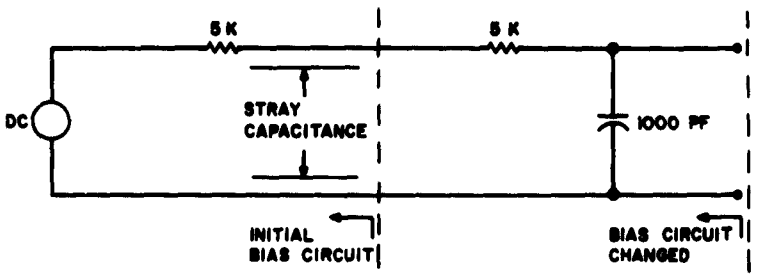

A. BIAS CIRCUIT OF PARAMETRIC AMPLIFIER

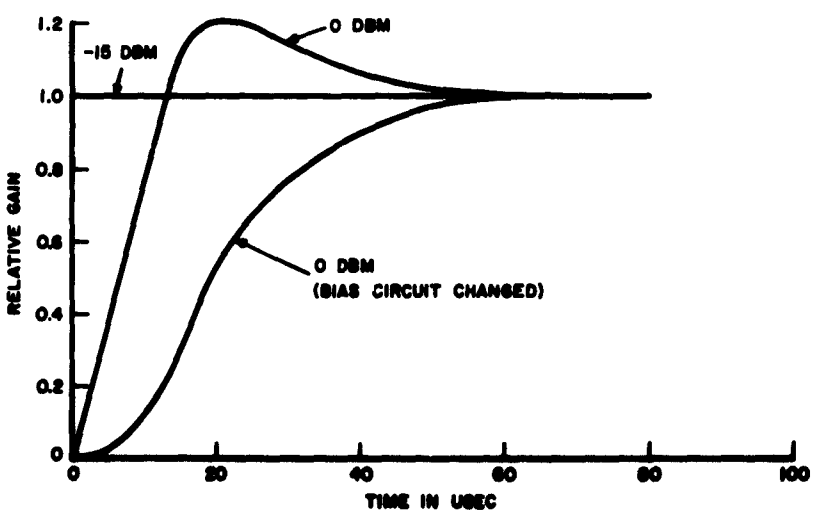

B. GAIN RECOVERY TIME OF PARAMETRIC AMPLIFIER

FIGURE 3-9. DEPENDENCE OF GAIN-RECOVERY TIME OF PARAMETRIC AMPLIFIER UPON AMPLIFIER BIAS CIRCUIT

IV. TUNNEL DIODES

A. HYBRID-COUPLED TUNNEL-DIODE AMPLIFIER

Measurements were performed on a hybrid-coupled tunnel-diode amplifier that was made available to AIL by RADC (reference 6). Gain, saturation, dynamic range, desensitization, intermodulation, and noise figure (as a function of source impedance) were evaluated during the testing of the hybrid-coupled amplifier. The amplifier consisted of two tunnel-diode amplifier modules, which used GE 1N3218A tunnel diodes attached to a 3-db 90-degree hybrid (Figure 4-1). The major advantage of this configuration is that it obviates the circulator (and its associated narrow-band properties) that would be used in conjunction with a negative-resistance amplifier.

The hybrid is a three-quarter wave coupled device that has wide bandwidth. It is a four-port device that splits an incident signal into two equal amplitude components in phase quadrature and couples them to two other ports. The remaining port is isolated from the input port. Figure 4-2 shows the action of the hybrid when an input voltage of amplitude E and zero phase ($E\angle 0^\circ$) is applied to port 1. The voltages coupled to ports 2 and 3 are ($\frac{E}{\sqrt{2}}\angle 0^\circ$) and ($\frac{E}{\sqrt{2}}\angle -90^\circ$), respectively. If two identical amplifier modules are attached at ports 2 and 3, the two amplified components add in-phase in arm 2 and out-of-phase in arm 1. Hence, complete coupling to port 4 is achieved.

Each amplifier module consists of a germanium tunnel diode with its associated bias circuit, and a shorted coaxial line. The shorted line presents an inductance at the diode terminals that resonates with the diode junction capacitance at the operating frequency. The RF equivalent circuit for

each amplifier module is shown in Figure 4-3, where $-g_d$ is the negative conductance of the diode and C is the diode junction capacity, R_S is the diode series resistance, and L_T is the combination of the intrinsic diode inductance and the inductance from the shorted line.

The equivalent circuit is assumed to be a negative resistance ($-R_d$) for the nonlinear analysis of the amplifier performance.

Because of the negative resistance at the tunnel diode, the reflection coefficient (Γ) of the device is greater than unity. This results in a transducer power gain of

$$\Gamma^2 = \left| \frac{R_d - R_o}{R_d + R_o} \right|^2 \qquad (4\text{-}1)$$

where R_o is the source impedance. The power gain in db is given by

$$G = 10 \log \Gamma^2 \qquad (4\text{-}2)$$

1. THEORY

a. TUNNEL DIODE i-v CHARACTERISTICS

A mathematical expression for the tunnel diode i-v characteristic was derived in reference 7. The resulting equation is:

$$I = \frac{I_p}{V_p} V \exp\left(1 - \frac{V}{V_p}\right) + I_o\left[\left(\exp \frac{qv}{KT_o}\right) - 1\right] \qquad (4\text{-}3)$$

where

I = tunnel-diode current
V = tunnel-diode voltage
V_p = peak voltage

I_p = peak current

I_o = bias current

q = electronic charge

K = Boltzmann's constant

T_o = 290°K

The first half of this expression expresses the i-v characteristic of the diode over the tunneling region, and the remaining half is an expression of the diffusion current of the diode. Since only the negative resistance region (tunneling region) is of interest, the current can be approximated to be:

$$I = \frac{I_p}{V_p} V \exp\left(1 - \frac{V}{V_p}\right) \tag{4-4}$$

$$I = AV\, e^{\alpha V} \tag{4-5}$$

where

$$A = \frac{I_p}{V_p} e$$

$$\alpha = -\frac{1}{V_p}$$

By differentiating equation 4-5, the negative resistance of the tunnel diode can be derived as follows:

$$R_d = \frac{1}{\frac{dI}{dV}} = \frac{1}{A\, e^{\alpha V}(V\alpha + 1)} \tag{4-6}$$

b. NONLINEAR ANALYSIS

A nonlinear analysis of the tunnel diode can be performed using equation 4-5; the theoretical i-v characteristic is:

$$I = AV\ e^{\alpha V}$$

Dividing the current and voltage into its AC and DC components:

$$I_o + i = A(V_o + v)e^{\alpha(V_o+v)} \qquad (4\text{-}7)$$

where

I_o = DC current in the tunnel diode

V_o = DC voltage across the tunnel diode

i = AC current

v = AC voltage

Expanding equation 4-7,

$$I_o + i = BV_o\ e^{\alpha v} + Bv\ e^{\alpha v} \qquad (4\text{-}8)$$

where

$$B = A\ e^{\alpha V_o} \qquad (4\text{-}9)$$

Dividing equation 4-8 into I_a and I_b to handle the analysis separately

$$I_a = BV_o\ e^{\alpha v} \qquad (4\text{-}10)$$

$$I_b = Bv\ e^{\alpha v} \qquad (4\text{-}11)$$

Assuming the AC voltage across the diode to be the sum of two sinusoidal signals, ω_1 and ω_2:

$$v = v_1 \cos \omega_1 t + v_2 \cos \omega_2 t \tag{4-12}$$

Substituting equation 4-12 into equation 4-10

$$I_a = BV_o \, e^{\alpha v_1 \cos \omega_1 t} \, e^{\alpha v_2 \cos \omega_2 t} \tag{4-13}$$

Each exponential part of equation 5-13 can now be expanded into a Fourier Series (reference 8):

$$e^{\alpha v_1 \cos \omega_1 t} = \sum_{n=-\infty}^{\infty} C_n \; e^{jn\omega_1 t} \tag{4-14}$$

$$C_n = \frac{1}{2\pi} \int_0^{2\pi} e^{\alpha v_1 \cos \omega_1 t} \; e^{-jn\omega_1 t} \, dt \tag{4-15}$$

$$C_n = I_n(\alpha v_1) \tag{4-16}$$

where $I_n(\alpha v_1)$ is a modified Bessel function of the first kind (reference 8). Substituting equation 4-16 into equation 4-14 and using

$$\cos n\omega_1 t = \frac{e^{jn\omega_1 t} + e^{-jn\omega_1 t}}{2} \tag{4-17}$$

then,

$$e^{\alpha v_1 \cos \omega_1 t} = I_0(\alpha v_1) + 2 \sum_{n=1}^{\infty} I_n(\alpha v_1) \cos n\omega_1 t \tag{4-18}$$

By a similar analysis,

$$e^{\alpha v_2 \cos \omega_2 t} = I_0(\alpha v_2) + 2 \sum_{m=1}^{\infty} I_m(\alpha v_2) \cos m\,\omega_2 t \tag{4-19}$$

Substituting equations 4-18 and 4-19 into equation 4-13:

$$\begin{aligned} I_a = BV_o \Big[& I_0(\alpha v_1) I_0(\alpha v_2) + && \text{(DC term)} \\ & 2I_0(\alpha v_2) \sum_{n=1}^{\infty} I_n(\alpha v_1) \cos n\,\omega_1 t + && \text{(harmonics of } \omega_1\text{)} \\ & 2I_0(\alpha v_1) \sum_{m=1}^{\infty} I_m(\alpha v_2) \cos m\,\omega_2 t + && \text{(harmonics of } \omega_2\text{)} \\ & 4 \sum_{n=1}^{\infty} I_n(\alpha v_1) \cos n\,\omega_1 t \sum_{m=1}^{\infty} I_m(\alpha v_2) \cos m\,\omega_2 t \Big] \end{aligned}$$

(intermodulation frequencies)

(4-20)

Then, equation 4-11 is $1/V_o$ times the derivative with respect to α of I_a (equation 4-10). That is,

$$I_b = \frac{1}{V_o} \frac{dI_1}{d\alpha} \tag{4-21}$$

Therefore differentiating equation 4-20 and substituting into equation 4-21

$$
\begin{aligned}
I_b = B\Big[& I_0(\alpha v_1)I_0'(\alpha v_2)v_2 + I_0(\alpha v_2)I_0'(\alpha v_1)v_1 + && \text{(DC term)} \\
& 2I_0(\alpha v_2) \sum_{n=1}^{\infty} I_n'(\alpha v_1)v_1 \cos n\omega_1 t + \\
& && \text{(harmonics of } \omega_1\text{)} \\
& 2I_0'(\alpha v_2)v_2 \sum_{n=1}^{\infty} I_n(\alpha v_1) \cos n\omega_1 t + \\
& 2I_0(\alpha v_1) \sum_{m=1}^{\infty} I_m'(\alpha v_2)v_2 \cos m\omega_2 t + \\
& && \text{(harmonics of } \omega_2\text{)} \\
& 2I_0'(\alpha v_1)v_1 \sum_{m=1}^{\infty} I_m(\alpha v_2) \cos m\omega_2 t + \\
& 4 \sum_{n=1}^{\infty} I_n(\alpha v_1) \cos n\omega_1 t \sum_{m=1}^{\infty} I_m(\alpha v_2)v_2 \cos m\omega_2 t + \\
& 4 \sum_{n=1}^{\infty} I_n'(\alpha v_1)v_1 \cos n\omega_1 t \sum_{m=1}^{\infty} I_m(\alpha v_2) \cos m\omega_2 t\Big] \\
& && \text{(intermodulation frequencies)}
\end{aligned}
\tag{4-22}
$$

The sum of equations 4-20 and 4-22 is the total current in the tunnel diode due to the application of two sinusoidal voltages across the tunnel diode.

c. **GAIN**

The gain characteristics of the tunnel-diode amplifier can be estimated by using the nonlinear analysis of the tunnel diode i-v characteristic. Summing the terms in equations 4-20 and 4-22, which contribute to the current i_1 at ω_1, results in:

$$i_1 = 2BV_oI_0(\alpha v_2)\ I_1(\alpha v_1)\ \cos\omega_1 t + 2B[I_0(\alpha v_2)\ I_1'(\alpha v_1)\ v_1 \cos\omega_1 t + I_0'(\alpha v_2)\ v_2\ I_1(\alpha v_1)\ \cos\omega_1 t] \qquad (4\text{-}23)$$

Substituting equation 4-9 and letting $v_2 = 0$,

$$i_1 = 2A\ e^{\alpha V_o} V_o[I_1(\alpha v_1) + \frac{v_1}{V_o} I_1'(\alpha v_1)]\ \cos\omega_1 t \qquad (4\text{-}24)$$

From the properties of the modified Bessel function for small arguments (reference 8):

$$I_n(\alpha v_1) = \frac{(\alpha v_1)^n}{2^n n!} \qquad \text{for } \alpha v_1 << 1 \qquad (4\text{-}25)$$

$$I_n'(\alpha v_1) = \frac{(\alpha v_1)^{n-1}}{2^n (n-1)!} \qquad \text{for } \alpha V_1 << 1 \qquad (4\text{-}26)$$

Substituting equations 4-25 and 4-26 into equation 4-24

$$i_1 = A\ e^{\alpha V_o} v_1(\alpha V_o + 1)\ \cos\omega_1 t \qquad (4\text{-}27)$$

Since the resistance of the diode is:

$$R_d = \frac{v_1}{I_1} \cos \omega_1 t \tag{4-28}$$

Substituting equation 4-27 into equation 4-28

$$R_d = \frac{1}{A\, e^{\alpha V_o}(\alpha V_o + 1)} \tag{4-29}$$

This result corresponds exactly with equation 4-6 when v_1 is small. The power gain can be found from equations 4-1 or 4-2.

d. SATURATION

For large v_1, the saturation characteristics of the tunnel diode due to a change in the diode resistance can be derived from equation 4-24. A property of the modified Bessel function is:

$$I_n'(\alpha v_1) = \frac{I_{n-1}(\alpha v_1) + I_{n+1}(\alpha v_1)}{2} \tag{4-30}$$

Substituting this relation into equation 4-24:

$$R_d = \frac{1}{A\, e^{\alpha V_o}\left[I_0(\alpha v_1) + I_2(\alpha v_1) + \frac{2V_o}{v_1} I_1(\alpha v_1)\right]} \tag{4-31}$$

where v_1 is the peak voltage across the diode at the fundamental frequency. The voltage across the diode is a function

of the input voltage to the amplifier and the reflection coefficient Γ:

$$v_1 = (1 + |\Gamma|)\ v_i \tag{4-32}$$

where v_i is the input peak voltage to the amplifier.

In the hybrid-coupled device with two amplifier modules, the actual input voltage to the hybrid amplifier is:

$$v_a = \sqrt{2}\ v_i \tag{4-33}$$

where v_a is the input peak voltage to the hybrid amplifier.

The input power to the hybrid-coupled amplifier is:

$$p = \frac{v_a^{\ 2}}{2R_o} \tag{4-34}$$

Substituting equations 4-32 and 4-33 into equation 4-34 gives:

$$p_1 = \frac{v_1^{\ 2}}{(1 + |\Gamma|)^2 R_o} \tag{4-35}$$

By substituting equation 4-31 into equations 4-1 and 4-2, the gain, Γ^2, can be found for v_1. Using equation 4-35, the power input into the hybrid-coupled amplifier can then be determined from v_1 and Γ. By successively choosing values for v_1 the gain as a function of input power can now be found.

e. DESENSITIZATION

The loss of gain of a desired signal v_1 in the tunnel diode when a large interfering signal v_2 is present can be estimated. Substituting the conditions for small-signal v_1 (equations 4-25 and 4-26) and equation 4-9 into equation 4-23 gives:

$$i_1 = A e^{\alpha V_o} v_1 \left[V_o \alpha I_0(\alpha v_2) + I_0(\alpha v_2) + \alpha v_2 I_0'(\alpha v_2) \right] \cos \omega_1 t \quad (4\text{-}36)$$

Substituting equation 4-36 into equation 4-28:

$$R_d = \frac{1}{A e^{\alpha V_o} \left[V_o \alpha I_0(\alpha v_2) + I_0(\alpha v_2) + \alpha v_2 I_0'(\alpha v_2) \right]} \quad (4\text{-}37)$$

Since the peak voltage v_2 is a function of the input voltage to the amplifier and the reflection coefficient Γ,

$$v_2 = (1 + |\Gamma|)\, v_1 \quad (4\text{-}38)$$

where v_1 is the input peak voltage to the amplifier using equations 4-33 and 4-34; and the input power at ω_2 is

$$p_2 = \frac{v_2^2}{(1 + |\Gamma|)^2 R_o} \quad (4\text{-}39)$$

By substituting equation 4-37 into equations 4-1 and 4-2, gain G can be found for a given value of v_2. Using equation 4-39, the power input into the hybrid-coupled amplifier can then be determined from v_2 and Γ. By choosing successive values for v_2, the desensitization as a function of interfering input power can be found.

f. INTERMODULATION

The intermodulation products can be evaluated by using the nonlinear analysis of the tunnel diode i-v characteristic. Summing the terms in equations 4-20 and 4-22 that contain the intermodulation products, substituting equation 4-9, and choosing the m, n current term gives:

$$i_{mn} = 2A\, e^{\alpha V_o} \Big[V_o I_n(\alpha v_1)\, I_m(\alpha v_2) + v_2 I_n(\alpha v_1)\, I_m'(\alpha v_2) + v_1 I_n'(\alpha v_1)\, I_m(\alpha v_2) \Big] \Big[\cos(m\omega_2 t + n\omega_1 t) + \cos(m\omega_2 t - n\omega_1 t) \Big] \tag{4-40}$$

Substituting equations 4-25, 4-26, and 4-30 into equation 4-40 for small v_1 and v_2 and considering the coefficient of the current term:

$$i_{mn} = \left[\frac{A\, e^{\alpha V_o} \left(\frac{\alpha}{2}\right)^{m+n-1}}{n!\,m!} \Big[V_o\alpha + (m+n) \Big]\, v_1^n\, v_2^m \right] \tag{4-41}$$

Substituting equations 4-32, 4-33, 4-34, 4-35, 4-38, and 4-39 into equation 4-41 gives:

$$p_{mn} = \left[\frac{A\, e^{\alpha V_o} \left(\frac{\alpha}{2}\right)^{m+n-1}}{\Gamma\, n!\,m!} \Big[V_o\alpha + (m+n) \Big]\, (1+\Gamma)^{m+n} \left(\frac{1}{2}\right)^{\frac{m+n}{2}} \right]^2 (2R_o)^{m+n+1}\, p_1^n\, p_2^m \tag{4-42}$$

where p_{mn} = equivalent input power at $\omega = n\omega_1 t \pm m\omega_2 t$. Stated more simply:

$$p_{mn} = C\ p_1^n\ p_2^m \tag{4-43}$$

g. NOISE FIGURE AS A FUNCTION OF SOURCE IMPEDANCE

A hybrid-coupled tunnel diode amplifier used as a high-gain low-noise device requires a well-matched source impedance. Assuming a match at the input, the noise figure of the amplifier is given by:

$$F_o = 1 + \frac{T_a}{T_o} \tag{4-44}$$

where

T_a = noise temperature of the amplifier in ^oK,
T_o = 290^oK.

Since the hybrid-coupled amplifier has a reciprocal transmission characteristic, the noise generated by the second stage T_{ss} passes through the amplifier and is amplified. With a mismatch at the input, a portion of this noise is reflected back into the amplifier. If the input is matched there will not be any load noise appearing at the input of the device. The noise temperature of the second stage T_{ss} is amplified to G_aT_{ss} and it appears at the input of the device. and $|\Gamma_1|^2G_aT_{ss}$ is the effective noise temperature reflected back into the amplifier due to the input voltage reflection coefficient Γ_1. An additional contribution from the noise temperature emitted by the amplifier to the input G_aT_a is reflected back to the amplifier $|\Gamma_1|^2G_aT_a$. Therefore the total noise temperature of the device is:

$$T_{total} = T_a + |\Gamma_1|^2G_aT_{ss} + |\Gamma_1|^2G_aT_a \tag{4-45}$$

Assuming

$$T_{ss} = T_o, \tag{4-46}$$

$$F_m = 1 + \frac{T_T}{T_o} = 1 + \frac{T_a + |\Gamma_1|^2 G_a T_{ss} + |\Gamma_1|^2 G_a T_a}{T_o} \tag{4-47}$$

$$= F_o(1 + |\Gamma_1|^2 G_a) \tag{4-48}$$

where F_m is degraded noise figure due to mismatch Γ_1. This derivation is based on ideal hybrid action and identical amplifier modules.

2. MEASUREMENTS

a. TUNNEL DIODE i-v CHARACTERISTIC

The germanium tunnel diodes (1N3218A) that were used in the amplifier modules were manufactured by General Electric. The typical specifications given by the manufacturer are:

Peak current	I_p	1.0 ma
Valley current	I_v	0.13 ma
Peak voltage	V_p	60 mv
Valley voltage	V_v	350 mv
Negative conductance	$-g_d$	9×10^{-3} mho
Series resistance	R_s	1.5 ohms
Series inductance	L_s	0.3 mμh
Total capacity	C_t	4 pf

The measured i-v characteristic of the tunnel diode is shown in Figure 4-4. The voltage drop across the series resistance

(R_s) of 1.5 ohm was considered negligible. The following parameters of the tunnel diode were found using Figure 4-4.

Peak current	1.22 ma
Valley current	0.15 ma
Peak voltage	55 mv
Valley voltage	310 mv

The substitution of these values into equation 4-4 results in a curve that does not agree with the measured curve shown in Figure 4-4. Therefore, two points in the negative resistance region of the measured i-v characteristic were substituted into equation 4-5 and A and α were found. The resulting equation for the tunnel diode i-v characteristic is:

$$I = 0.0805\ V\ e^{-22.2V} \tag{4-49}$$

This is a good approximation in the negative resistance region and a fair approximation in the peak and valley areas. The negative resistance of the tunnel diode ($-R_d$) was measured as a function of bias voltage using the audio bridge circuit shown in Figure 4-5. The series resistance of the tunnel diode (R_s = 1.5 ohm) was considered negligible. The results plotted in Figure 4-5 indicate a minimum negative resistance of 85 ohms that occurs at the inflection point of the i-v characteristic. The bias voltage associated with the inflection point is approximately 100 mv and the bias current is 0.9 ma. Substituting into equation 4-6, the values of A and α from equation 4-49, results in a diode negative resistance at the inflection point (V_o = 100 mv) of

$$R_d = \frac{1}{A\ e^{\alpha V}(V\alpha + 1)} = -93.7 \text{ ohms} \tag{4-50}$$

This value is fairly close to the measured negative resistance at the inflection point shown in Figure 4-5.

b. GAIN

The measurement of the gain of the hybrid-coupled amplifier was made using the test setup shown in Figure 4-6. The amplifier was padded at the input and output to assure stable operation. The bias voltage was maintained at 100 mv and the frequency of the signal generator was varied in 50-Mc increments from 50 Mc to 500 Mc. The signal generator was modulated by a square-wave generator, and the detector used was of the crystal type with a standing wave indicator. Figure 4-6 is a plot of the broad-band frequency response of the amplifier.

The power gain derived by substituting the negative resistance described in equation 4-50 into equation 4-1 is:

$$G = \Gamma^2 = \left|\frac{R_d - R_o}{R_d + R_o}\right|^2 = \left|\frac{(-93.7) - 50}{(-93.7) + 50}\right|^2 = 10.82 \qquad (4\text{-}51)$$

assuming R_o = 50 ohms.

The gain in db is given by equation 4-2. Substituting equation 4-51 into equation 4-2:

$$G = 10.4 \text{ db} \qquad (4\text{-}52)$$

This gain is close to the measured gain if the simplified equivalent circuit of a negative resistance is assumed.

c. DYNAMIC RANGE

The dynamic range of the hybrid-coupled amplifier was measured at 350 Mc using the test circuit shown in Figure 4-7. The bias voltage on the tunnel diode was maintained at 100 mv during the test. The input power was varied from -79 dbm to -4 dbm, and the change in the output power was

measured (Figure 4-7). The input power level to the mixer was kept constant by using a variable attenuator that ensured that the mixer would not saturate at high input levels. The 3-db deviation from linearity in the dynamic range curve is at an input power of approximately -20 dbm.

Figure 4-8 is a plot of the gain characteristic derived from the power transfer curve in Figure 4-7. This figure also shows a 3-db deviation from linearity at -20 dbm. The theoretical values plotted in Figure 4-8 predict a larger low-level gain of 10.4 db and a 3-db deviation from linearity at -20.5 db. The measurements agree closely with the predictions considering that the tunnel diode i-v characteristic was approximated.

d. DESENSITIZATION

The test setup for the measurement of desensitization is shown in Figure 4-9. The desired signal frequency was 250 Mc and the interfering signal was 280 Mc. The input power for the desired signal was -36 dbm. The bias of the tunnel diode was maintained at 125 mv. The plot of gain as a function of the input power of the interfering signal is shown in Figure 4-9. The 3-db loss in gain point corresponds to an input power of -22 dbm in the interfering signal. A plot of theoretical loss in gain as a function of input power of the interfering signal is also shown in Figure 4-9. The predicted input power, corresponding to a loss of 3 db in gain, is shown to be -18 dbm.

e. INTERMODULATION CHARACTERISTICS

The test setup for the measurement of intermodulation products is shown in Figure 4-9. The tunnel-diode bias was kept at 100 mv. The two signal generators at f_1 and f_2 were isolated by at least 30 db by using a cross-over 3-db hybrid. The narrow-band cavity at the output of the hybrid-coupled amplifier is used to select the proper intermodulation

product, in this case $2f_2 - f_1$. When f_1 is equal to 250 Mc and f_2 is equal to 300 Mc, $2f_2 - f_1$ is equal to 350 Mc. Figure 4-10 shows the variation of the equivalent input power of the third order intermodulation product (p_{12}) as a function of the input power at $f_2(p_2)$ with the input power at $f_1(p_1)$ as a parameter. The third-order intermodulation product can be expressed in db as:

$$p_{12} = 2p_2 + p_1 + C \qquad (4\text{-}53)$$

As shown in Figure 4-10, the measured value of C is 52 dbm and the predicted value of C is 37 db. The theoretical results are plotted in Figure 4-10.

f. NOISE FIGURE

The test circuit used to measure the noise figure is illustrated in Figure 4-11. The bias voltage was maintained at 100 mv. The noise source used was an AIL Type 74 noise diode. The source impedance was varied by adding a series or parallel resistance at the output of the noise diode.

The diode current was measured for source impedances of 50.15, 25.46, 28.98, 74.0, and 100.9 ohms with a sensitive milliammeter. A Wheatstone bridge was used to measure the resistance.

The noise figure and gain of the hybrid-coupled amplifier at 200 Mc were determined by varying the attenuator (L) between the device and a second-stage receiver that had a noise figure F_2. Since the overall noise figure F_o is equal to

$$F_o = F_1 + \frac{LF_2 - 1}{G_a} = \left[F_1 - \frac{1}{G_a}\right] + \left[\frac{F_2}{G_1}\right] L \qquad (4\text{-}54)$$

the noise figure of the amplifier F_1 and its gain (G_a) can be determined. The noise figure was also plotted as a function of the input reflection coefficient (Figure 4-11) using equation 4-48. These results agree fairly well with theory under the assumptions of ideal hybrid action, matched output terminations, and identical amplifier modules.

B. BALANCED TUNNEL-DIODE AMPLIFIER

An arrangement of two tunnel diodes in a balanced push-pull configuration was suggested (reference 9) to increase the dynamic range of the tunnel-diode amplifier. A balanced amplifier has been designed and fabricated, and its interference characteristics investigated. This amplifier consists of two Micro State 233 gallium-antimonide tunnel diodes in a balanced mount. The mount is constructed of stripline with the two diodes positioned across the line between the center conductor and the ground plane. The diodes are tuned by a sliding short across the stripline. The mount has a bypass capacitor across the diode to the ground plane. A wide-band circulator is used in conjunction with the amplifier mount.

1. THEORY

a. TUNNEL-DIODE COMPOSITE CHARACTERISTIC

A mathematical expression for the single tunnel-diode characteristic shown in Figure 4-12 is given by equation 4-5. The composite characteristic (Figure 4-13) can be expressed as the sum of two currents:

$$I = I_c + I_d \tag{4-55}$$

The first term of this composite current, which is the current through the first diode expression is the same as equation 4-5:

$$I_c = AV\, e^{\alpha V} \tag{4-56}$$

The second term can be obtained by transforming equation 4-56 to an expression that describes the second diode current (Figure 4-13). Thus,

$$I_d = A(V - 2V_o)\, e^{-\alpha(V-2V_o)} \qquad (4\text{-}57)$$

where V_o is the bias voltage.

b. NONLINEAR ANALYSIS

A nonlinear analysis of the balanced tunnel-diode amplifier can be performed using the expression for the composite characteristic (equation 4-55). A nonlinear analysis of the first term (I_c) in the composite characteristic was made previously; the nonlinear components are given in equations 4-20 and 4-22. It is now necessary to analyze the second term (I_d).

Using equation 4-57, and separating the voltage and current into its AC and DC components,

$$I_o + i = A(V_o + v - 2V_o)\, e^{-\alpha(V_o+v-2V_o)} \qquad (4\text{-}58)$$

where

I_o = DC component of tunnel-diode current,
V_o = DC component of tunnel-diode voltage,
i = AC component of tunnel-diode current,
v = AC component of tunnel-diode voltage.

Expanding equation 4-58,

$$I_o + i = Bv\, e^{-\alpha v} - BV_o\, e^{-\alpha v} \qquad (4\text{-}59)$$

where $B = A\, e^{\alpha V_o}$

Writing I_e and I_f from equation 4-59,

$$I_e = Bv\ e^{-\alpha v} \tag{4-60}$$

$$I_f = BV_o\ e^{-\alpha v} \tag{4-61}$$

It can be seen that I_e is the same as in equation 4-11, and I_f is the same as in equation 4-10, except for the negative sign of α in both equations. When two sinusoidal signals (ω_1 and ω_2) are applied across the diode, the voltage across the diode is given by equation 4-12. Substituting equation 4-12 into equations 4-60 and 4-61, the solution of the Fourier series expansion of I_e is given in equation 4-22 and the solution for I_f is given in equation 4-20 except that $-\alpha$ is substituted for α.

c. GAIN

The gain characteristics of the tunnel-diode amplifier can be estimated by using the nonlinear analysis of the tunnel-diode i-v characteristic. Summing the terms in the solution of equation 4-55 that contribute to the current i_1 at the fundamental ω_1 (equations 4-20 and 4-22), letting $v_2 = o$, and using the relation

$$\begin{aligned} I_n(-\alpha v) &= I_n(\alpha v),\ n \text{ even} \\ I_n(-\alpha v) &= -I_n(\alpha v),\ n \text{ odd} \end{aligned} \tag{4-62}$$

the resulting expression is

$$i_1 = 4A\ e^{\alpha V_o}\ V_o\left[I_1(\alpha v_1) + \frac{v_1}{V_o}\ I_1'\ (\alpha v_1)\right]\ \cos\ \omega_1 t \tag{4-63}$$

where v_1 is the peak AC diode voltage.

Using equations 4-25 and 4-26, the composite current in the tunnel diodes is

$$i_1 = 2A\, e^{\alpha V_o}\, v_1(\alpha V_o + 1) \cos \omega_1 t \qquad (4\text{-}64)$$

This is exactly twice the fundamental current in one tunnel diode. Substituting equation 4-63 into 4-28, the small-signal resistance of the diode is

$$R_d = \frac{1}{2A\, e^{\alpha V_o}\, (\alpha V_o + 1)} \qquad (4\text{-}65)$$

The resistance is half of the resistance of a single tunnel diode. The power gain can be computed from equations 4-1 and 4-2.

d. SATURATION

For large v_1, the saturation characteristics of the balanced tunnel-diode amplifier caused by a change in the diode resistance can be derived from equation 4-63. Substituting equation 4-30 into equation 4-63,

$$R_d = \frac{1}{2A\, e^{\alpha V_o}[I_0(\alpha v_1) + I_2(\alpha v_1) + 2\frac{V_o}{v_1} I_1(\alpha v_1)]} \qquad (4\text{-}66)$$

This large-signal resistance is half of the large-signal resistance of a single tunnel diode.

By substituting equation 4-66 into equations 4-1 and 4-2, the gain Γ^2 can be found for v_1. Using equation 4-35, the power into the amplifier can then be determined from v_1 and Γ. By successively choosing values for v_1, the gain as a function of input power can now be found.

e. DESENSITIZATION

The loss of gain of a desired signal v_1 in the tunnel-diode amplifier can be estimated when a large interfering signal v_2 is present. Since the composite current at the fundamental frequency in the balanced tunnel-diode amplifier is twice the current in a single tunnel-diode amplifier, the composite current is twice the value given in equation 4-36.

$$i_1 = 2A\, e^{\alpha V_o}\, v_1\left[V_o\alpha\, I_0(\alpha v_2) + I_0(\alpha v_2) + \alpha v_2\, I_0'(\alpha v_2)\right] \cos \omega_1 t \tag{4-67}$$

Substituting equation 4-67 into equation 4-28, the diode resistance in the presence of a strong interfering signal is

$$R_d = \frac{1}{2A\, e^{\alpha V_o}\left[V_o\alpha\, I_0(\alpha v_2) + I_0(\alpha v_2) + \alpha v_2\, I_0'(\alpha v_2)\right]} \tag{4-68}$$

By substituting equation 4-68 into equations 4-1 and 4-2, the gain can be found for a given value of v_2. Using equation 4-39, the power input to the balanced amplifier can be determined from v_2 and Γ. By choosing successive values for v_2, the desensitization as a function of interfering power can be found.

f. INTERMODULATION

The intermodulation products can be evaluated by using the nonlinear analysis of the tunnel-diode i-v characteristic. Summing the terms in equation 4-20 and 4-22, substituting into equation 4-55, and using 4-25, 4-26, and 4-30, the coefficient of the current terms is:

$$i_{mn} = \left\{ \frac{2A\, e^{\alpha V_o} \left(\frac{\alpha}{2}\right)^{m+n-1}}{n!m!} \left[V_o\alpha + (m + n)\right] v_1^n\, v_2^m \right\} \quad \text{for } m + n \text{ odd}$$

$$= 0 \text{ for } m + n \text{ even} \tag{4-69}$$

Substituting equations 4-35 and 4-39 into equation 4-69, and solving for the intermodulation coefficient C in equation 4-43,

$$C = \left\{ \frac{2A\, e^{\alpha V_o} \frac{\alpha}{2}^{m+n-1}}{\Gamma\, m!n!} \left[V_o\alpha + (m + n)\right] (1 + \Gamma)^{m+n} \left(\frac{1}{2}\right)^{\frac{m+n}{2}} (2R_o)^{m+n+1} \right\} \quad \text{for } m + n \text{ odd}$$

$$= 0 \text{ for } m + n \text{ even}$$

It can be seen that, since α is negative, a theoretical null exists for the intermodulation coefficient where the bias voltage is equal to $\frac{m + n}{\alpha}$.

2. MEASUREMENTS

a. TUNNEL DIODE i-v CHARACTERISTIC

The i-v characteristic (MS 233 diode) was measured (Figure 4-12) using the test setup shown in Figure 4-4. The inflection point is approximately 0.66 ma and 70 mv. During the testing of the balanced amplifier, the bias was kept at about 0.38 ma and 93 mv to achieve a low noise figure. The composite characteristics were plotted for a bias of 0.38 ma from the measured i-v characteristic shown in Figure 4-13. This shows a fairly linear region in the plot of the composite characteristic which yields a good dynamic range. The negative resistance of the tunnel diode was measured as a function of bias voltage (Figure 4-14) using the test setup shown in Figure 4-5.

Two points in the negative resistance region of the measured i-v characteristic were substituted in equation 4-5 to find A and α. The points chosen were near the peak (V = 45 mv, I = 1.05 ma) and at the low-noise operating point (V = 93 mv, I = 0.38 ma). These points bound the usual operating-bias region for the tunnel-diode amplifier and result in a good approximation to the measured i-v characteristic. The resulting theoretical tunnel-diode i-v characteristic obtained from equation 4-5 is:

$$I = 0.12\ V\ e^{-36.4V}$$

This is shown plotted in Figure 4-12 along with the experimental points chosen.

b. <u>GAIN</u>

Gain of the balanced amplifier was measured using the test circuit shown in Figure 4-15. The bias voltage was maintained at 93 mv during the test. Insertion measurements were taken in 100-Mc increments of the signal generator; they are plotted in Figure 4-15. This plot shows a very flat response from 1100 to 1400 Mc with a gain of about 10 db. Since the diode is biased at the low-noise point of the tunnel diode i-v characteristic, there is less gain that if it were biased at the inflection point.

The power gain derived by substituting the negative resistance of equation 4-65 at the low-noise bias point (V = 93 mv) into equation 4-1 is

$$\Gamma = 4.28$$

$$G = 12.6 \text{ db}$$

using R_o = 32 ohms, which is the transformed generator impedance at the diode terminals. This gain is close to the measured gain if the simplified equivalent circuit of a negative resistance is assumed.

c. DYNAMIC RANGE

Dynamic range measurements were performed using the test circuit shown in Figure 4-15. The bias voltage was maintained at 93 mv. A variable attenuator was inserted between the amplifier and mixer to ensure that the level into the mixer remained constant and did not saturate. The output power of the signal generator was varied; the receiver level was recorded and is plotted in Figure 4-16. This shows a 3-db deviation from linearity at -23.5 dbm input power.

Figure 4-17 is a plot of the gain characteristic at V = 93 mv derived from the power transfer curve in Figure 4-16. Figure 4-17 also shows a 3 db loss of gain at an input of -23.5 dbm. The theoretical values plotted in Figure 4-17 predict a larger small-signal gain of 12.6 db and a 3-db loss of gain at an input of -21 dbm. The 0.6 db increase in gain from its small-signal value before the gain drops off because of saturation is due to the change in negative resistance with increasing signal strength. The measured results do not indicate this small increase, probably because of measurement inaccuracy.

Using equations 4-31 and 4-35, the theoretical gain characteristics of a single MS 233 tunnel diode biased at the inflection point of 70 mv and at the low-noise point of 93 mv are obtained (Figure 4-18). This figure shows an increase of 3 db in the dynamic range when operating in the low-noise region. The upper end of the dynamic range is taken to the point at which there is a 3-db decrease in gain. For this analysis, the gain at the inflection point was made equal to the gain at the low-noise point by adjusting the source impedance.

d. DESENSITIZATION

The loss in gain for a desired signal caused by an interfering signal was measured. The bias voltage was maintained at 93 mv. The desired signal frequency was 1300 Mc and the interfering signal was at 1200 Mc. A hybrid was used to isolate the two signal generators producing the desired and interfering signals. The output power of the signal generator producing the interfering signal was increased and the decrease in gain at the desired frequency was recorded (Figure 4-19). A 3-db loss in gain at -15 dbm was indicated. The theoretical desensitization characteristic is also given in Figure 4-19, which shows a 3-db loss in gain at -23 dbm.

e. INTERMODULATION

The third-order intermodulation product $(2f_2 - f_1)$, produced by two in-band signals into the amplifier, was measured on the balanced amplifier. The frequency of p_1 was 1200 Mc and of p_2 was 1300 Mc producing a signal output from the amplifier at 1400 Mc. The test setup for this measurement is shown in Figure 4-20. The two signal generators are isolated from each other by a hybrid and a circulator used as an isolator at the output of one of the signal generators. A cavity tuned to 1400 Mc is used to select the third-order intermodulation product at the output of the amplifier. The equivalent input power at $2f_2 - f_1$ was determined. It is plotted in Figure 4-20 as a function of the input power at f_2 with the input power at f_1 as a parameter. The resulting C is 52 dbm. The dips in the intermodulation characteristic in the saturation region are probably caused by a shift in the bias point of the diodes when they are saturated. The theoretical value of C is 84 dbm (equation 4-70). A possible reason for the large difference between the measured and theoretical intermodulation coefficients is that the bias point is near a theoretical null in third-order intermodulation products--that is, when $V_o = \frac{3}{\alpha} = 82.5$ mv. Therefore the intermodulation product is a sensitive function of bias in this region.

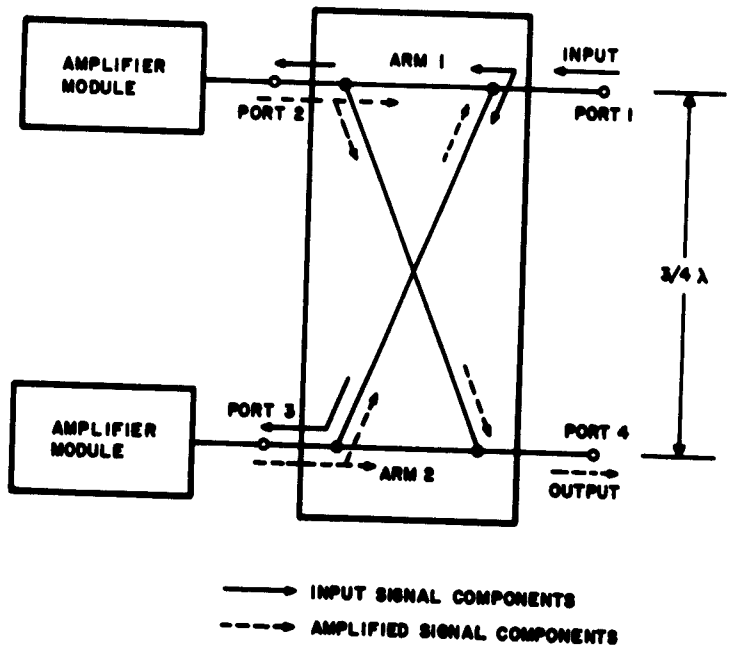

FIGURE 4-1. HYBRID-COUPLED TUNNEL-DIODE AMPLIFIER

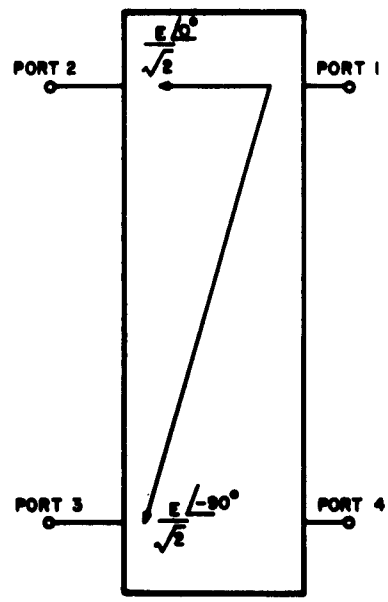

FIGURE 4-2. VOLTAGE COUPLING IN 3-DB HYBRID

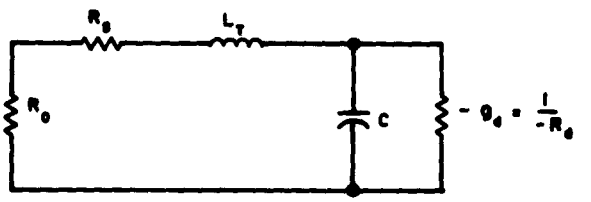

FIGURE 4-3. TUNNEL-DIODE EQUIVALENT CIRCUIT

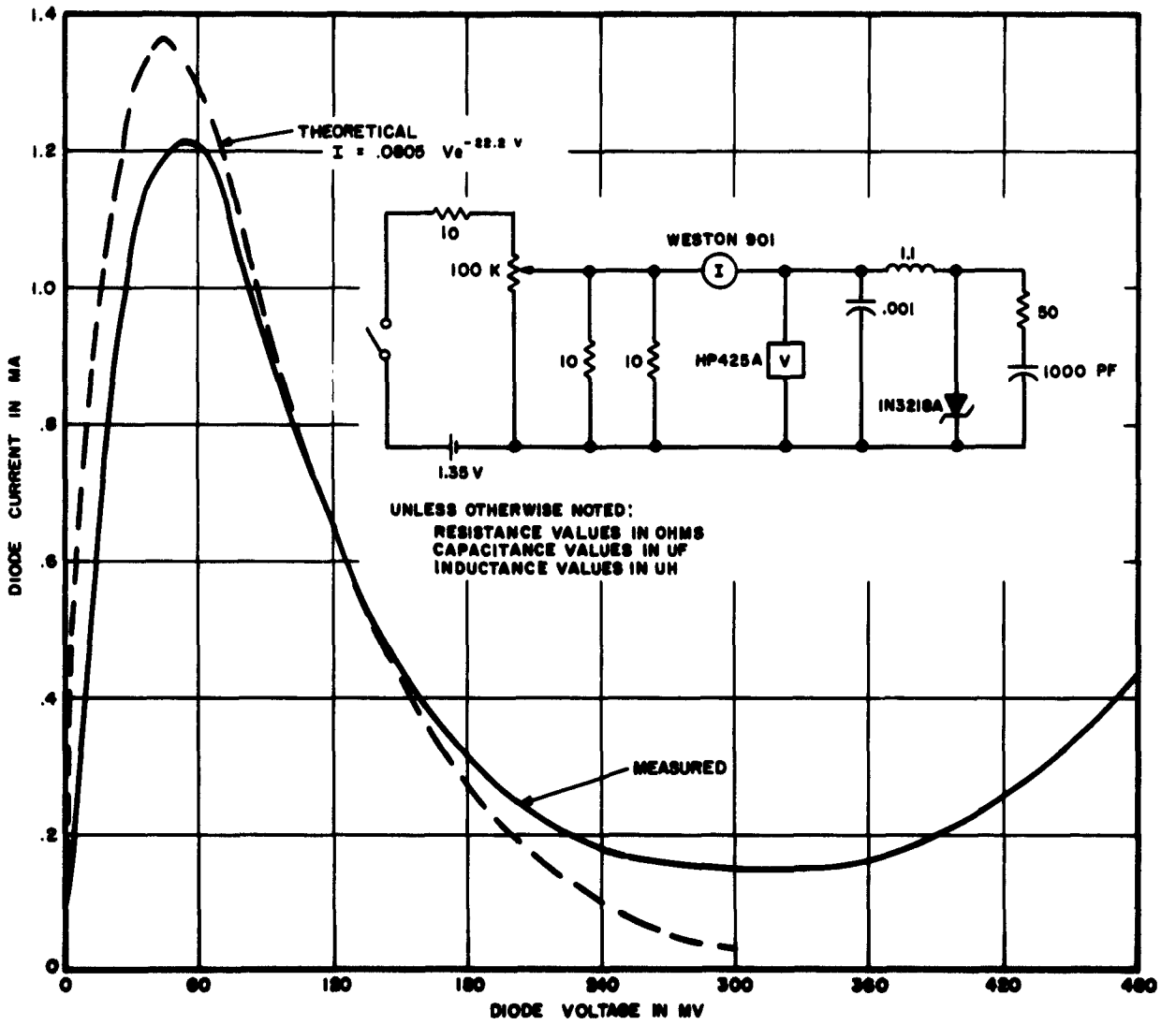

FIGURE 4-4. TUNNEL-DIODE 1N3218A i-v CHARACTERISTIC

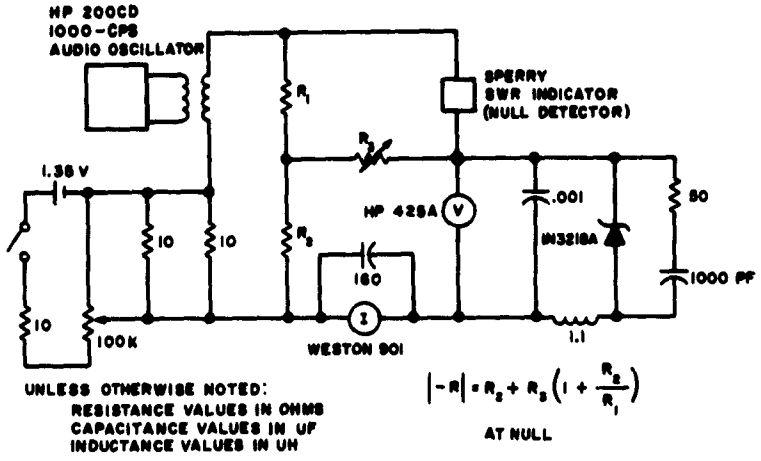

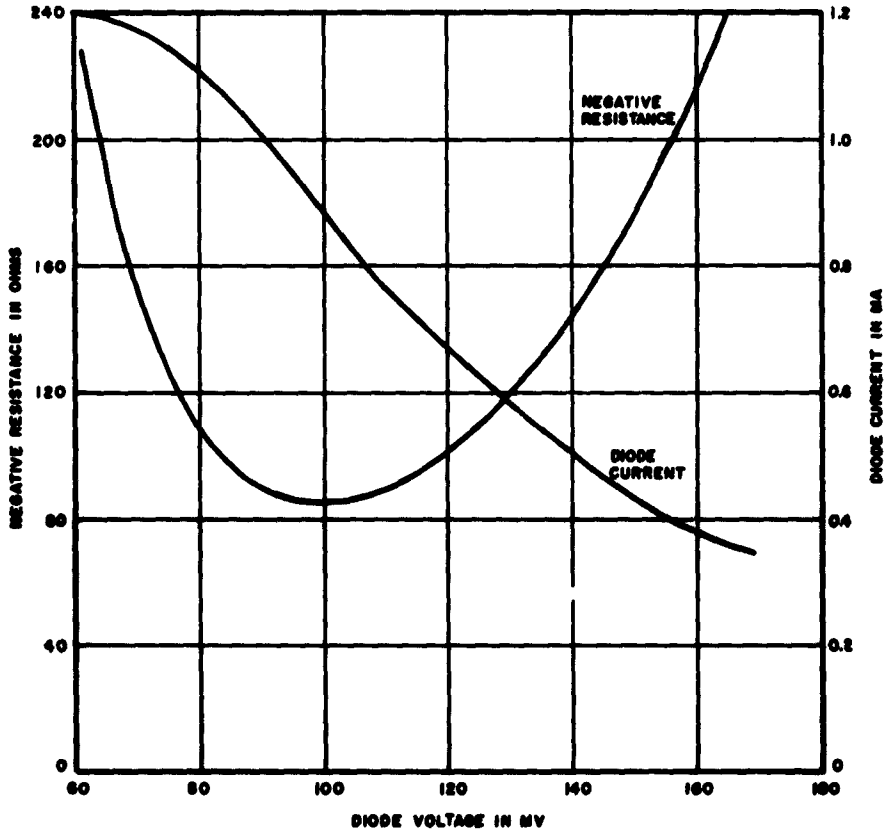

FIGURE 4-5. TUNNEL-DIODE 1N3218A NEGATIVE RESISTANCE

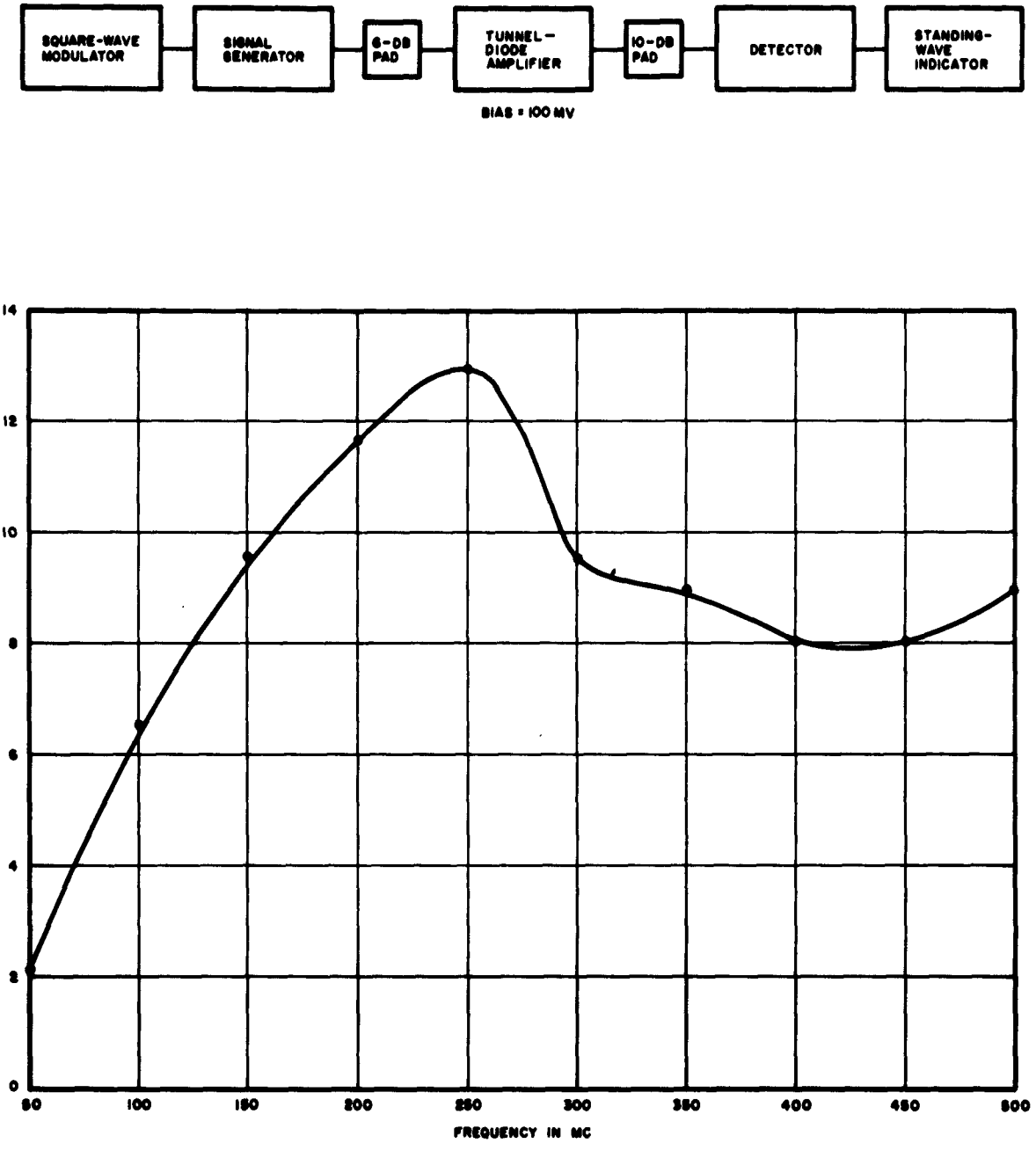

FIGURE 4-6. GAIN VS FREQUENCY OF HYBRID-COUPLED AMPLIFIER

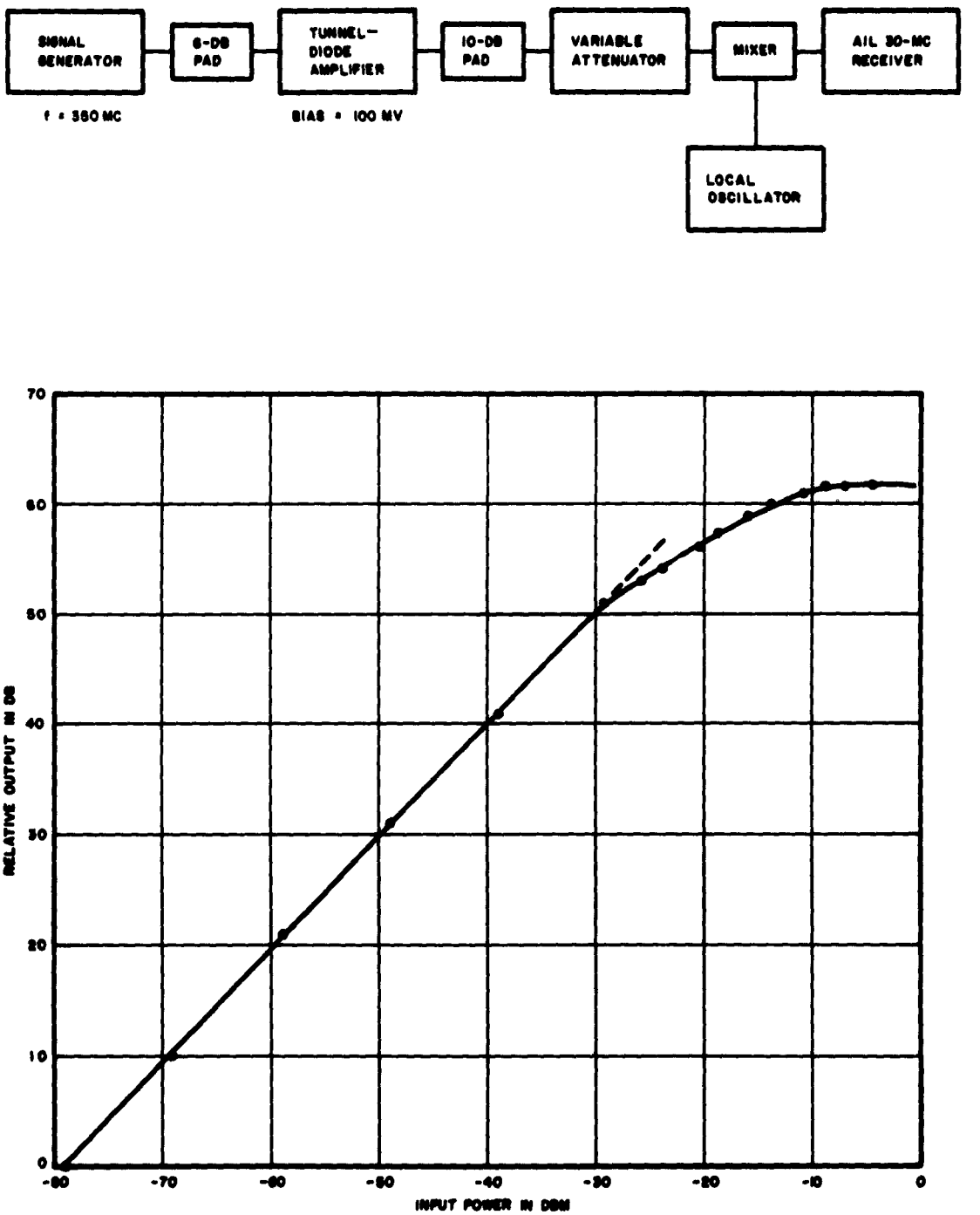

FIGURE 4-7. POWER TRANSFER CHARACTERISTIC OF HYBRID-COUPLED AMPLIFIER

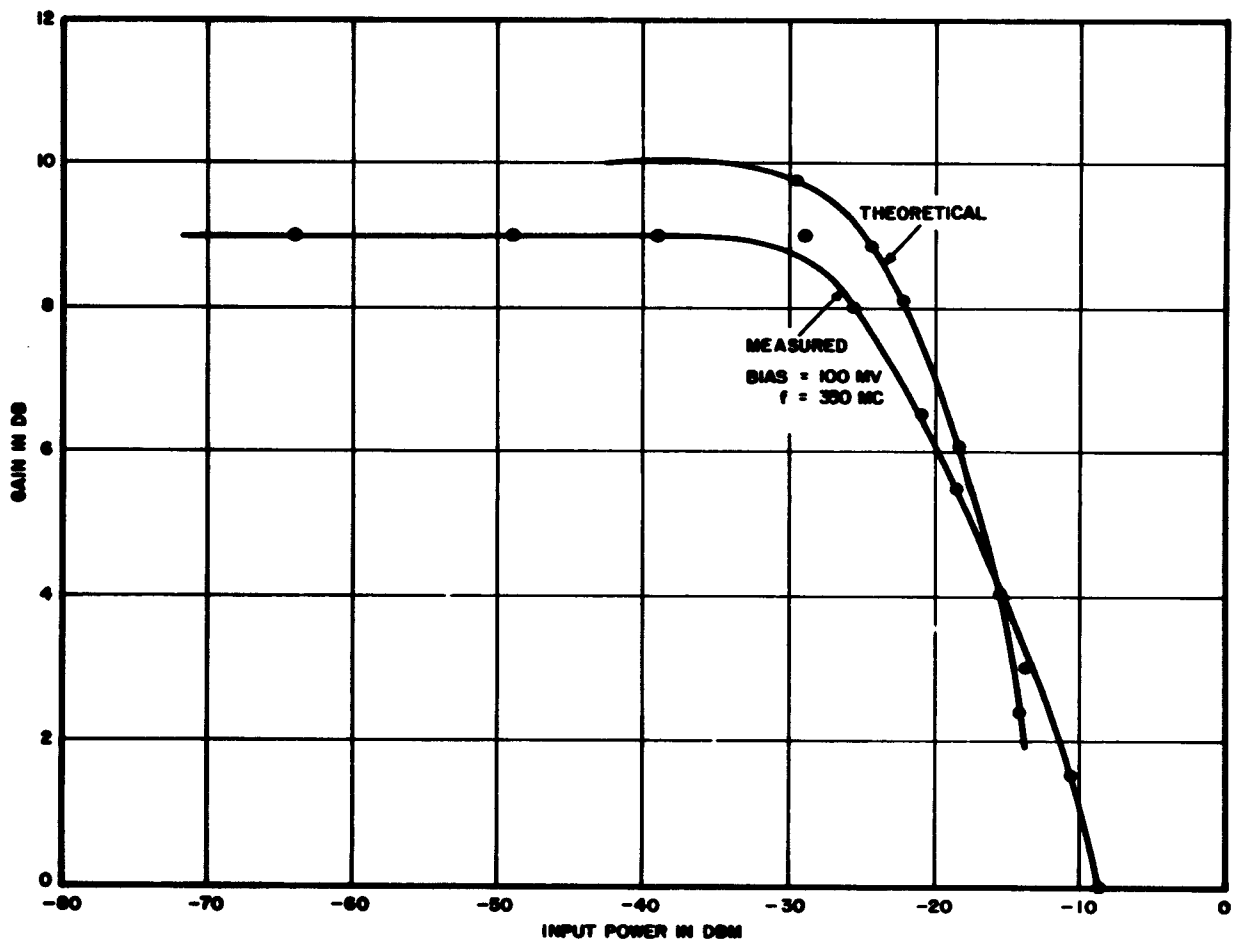

FIGURE 4-8. GAIN VS INPUT POWER FOR HYBRID-COUPLED AMPLIFIER

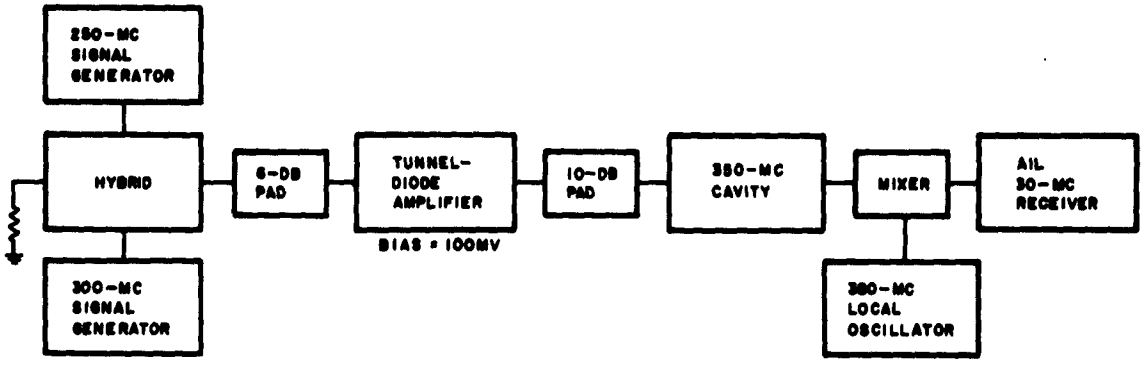

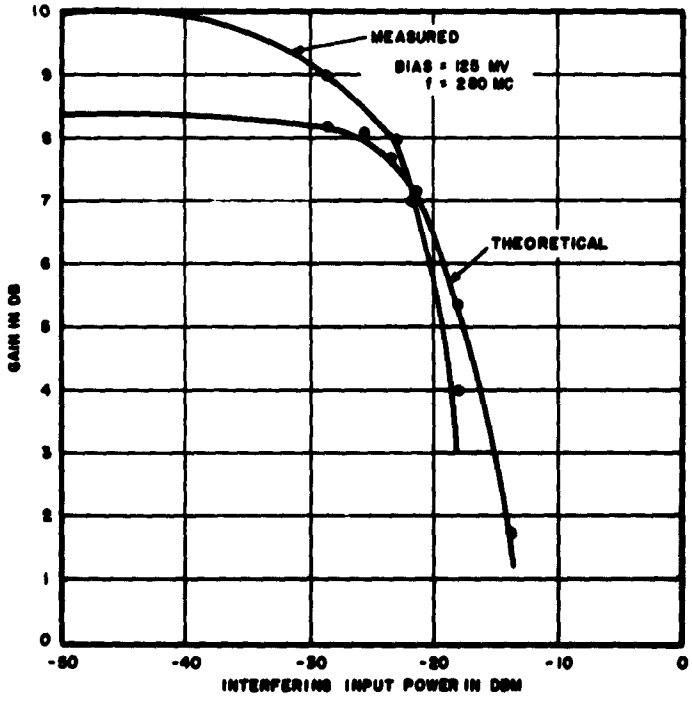

FIGURE 4-9. GAIN VS INTERFERING INPUT POWER FOR HYBRID-COUPLED AMPLIFIER

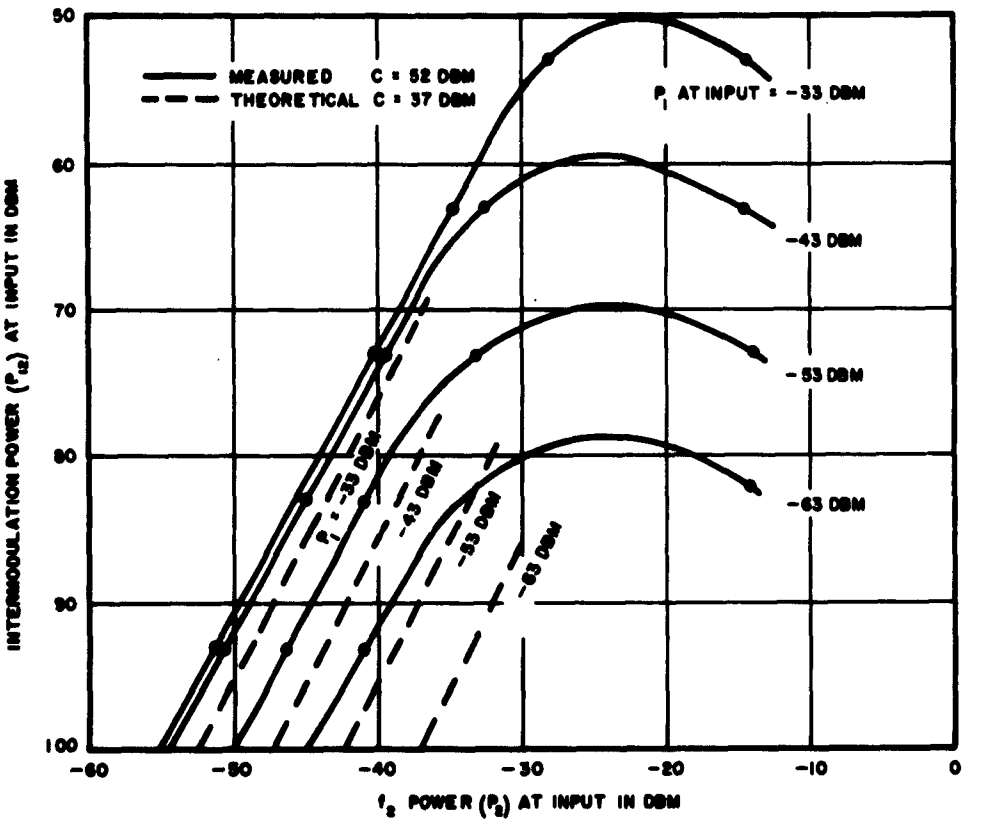

FIGURE 4-10. THIRD-ORDER INTERMODULATION VS INPUT POWER OF HYBRID-COUPLED AMPLIFIER

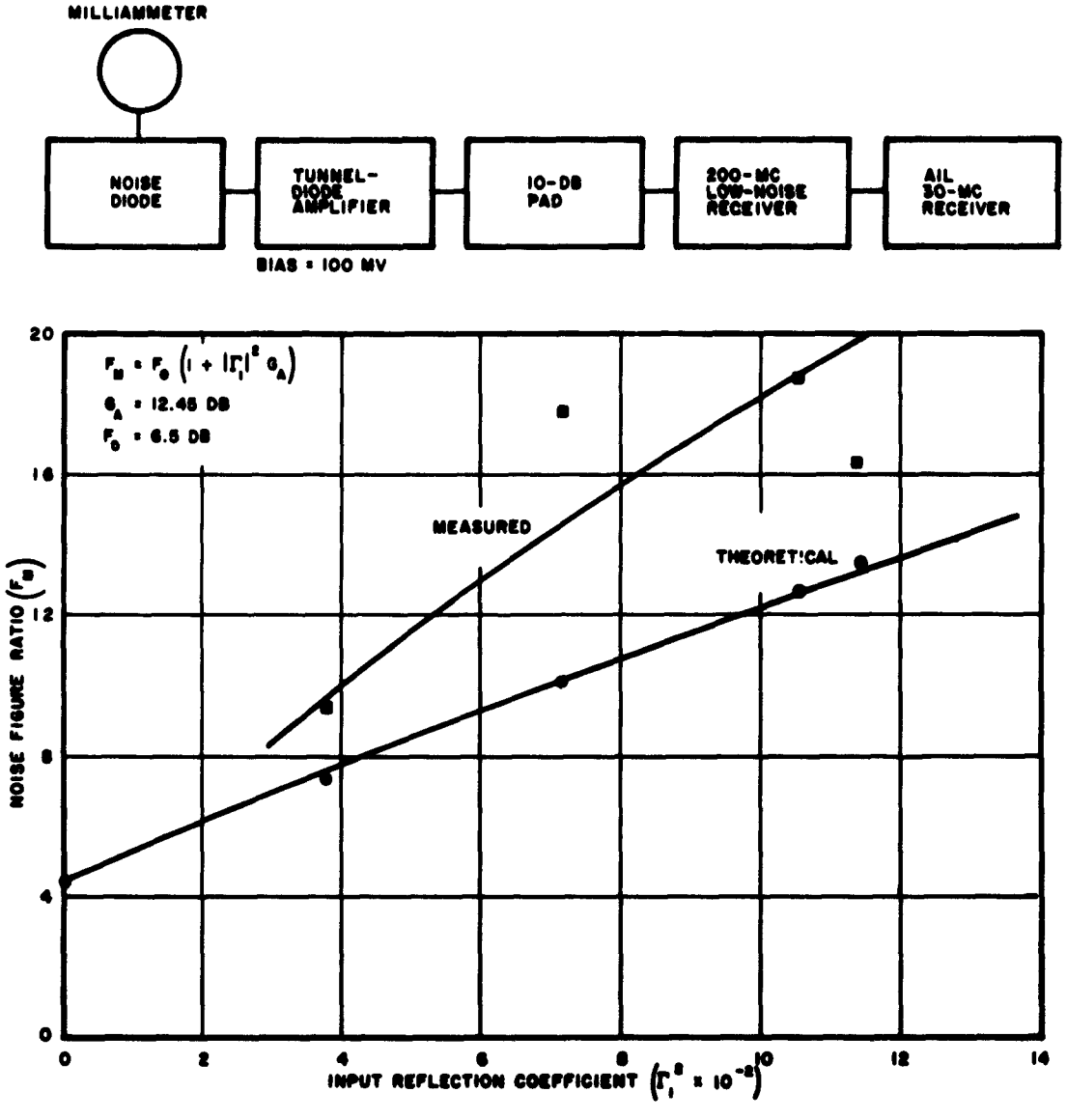

FIGURE 4-11. NOISE FIGURE VS INPUT REFLECTION COEFFICIENT FOR HYBRID-COUPLED AMPLIFIER

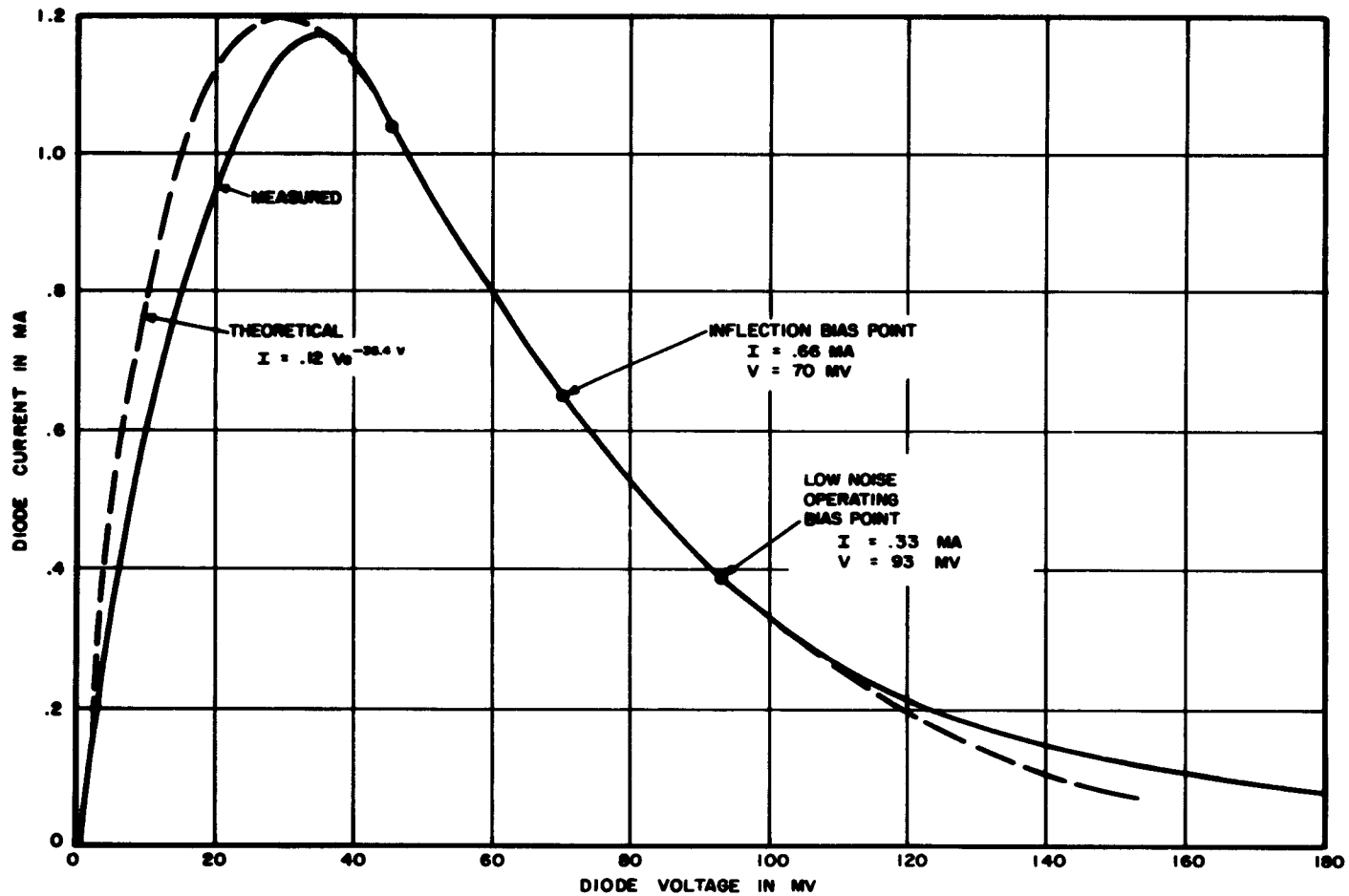

FIGURE 4-12. TUNNEL-DIODE MS233 i-v CHARACTERISTIC

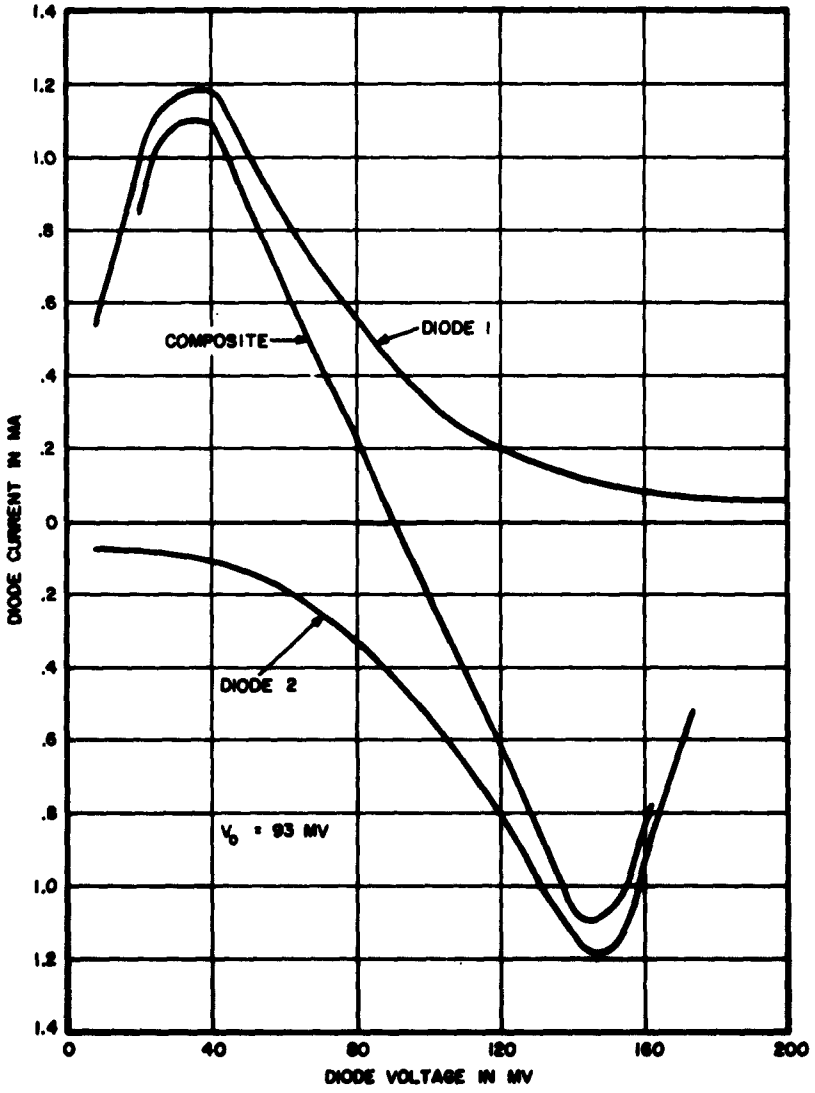

FIGURE 4-13. TUNNEL-DIODE MS233 COMPOSITE 1-v CHARACTERISTIC

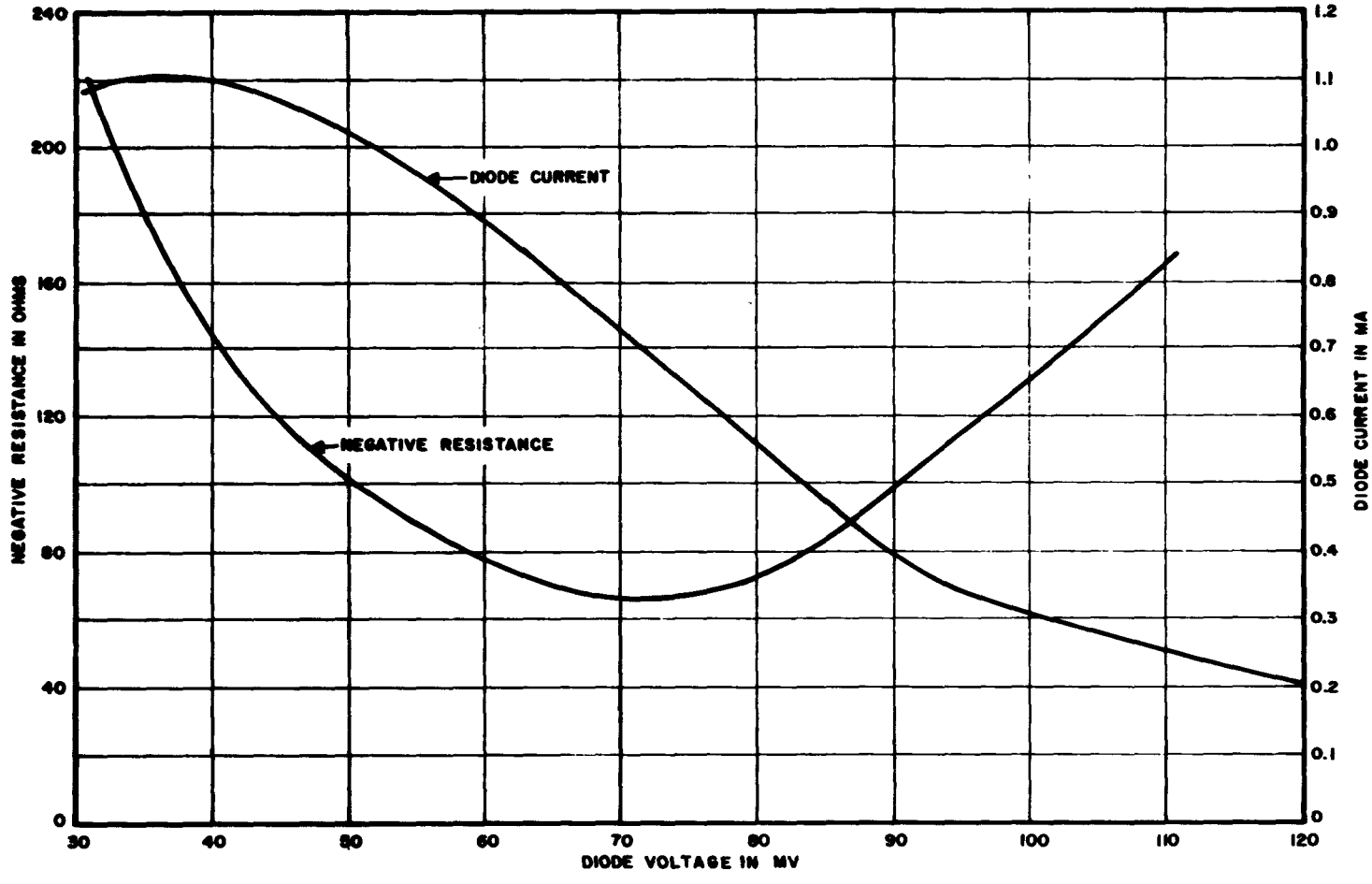

FIGURE 4-14. TUNNEL-DIODE MS233 NEGATIVE RESISTANCE

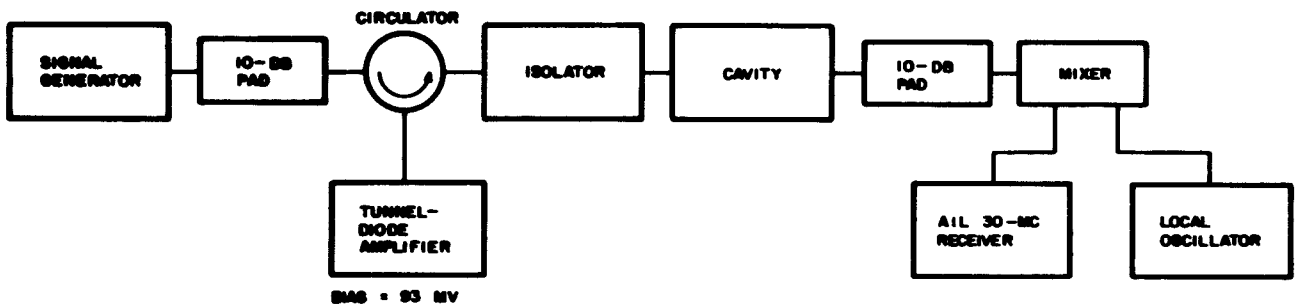

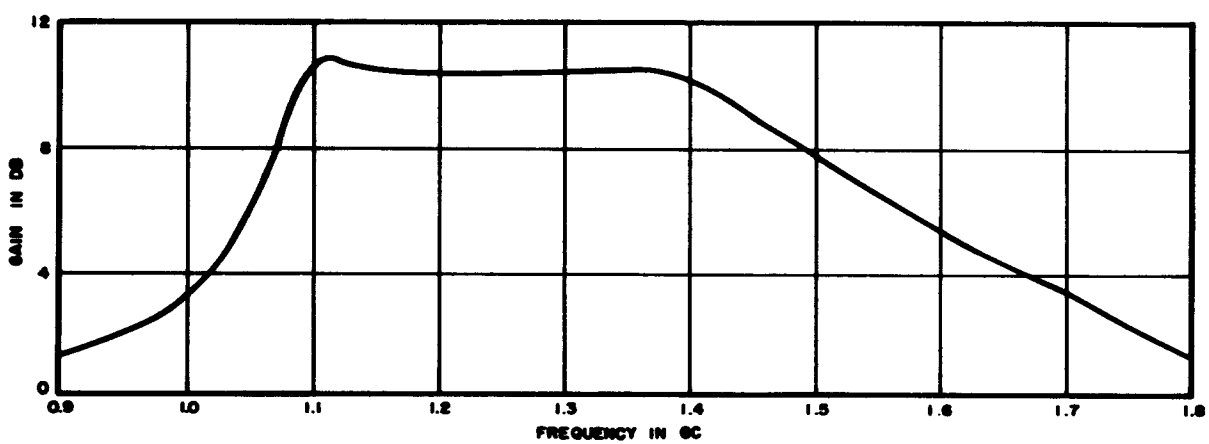

FIGURE 4-15. GAIN VS FREQUENCY OF BALANCED AMPLIFIER

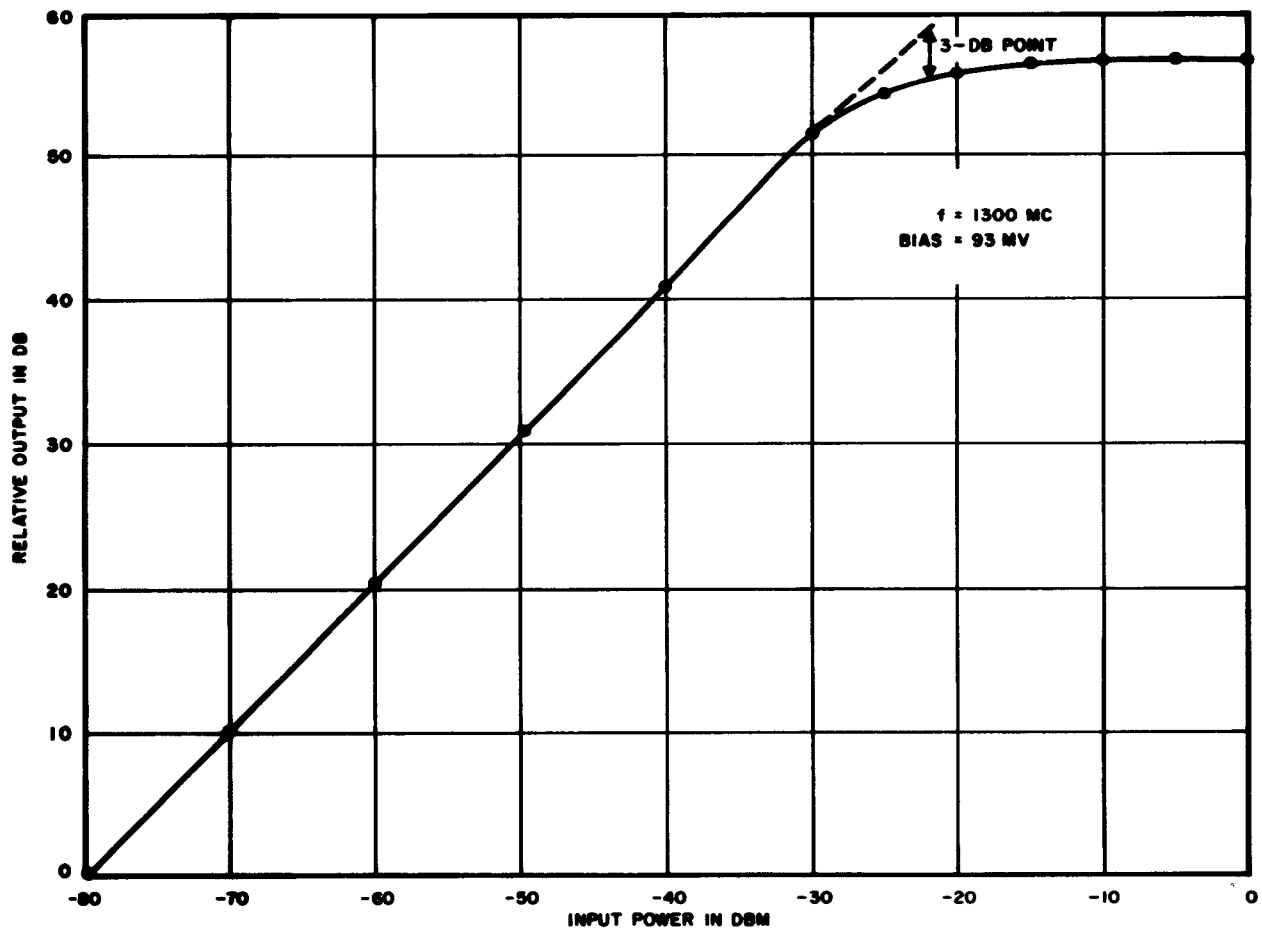

FIGURE 4-16. POWER TRANSFER CHARACTERISTIC OF BALANCED AMPLIFIER

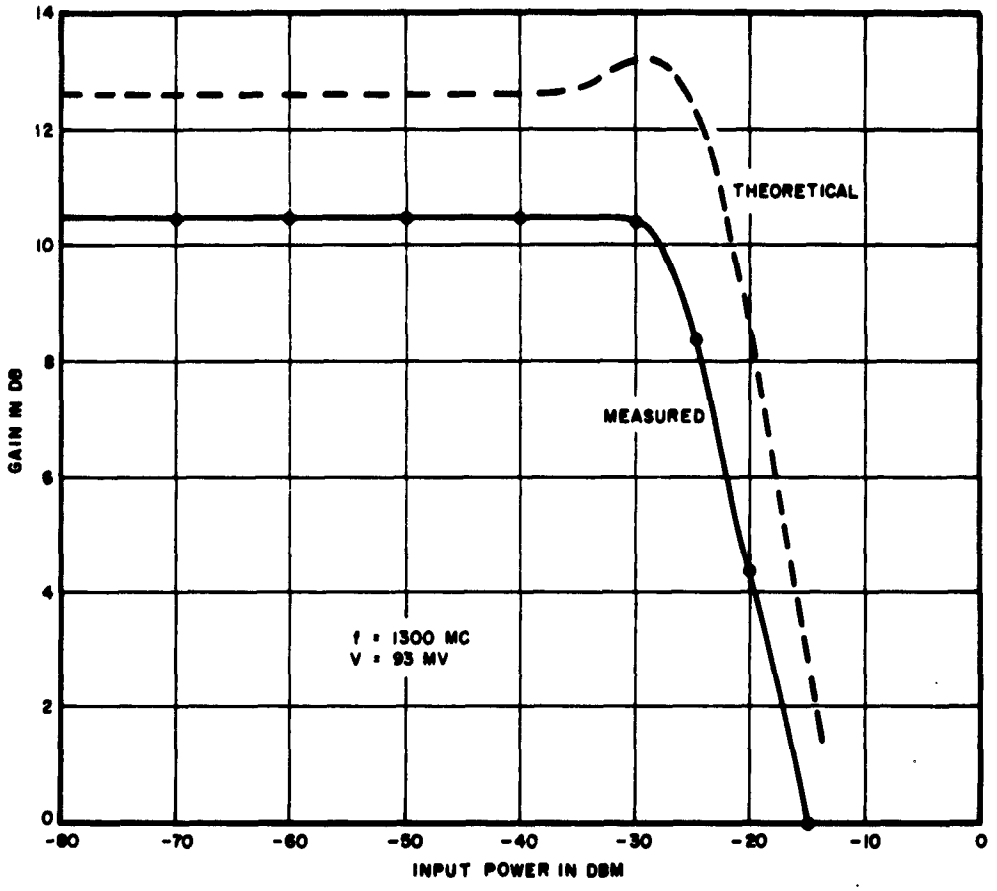

FIGURE 4-17. GAIN VS INPUT POWER FOR BALANCED TUNNEL-DIODE AMPLIFIER

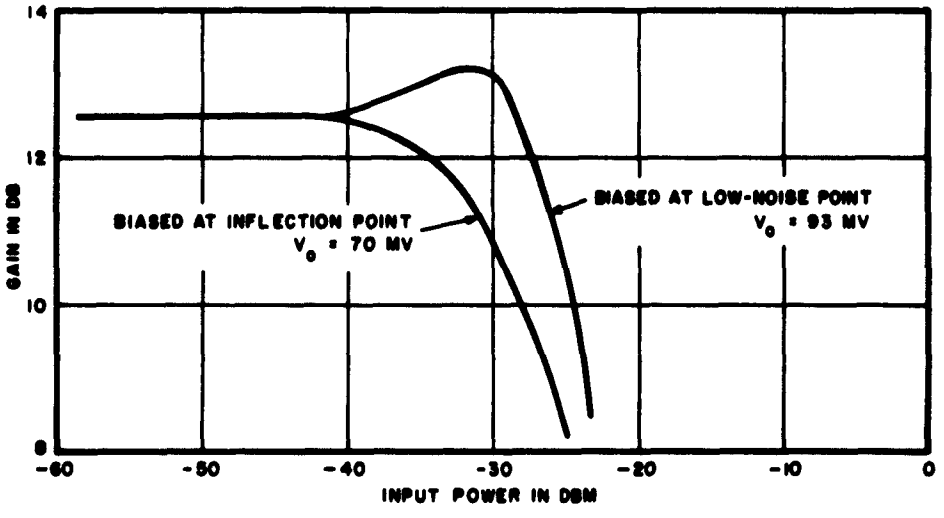

FIGURE 4-18. THEORETICAL GAIN VS INPUT POWER FOR SINGLE TUNNEL-DIODE AMPLIFIER

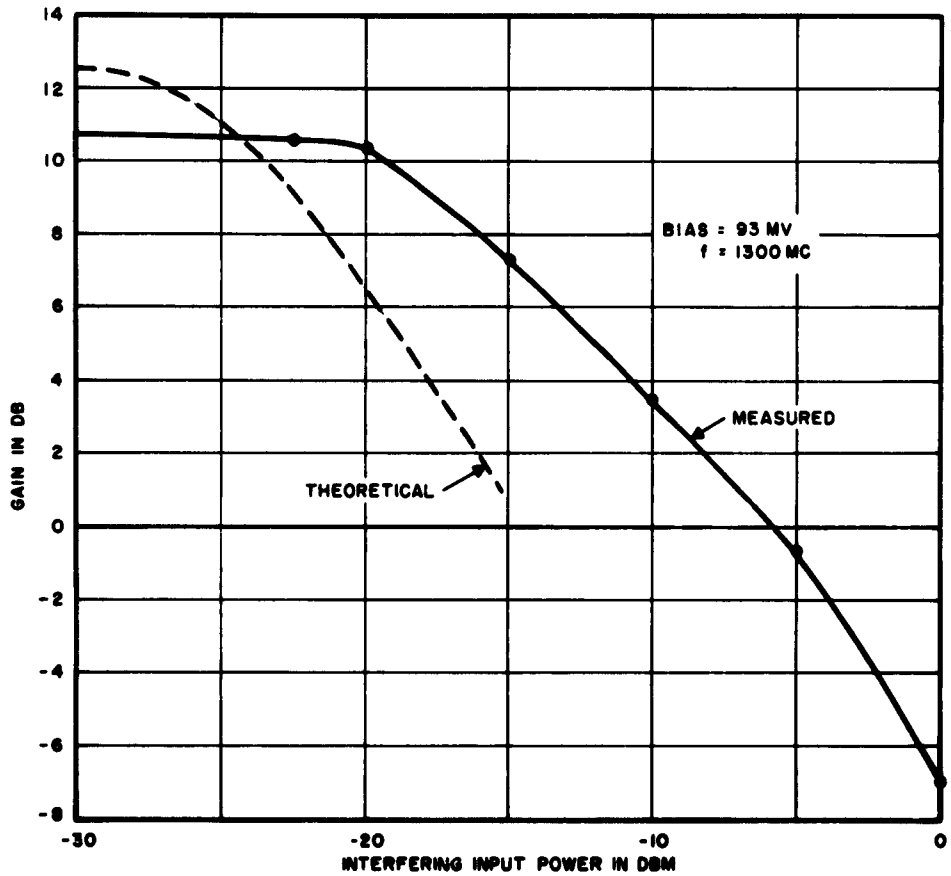

FIGURE 4-19. GAIN VS INTERFERING INPUT POWER FOR BALANCED AMPLIFIER

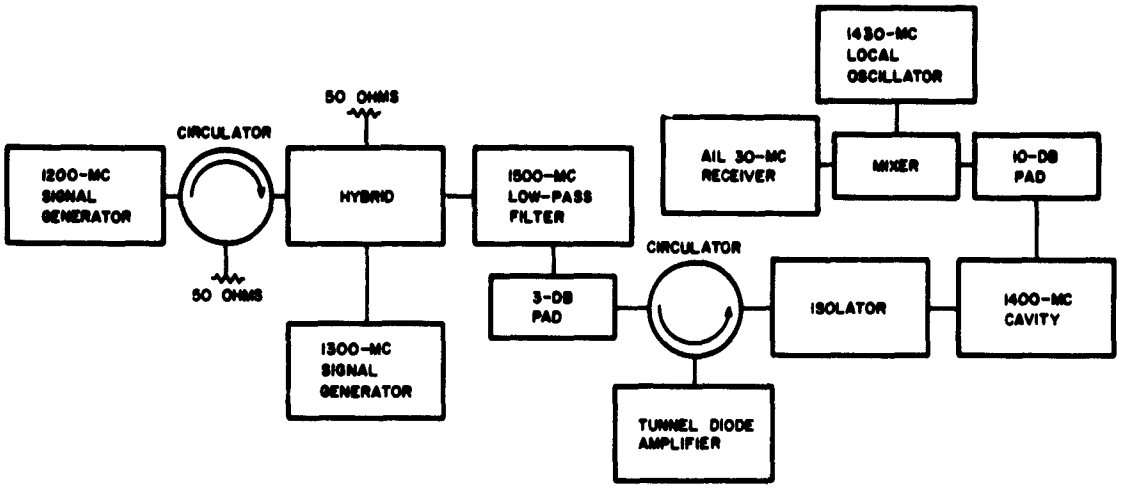

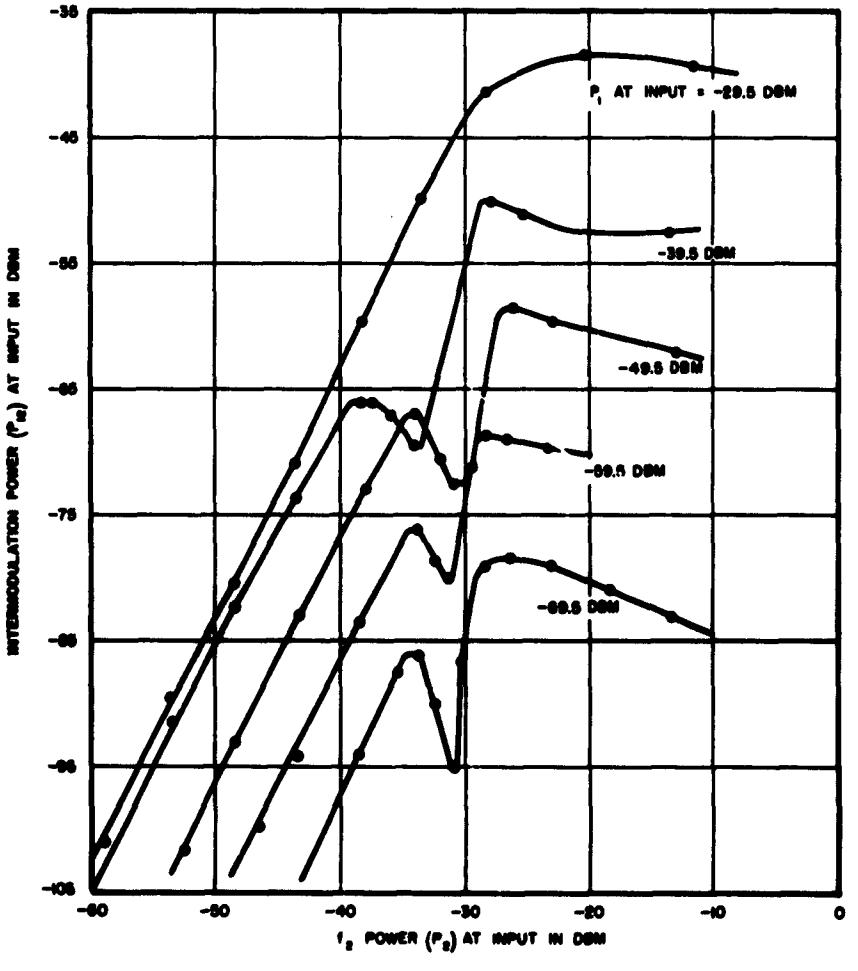

FIGURE 4-20. THIRD-ORDER INTERMODULATION VS INPUT POWER OF BALANCED AMPLIFIER

V. TRANSISTORS

The interference problems associated with transistor amplifiers pose a complex analysis problem because the nonlinear effects that arise in practice are voltage, current, and frequency dependent. Approximate relationships can be derived theoretically to predict interference output for simple transistor amplifiers. It is also possible to make certain generalizations concerning the selection of appropriate transistor types for minimum interference susceptibility.

Transistor-amplifier interference characteristics such as dynamic range, desensitization, cross modulation, intermodulation, and gain-recovery time for a low-frequency power amplifier and a high-frequency tuned amplifier are discussed in this section. The effects of transistor biasing and frequency on the interference characteristics are described.

A. THEORY

The nonlinear characteristics of transistors are produced by (reference 1): (1) the nonlinear volt-ampere characteristic of the forward-biased base-emitter function, and (2) the variations of the current-amplification factor with voltage and current. These nonlinear effects are frequency dependent because of the existence of intrinsic diffusion and barrier capacitances and parasitic elements. In general, it is an impossible task to derive the amplifier transfer function that will yield the correct levels of nonlinear output at all frequencies. However, approximate results can be found by assuming that the current amplification

factor of the transistor is constant and that the frequency dependence can be approximated by making a simple substitution in the low-frequency formulas.

Certain generalizations can be made concerning the nonlinear characteristics of high-frequency transistors that are important for low-interference operation. The simplified equivalent circuit for a high-frequency amplifier operating at $f \gg f_\beta$ is shown in Figure 5-1. For this circuit, the current gain G_i is given by:

$$G_i = \frac{i_c}{i_b} \approx \omega_t R_L C_{b'c} \left(1 + j\frac{g_m}{\omega C}\right) \tag{5-1}$$

where

$\omega_t = g_m/C_{b'e}$, the radian frequency at which $|\beta| = 1$,

$C \cong g_m R_L C_{b'c}$.

A further simplification can be made when $\omega \ll \omega_t$ because, in general, $C_{b'e} > C$ and thus, $g_m/\omega C > \omega_t/\omega > 1$. This gives:

$$G_i \approx \omega_t/\omega = f_t/f \tag{5-2}$$

Equation 5-2 shows the gain as a function of f_t. Since f_t is a function of voltage and current, it is an important reason for nonlinearity in a high-frequency transistor amplifier. The other important reason for nonlinearity for non-current-source drivers is the base current i_b variation, which is approximately an exponential function of the applied voltage.

The gain-bandwidth product, f_t, is an important parameter for high-frequency transistors and its value is

usually given by the manufacturer at some value of bias voltage and current. According to equation 5-1, the value of f_t is independent of current because both g_m and $C_{b'e}$ are proportional to current. But, in references 11, 12, and 13 it is shown that f_t is a function of voltage and current, and that for drift transistors (all high-frequency transistors are variations of this type) f_t increases at first with current until it reaches a maximum value for some value of current and then decreases with higher current. Reference 13 shows that under large-signal high-frequency conditions, the base resistance $r_{bb'}$ may be decreased and this, in turn, changes the value of f_t.

The variation of f_t is similar to that of the low-frequency current-amplification factor β_o. In low-frequency amplifiers, it is desirable from an interference standpoint to choose a transistor that has a "flat β_o" over the desired output-signal range. Likewise in high-frequency amplifiers it is also desirable to choose a transistor type (MADT, mesa, epitaxial, planar, etc.) that displays a "flat f_t" over the desired output-signal range. Although it is not standard practice, some manufacturers give the typical variation of f_t with bias for their high-frequency transistors. If this information is not available, then it can be calculated from the measurement of the high-frequency current-amplification factor with a high-frequency bridge.

The following discussion gives the relationships derived in reference 1 for desensitization, cross modulation, and intermodulation in the active region of the amplifier (linear region). These relationships were derived considering that the transfer characteristic is given by a linearized exponential function, which is then approximated by a finite power-series expansion. An alternate method for calculating the nonlinear output is presented in Appendix II. This

alternate method assumes that the transfer characteristic is given by a pure exponential function; thus, it neglects the linearizing effect of the input-circuit resistance. The advantage over the power-series approximation is that the output signal is given exactly in closed-form solution. However, the pure exponential function is in theory a poorer approximation of the transfer characteristic than the linearized exponential function.

1. DYNAMIC RANGE AND DESENSITIZATION

The dynamic range of an amplifier is defined as that portion of the input-signal range over which the gain does not change by more than 1 db from its small-signal value. The smallest signal that can be linearly amplified is a few db above the amplifier-generated noise level. The largest signal nominally drives the transistor to saturation or cutoff; its value can be calculated from the bias point and output circuit configuration of the amplifier. Higher-level signals are said to be in the saturation region of the amplifier.

The saturation output level is calculated by representing the amplifier output circuit as shown in Figure 2A. The output impedance of the transistor is inside block A. The collector current $i_{c_{max}}$ is the maximum undistorted sinusoidal current that can flow in the transistor. For example, the value of $i_{c_{max}}$ can be obtained from DC and AC load lines for the amplifier (Figure 2B). It is assumed that the AC load is resistive. The peak positive current is $i^{+}_{c_{max}} = V_{ce}/R_{ac}$ and the peak negative current is $i^{-}_{c_{max}} = I_c$. The peak value of the maximum possible symmetrical swing is the smaller of $i^{+}_{c_{max}}$ and $i^{-}_{c_{max}}$ as shown in Table 5-I.

TABLE 5-I

VALUES OF $i_{c_{max}}$

$i_{c_{max}}$	Condition
I_c	$I_C < V_{ce}/R_{ac}$
V_{ce}/R_{ac}	$I_C > V_{ce}/R_{ac}$

For maximum dynamic range, I_c must equal V_{ce}/R_{ac}. In low-level high-frequency amplifiers, I_c is usually less than 5 ma, and V_{ce}/R_{ac} is usually above 5 ma. Thus, $i_{c_{max}} = I_c$ and maximum dynamic range is not obtained. After the value of $i_{c_{max}}$ has been determined, the output power at which the amplifier saturates is given by:

$$P_{sat} = \frac{(A\ i_{c_{max}})^2}{2} R_L \tag{5-3}$$

As shown in reference 1, when two signals are applied to an amplifier (a low-level desired signal and a high-level interfering signal), the interfering signal reduces the output of the desired signal. This loss of gain for small signals is called desensitization and for two continuous-wave signals the desensitization is approximately equal to the loss of gain caused by saturation. Thus, when the interfering-signal level is at the upper limit of the dynamic range, the desensitization is about 1 db.

For other types of interfering waveforms, the value of desensitization is a matter of definition. Desensitization can be defined as the loss of average-power gain. For example, for a continuous-wave low-level signal and a 100 percent square-wave-modulated saturating signal, the desensitization (assuming zero gain-recovery time) for average power can not exceed 3 db.

For two continuous-wave input signals p_1 and p_2 (and $p_1 \gg p_2$), the current desensitization D_i in the active region (linear region) is (reference 1):

$$\begin{aligned} D_i &\approx 1 + 12\ R_g \frac{a_3}{a_1} p_2 \\ D &= 20 \log D_i \end{aligned} \tag{5-4}$$

where

D = desensitization in db,

p_1 = available interfering power at the input (power delivered to the amplifier if its input impedance $Z_i = R_g$),

R_g = interfering-signal source impedance,

a_1 and a_3 = first- and third-order curvatures of the transfer characteristic in the active region of the amplifier.

In the low-frequency range of a common-emitter amplifier where all transistor and external reactances in the input circuit of the amplifier can be neglected, the terms a_1 and a_3 are given by (reference 1):

$$a_1 = \frac{1}{R + r_{b'e}} \tag{5-5}$$

$$a_3 = \frac{1 - 2R/r_{b'e}}{6V_t^2\, r_{b'e}(1 + R/r_{b'e})^5} \tag{5-6}$$

where

I_b = base bias current,

I_c = collector bias current,

β_o = low-frequency current amplification factor of common emitter stage,

$V_t = \frac{KT}{q}$, thermal-junction voltage (about 25 mv at room temperature,

$r_{b'e} = \frac{V_t}{I_b} = \frac{\beta_o V_t}{I_c}$, the dynamic resistance of the forward-biased base-emitter junction,

$R = R_g + r_{bb'}$,

$r_{bb'}$ = extrinsic base resistance of transistor.

Equation 5-4 is obtained from a power-series approximation of the transfer characteristic; it neglects the higher-order curvature terms of the transfer characteristic.

The resistance $r_{b'e}$ in equations 5-5 and 5-6 approximates the transistor nonlinearity at mid-band frequencies. In a high-frequency amplifier, operating at frequencies where transistor capacitances must be considered, the transistor nonlinearity can no longer be approximated by a resistance. Instead it can be approximated by a complex impedance $Z_{b'e}$ given by the parallel combination of $r_{b'e}$ and the capacitance $C_{b'e}$ (Figure 5-3). Thus,

$$Z_{b'e} = \frac{r_{b'e} \times \frac{1}{j\omega C_{b'e}}}{r_{b'e} + \frac{1}{j\omega C_{b'e}}} = \frac{r_{b'e}}{1 + jf/f_\beta} \tag{5-7}$$

where $f_\beta = \frac{1}{2\pi r_{b'e} C_{b'e}}$, the β-cutoff frequency of the transistor. The capacitance $C_{b'e}$ and the resistance $r_{b'e}$ have a similar exponential dependence upon the intrinsic junction voltage $v_{b'e}$ that is given by:

$$\begin{aligned} r_{b'e} &\propto \exp -(v_{b'e}/V_t) \\ C_{b'e} &\propto \exp (v_{b'e}/V_t) \end{aligned} \tag{5-8}$$

At frequencies $f \gg f_\beta$, $\omega r_{b'e} C_{b'e} \gg 1$, and $Z_{b'e}$ can be simplified to:

$$Z_{b'e} \approx -j\beta r_e \tag{5-9}$$

where

$r_e = \frac{26}{I_e \text{ in ma}}$ in ohms,

$\beta = \beta_o f_\beta / f$, high-frequency magnitude of β_o,

I_e = emitter bias current.

At high frequencies, a first-order approximation of desensitization can be calculated by substituting $|Z_{b'e}|$ for $r_{b'e}$ in equations 5-5 and 5-6.

2. CROSS MODULATION

Cross modulation is the transfer of modulation from one signal to a second signal as a result of the nonlinear transfer characteristic of the active element that processes the two signals. When a low-level CW signal and a high-level modulated interfering signal are applied to an amplifier, the percent of cross modulation k is defined by:

$$k = 100\ m_k/m_i \tag{5-10}$$

where

m_k = modulation index acquired by the CW signal through nonlinear action,

m_i = modulation index of the interfering signal.

As shown in reference 1, the output cross-modulation voltage in the active region is approximately proportional to the interfering input power. The proportionality constant depends on the interfering-signal waveshape. When the interfering signal is 100-percent square-wave modulated, the cross modulation k is related to the current desensitization D_i as follows:

$$k = \left|\frac{1 - D_i}{1 + D_i}\right| \times 100 \text{ percent} \tag{5-11}$$

$$k \approx \frac{6R_g \frac{a_3}{a_1} p_i}{1 + 6R_g \frac{a_3}{a_1} p_i} \times 100 \text{ percent} \tag{5-12}$$

A plot of the theoretical k (equation 5-11) as a function of desensitization is shown in Figure 5-4.

Equation 5-12 assumes that the emitter-to-ground impedance of the amplifier is negligible at RF and the modulation frequencies. The equations when the emitter-to-ground impedance is not negligible at modulation frequencies, are given in Section V of reference 1.

The variation of k with bias current (for constant p_1) is shown in Figure 5-5. The coordinates of the critical points, the minimum and maximum values on the curve, depend on the value of the emitter-to-ground impedance at modulation frequencies. For negligible emitter impedance, the zero occurs for:

$$I_{c_{min}} = \frac{13\beta}{R_g + r_{bb}} \qquad (5\text{-}13)$$

3. INTERMODULATION

The n-order intermodulation output of a nonlinear device at $f = af_1 \pm bf_2$ is given approximately by $P_{ab} = K_{ab} P_1^a P_2^b$ where P_1 and P_2 are the output powers for two CW input signals at frequencies f_1 and f_2--$(a + b = n)$. K_{ab} is a constant only for a particular amplifier using a particular transistor, and specified source and load resistances. The most important practical case of interference in narrow-band amplifiers caused by intermodulation is third-order intermodulation. Second-order intermodulation and higher-order intermodulation are of concern in wide-band amplifiers.

The second-order intermodulation output is given in dbw as follows:

$$P_{11} = P_1 + P_2 + K_2 \quad (f_1 \pm f_2) \text{ component} \qquad (5\text{-}14)$$

where $K_{11} = K_2$, and P_1, P_2, and K_2 are in dbw.

From reference 1, for a common-emitter amplifier at mid-band frequencies, K_2 is given by:

$$K_2 = \frac{2R_g}{G}\left[\frac{1}{V_t(1 + R/r_{b'e})^2}\right]^2 \tag{5-15}$$

where G = amplifier power gain.

The third-order intermodulation output is given in dbw as follows:

$$\begin{aligned} P_{21} &= 2P_1 + P_2 + K_3 \qquad (2f_1 - f_2) \text{ component} \\ P_{12} &= P_1 + 2P_2 + K_3 \qquad (2f_2 - f_1) \text{ component} \end{aligned} \tag{5-16}$$

where $K_3 = K_{21} = K_{12}$, and P_1, P_2, and K_3 are in dbw. From reference 1, K_3 is given by:

$$K_3 = \left(\frac{R_g}{G}\right)^2\left[\frac{1 - 2R/r_{b'e}}{V_t^2\,(1 + R/r_{b'e})^4}\right]^2 \tag{5-17}$$

Equations 5-15 and 5-17 are derived from the mid-band equivalent circuit for the amplifier shown in Figure 5-6. This equivalent circuit shows a nonlinear current source that approximates the transistor nonlinearity in the frequency range where all transistor reactances can be neglected.

At high frequencies, a first-order approximation of K_2 and K_3 can be calculated by substituting $|Z_{b'e}|$ for $r_{b'e}$ (from either equation 5-7 or 5-9) into equations 5-15 and 5-17. G is calculated from the equivalent circuit of Figure 5-3, and its value for $f \gg f_\beta$ is given by:

$$G \approx \frac{4R_LR_g}{r_e^2 + (\omega C_{b'c}R_LR + R/\beta)^2} \tag{5-18}$$

4. GAIN-RECOVERY TIME

The gain-recovery time is the length of time required for the gain of the amplifier to return to its normal value after an interfering signal is removed. The gain-recovery time is composed of transistor storage-time effects and transient effects caused by external circuits. These effects should be minimized to minimize gain-recovery time. The storage time is zero for input signals below saturation and increases with input signals above saturation. Storage time effects cause pulse-stretching at the output. In turn, the stretched pulse can suppress either partially or totally the response for a small signal that immediately follows the saturating signal.

Storage time can be minimized by choosing a transistor with a large gain-bandwidth product, f_t, because the storage time is inversely proportional to f_t.

B. EXPERIMENT

1. PROCEDURES AND TEST SETUP

The basic test setup for measurements using the low-frequency power amplifier is shown in Figure 5-7. The summing network is resistive and has an output impedance of 600 ohms. It provides 34 db of isolation between the two input ports and a 20-db insertion loss between input and output ports.

The wave analyzer is an extremely narrow-band voltmeter that can be tuned from 20 cps to 50 Kc. It is connected to either the input or the output of the amplifier and is used to measure the rms voltage of the frequency components of a complex signal. For dynamic range measurements the output of one generator is set at zero. Then the gain of the amplifier is measured as a function of input power by a substitution technique with the operating point as a parameter.

For desensitization and intermodulation measurements, two input signals are fed to the amplifier. The output voltage at the desired and intermodulation frequencies is then measured as a function of input power with the operating point as a parameter.

To ensure accurate measurements, the signal fed to the wave analyzer must be below its saturation level. When the wave analyzer is overloaded by a complex signal, in particular by a frequency component other than the one to which it is tuned, the voltage reading for the frequency to which the analyzer is tuned is inaccurate because of the nonlinear effects generated in the instrument.

The basic test setup for measurements using the 385-Mc amplifier is shown in Figure 5-8. The low-pass filter having a cutoff frequency of 700 Mc attenuates generator harmonics. The band-pass filter is a very narrow-band tunable frequency meter that selects the frequency component to be measured. The selected frequency is heterodyned down to 30 Mc by the local oscillator and mixer. The AIL 30-Mc receiver is a highly sensitive receiver that incorporates a precision attenuator to permit accurate power measurements. The 1-kc meter is a narrow-band VTVM tuned to 1 kc. The two 10-db pads ensure a source and load impedance of 50 ohms for the amplifier.

To measure amplifier output power, the reading on the AIL receiver is calibrated with a signal applied to the 10-db pad that serves as the amplifier load. For the measurements presented in this series of experiments, a reading of 0 db was set on the AIL receiver for a signal 6 db above the noise level.

The procedures used for dynamic range, desensitization, and intermodulation measurements at high frequency were similar to those used at low frequency. Desensitization and

intermodulation were measured as a function of input power with the operating point as a parameter. CW input signals were fed to the amplifier.

For cross-modulation measurements, the desired signal is CW and the interfering signal is 100-percent square-wave modulated at 1 kc. An initial calibration is made to relate the voltage reading on the 1-kc meter to the corresponding percent of cross modulation. The calibration procedure consists of setting a convenient reference reading on the 1-kc meter, which corresponds to 100 percent cross modulation, by using a 100-percent square-wave-modulated signal at the desired signal frequency that has the same average amplitude as the CW desired signal used for the cross-modulation measurement. After the calibration is made, the transistor-generated cross modulation can be read directly on the 1-kc meter in db down from 100 percent.

To ensure accurate measurements, the signal fed to the mixer must be below the saturation level of the mixer. If the mixer is overloaded, the output reading for the frequency component that is being measured is inaccurate. In addition, the mixer will generate a family of spurious responses that can inadvertently be ascribed to the amplifier.

2. LOW-FREQUENCY POWER AMPLIFIER

The interference characteristics were measured for the one-stage common-emitter power amplifier shown in Figure 5-9. The transistor used was a 2N1046 (alloy-diffused type), which has a 30-watt dissipation rating and a typical gain-bandwidth product of 20 Mc. The extrinsic base resistance has a nominal value of 0.3 ohm. The effective source resistance for the amplifier is 300 ohms and the load resistance is 10 ohms. The small-signal characteristics of the amplifier are shown in Figure 5-10.

a. SATURATION

The saturation characteristics of the amplifier are shown in Figure 5-11. The saturation characteristics show the variation of gain as a function of input power.

Table 5-II shows the measured saturation output levels for several values of bias current and the corresponding levels calculated by using equation 5-3. In the calculations, the output impedance of the transistor is considered much larger than 10 ohms. It is seen that the calculated values are within 3 db of the measured values.

TABLE 5-II
SATURATION OUTPUT POWERS

I_c in amperes	0.50	0.75	1.0
Measured saturation output power (gain down 1 db) in dbm	33.4	37.3	38.6
Calculated saturation output power in dbm	31	34.5	37

According to equation 5-3, the dynamic range should increase 6 db when the bias current is doubled. The dynamic range measurements show an increase of 5.2 db when the current is increased from 0.5 to 1 ampere. The 0.8-db error is within the allowable accuracy of the experimental test setup.

b. DESENSITIZATION

The desensitization characteristics of the amplifier are shown in Figure 5-12. The frequency of the small signal is 6 kc; desensitization for interfering signals at 40 kc and at 80 kc is measured. The measurements show that for a given desensitization, the output power at 80 kc is about 1 db higher than the output at 40 kc. In addition, the interfering output for 1 db desensitization is approximately equal to the interfering output for a 1-db loss of gain caused by saturation.

c. INTERMODULATION

Figures 5-13, 5-14, and 5-15 show the intermodulation characteristics of the amplifier. For the audio-amplifier discussed in this section, the second-, third-, and some higher-order intermodulation products are potential sources of interference because of the wide-band characteristics of the amplifier.

Figure 5-13, shows curves for second- and third-order intermodulation outputs as a function of the desired signal output. However, an examination of intermodulation-output variations before the data was recorded showed that both second- and third-order intermodulation follow the predicted relationships $P_{11} = P_1 + P_2 + K_2$ and $P_{21} = 2P_1 + P_2 + K_3$ for outputs much lower than the saturation level. The P_{21} output deviates considerably from this relationship for desired output levels that are less than 15 db below saturation. The P_{11} output follows the predicted law at least up to 10 db below saturation. The value of K_3 for the region where P_{21} follows the predicted variation can be determined from the curve in Figure 5-13 as follows:

$$P_1 = 10 \text{ dbm} = -20 \text{ dbw}$$

$$P_2 = 23 \text{ dbm} = -7 \text{ dbw}$$

$$P_{21} = -48 \text{ dbm} = -78 \text{ dbw}$$

$$K_3 = P_{21} - 2P_1 - P_2 = -78 + 40 + 7 = -31 \text{ dbw}$$

The value of K_2 can also be determined from the curves in Figure 5-13 as follows:

$$P_1 = 10 \text{ dbm} = -20 \text{ dbw}$$

$$P_2 = 23 \text{ dbm} = -7 \text{ dbw}$$

$$P_{11} = -37 \text{ dbm} = -67 \text{ dbw}$$

$$K_2 = P_{11} - P_1 - P_2 = -67 + 20 + 7 = -40 \text{ dbw}$$

The values of K_2 and K_3 were calculated using equations 5-15 and 5-17 (power series approximation) and equation II-15 of Appendix II (exponential approximation). The values are compared in Table 5-III. The calculated values are in poor agreement with the measured values.

TABLE 5-III

K_2 AND K_3 FOR LOW-FREQUENCY POWER AMPLIFIER

I_c = 1 amp, V_{ce} = -10 volts	K_2 (dbw)	K_3 (dbw)
Measured	-40	-31
Calculated (series approximation)	-57.5	-69
Calculated (exponential approximation)	-18.1	-41.2

Table 5-III shows that K_2 and K_3 are negative constants and are therefore much lower than 1 watt. Thus, the intermodulation constants for this amplifier are much lower than the corresponding constants reported elsewhere in this report for the high-frequency amplifier and for other amplifiers described in reference 1.

Figure 5-14 shows the intermodulation output for the amplifier as a function of frequency. Input-signal frequencies f_1 and f_2 were varied over a wide range inside the pass band of the amplifier. The output powers P_1 (at f_1) and P_2 (at f_2) were kept constant for all frequencies and the variation of second- and third-order intermodulation output was measured. The variation of the intermodulation output is the variation of K_2 and K_3 with frequency since the signal output was kept constant. According to equations 5-15 and 5-17, the frequency dependence of K_2 and K_3 is related to the frequency dependence of the gain of the amplifier and the ratio f/f_β. Since both the gain and the ratio f/f_β vary in the pass band of the amplifier, the values of K_2 and K_3 can also be expected to vary. The measurements show a smooth variation for K_3 of

about 10 db from 500 cps to 50 kc. The variation for K_2 is not as smooth and it appears to be more dependent on the frequency pair f_1 and f_2 used for the measurement.

Figure 5-15 shows the measured intermodulation output as a function of bias current for constant inputs p_1 and p_2 and the calculated intermodulation output using the power series approximation. The calculated and measured values agree to within 13 db up to $I_C = 0.3$ ampere. For $I_C > 0.3$ ampere, the measured values show an unpredicted variation for which no explanation is known. For $I_C > 0.3$ ampere, the measured values are much larger than the calculated values.

Figure 5-15 also shows the variation in the values of measured K_3. The value of $K_{3\ min} = -68$ dbw at $I_C = 0.26$ ampere and $K_3 = -28$ dbw at $I_C = 1$ ampere.

The effect of other nonlinear elements in the amplifier could explain the difference between the measured intermodulation output and the theoretical predictions. The elements that probably have nonlinear characteristics are the large electrolytic capacitors used as input coupling and bypass capacitors. The cause of the nonlinearity is that in power amplifier applications these capacitors may operate at relatively high temperatures and may carry large values of AC. In fact, no special mounting considerations or component selection were made for the amplifier that was used in the measurements, and, thus, it is possible that high surrounding temperatures caused nonlinear effects in the electrolytic capacitors.

d. GAIN-RECOVERY

The gain-recovery characteristics of the amplifier are shown in Figure 5-16. Figure 5-16A shows the degree of pulse-stretching that results at the output when two different input-pulse levels saturate the amplifier. The pulse stretching (microseconds) is not proportional to the input-pulse amplitude. Figure 5-16B shows the output response of

the amplifier for an input signal consisting of two consecutive pulses of opposite polarity. The middle and lower traces show that the output for the second pulse is suppressed when the amplitude of the first pulse is increased above saturation.

3. HIGH-FREQUENCY TUNED AMPLIFIER

The interference characteristics were measured for the one-stage common-emitter tuned amplifier shown in Figure 5-17. The transistor used was a 2N2415 (diffused-base mesa type), which has a nominal gain-bandwidth product of 560 Mc and a nominal noise figure of 2.4 db at 200 Mc. The extrinsic base resistance $r_{bb'}$ has a nominal value of 6 ohms. The amplifier has a nominal bandwidth of 18 percent and a center frequency of 385 Mc. The source and load impedances are 50 ohms and the effective resistance "seen" by the collector of the transistor at resonance is 300 ohms. The small signal characteristics of the amplifier are shown in Figure 5-18.

a. SATURATION

The saturation characteristics of the amplifier are shown in Figure 5-19. In this figure, the calculated and measured saturation output levels are compared. The saturation levels were calculated from the bias current and the output circuit of the amplifier. In the calculations of saturation output level for each bias current, transistor output resistances were assumed to be several hundred ohms and infinite because the exact values were not known. As expected, the measured saturation levels fall between the two calculated values, and they indicate an output resistance of about 1 kilohm.

The saturation level should increase 6 db when the bias current is doubled if the output resistance of the transistor is constant. Measurements show an increase of 4 to 5 db in saturation level when the bias current is doubled in the range between 1 and 5 ma. The measured increase is lower than the theoretical increase because the output resistance of a common-emitter amplifier decreases with increasing current.

b. DESENSITIZATION

The desensitization characteristics of the amplifier are shown in Figure 5-20A. The measurements show that an increase in bias current decreases the desensitization for a given interfering input-signal level. The decrease of desensitization is caused by the increase of dynamic range produced by an increase of bias current. The curves show that the interfering input-signal level for 1 db of desensitization for a bias current of 2 ma is 5 db higher than for a bias current of 1 ma. The 5-db ratio is approximately equal to the corresponding increase of dynamic range.

Figure 5-20B compares calculated and measured values of desensitization for a bias current of 1 ma. The theoretical curve is calculated from the measured saturation characteristic. It assumes that the desensitization is equal to the loss of gain caused by saturation. The measurements, for desensitization caused by a continuous-wave or a 100-percent square-wave modulated interfering signal, show good agreement with the theoretical curve.

c. CROSS MODULATION

The cross-modulation characteristics of the amplifier are shown in Figures 5-21, 5-22, and 5-23. Figure 5-21 shows that, in the active region, the percent of cross modulation is doubled for every 3-db increase of interfering input power. This result is in agreement with the predicted value. Measurements show that for an interfering input signal that causes a 1-db loss in gain due to saturation, cross modulation is about 7 percent. If desensitization is equal to loss of gain due to saturation, the theoretical k, as shown in Figure 5-4, is 5.75 percent. Thus, measurements tend to verify that for this amplifier desensitization is approximately equal to the loss of gain due to saturation.

Figure 5-22 compares the measured relationship between cross modulation and desensitization with the theoretical relationship. In this figure, two sets of measurements are shown. One set of measurements is in better agreement with the theoretical values than the other; the largest measured deviation of cross modulation in either curve is 8 percent lower than predicted.

Figure 5-23 shows calculated and measured values of interfering input signals required for 1 percent cross modulation. Two calculated curves are shown. The first calculated curve shown in this figure uses the power-series approximation based on equations 5-3 and 5-9. Since a 100-percent square-wave-modulated interfering signal was used, equation 5-11 is used to calculate the required desensitization for 1 percent cross modulation. Then, equation 5-4 is used to obtain values of p_I for different bias currents. The values of a_1 and a_3 in equation 5-3 are calculated from equations 5-5 and 5-6 by substituting $|Z_{b'e}| = \beta r_e$ for $r_{b'e}$. A value of $\beta = 1.5$ is used for all calculations. The second calculated curve is based on an exponential approximation of the transfer characteristic. This approximation neglects the linearizing effect of source impedance R_g and extrinsic base resistance $r_{bb'}$ on the transfer characteristic, and it assumes that the voltage $v_{b'e}$ across the intrinsic base-emitter junction is proportional to the applied voltage v_g (Appendix II).

Figure 5-23 shows that, in the range from 0.8 ma to 3.0 ma, when the bias current is doubled, 5 db more interfering input power is required to produce 1-percent cross modulation. Thus, for reduced cross-modulation output, it is desirable to bias the transistor with $I_c > 1$ ma. The calculated and measured values using the power series approximation are different from the theoretical values by not more than 2 db in the range from 0.5 ma to 3 ma. The values

calculated with the exponential approximation are different from the theoretical values by not more than 8 db in the range from 0.3 ma to 3 ma. In addition, Figure 5-23 shows the variation of k with bias current for a given interfering input power. The shape of this curve shows good agreement with the theoretical curve for zero emitter impedance (Figure 5-5).

d. INTERMODULATION

Figures 5-24 and 5-25 show the intermodulation characteristics of the amplifier. Figure 5-24 shows the third-order intermodulation output P_{21} as a function of input signal p_1 at f_1 with input signal p_2 at f_2 as a parameter. The bias current is 1 ma. The curves follow the predicted relationship $P_{21} = 2P_1 + P_2 + K_3$ up to the highest input level available from the source--7 db above saturation. The value of K_3 can be determined from a sample point on the curves:

$$p_1 = p_2 = -50 \text{ dbw}$$

$$P_1 \approx P_2 = -50 + 7.7 = -42.3 \text{ dbw}$$

$$P_{21} = -82 \text{ dbw}$$

$$K_3 = P_{21} - 2P_1 - P_2 = -82 + 126.9 = 44.9 \text{ dbw}$$

The value of K_3 is calculated using equation 5-17 (the power-series approximation) and using equation II-15 (the exponential approximation) from Appendix II. The three values are compared in Table 5-IV.

In this table, the series approximation yields intermodulation levels that are 13 db higher than the measured levels, and the exponential approximation yields levels that are 9 db lower than the measured levels.

TABLE 5-IV

K_3 FOR 385-MC TUNED AMPLIFIER

Measured	44.9 dbw
Calculated (series approximation)	58.1 dbw
Calculated (exponential approximation)	35.9 dbw

Figure 5-24 also shows a curve of the fifth-order intermodulation output P_{32} at $f = 3f_1 - 2f_2$ as a function of input at f_1 and f_2, respectively. The measurement shows that P_{32} increases 4 db with each 1-db increase in p_1 for a constant value of p_2, whereas the predicted variation was a 3-db increase for each 1 db in p_1. Furthermore, a single measurement shown in Figure 5-23 verifies that P_{32} increases 2 db with each 1-db increase in p_2--in agreement with the predicted variations. According to theory, $P_{32} = 3P_1 + 2P_2 + K_{32}$ where P_1, P_2, P_{32}, and K_{32} are in dbw and the measured value of K_{32} is 102 dbw. The measured ratio $K_{32}/K_3 \cong 57$ db. Although the fifth-order intermodulation constant K_{32} is much greater than the third-order intermodulation constant K_3, the third-order intermodulation was always greater for a given set of input powers p_1 and p_2 in the active region of the amplifier. Experimentally, $P_{21}/P_{32} \gtrsim 26$ db.

Figure 5-25 shows the relative intermodulation output as a function of bias current for constant inputs p_1 and p_2.

Measurements show that for low intermodulation output it is desirable to bias the transistor with $I_c > 1$ ma since the value of K_3 decreases for higher values of bias current. For example, $K_3 = 44.9$ dbw for $I_c = 1$ ma, and $K_3 = 36$ dbw for $I_c = 2$ ma. The theoretical curve is based on the power-series approximation and measured values differ by not more than 15 db from theoretical in the range from 0.4 to 3 ma.

The predicted values of desensitization agree much better with experimental results than the predicted values of third-order intermodulation. As previously mentioned, the proposed equations for calculations of desensitization and intermodulation at high frequencies are first-order approximations; it appears that the approximation is more valid for desensitization than for intermodulation.

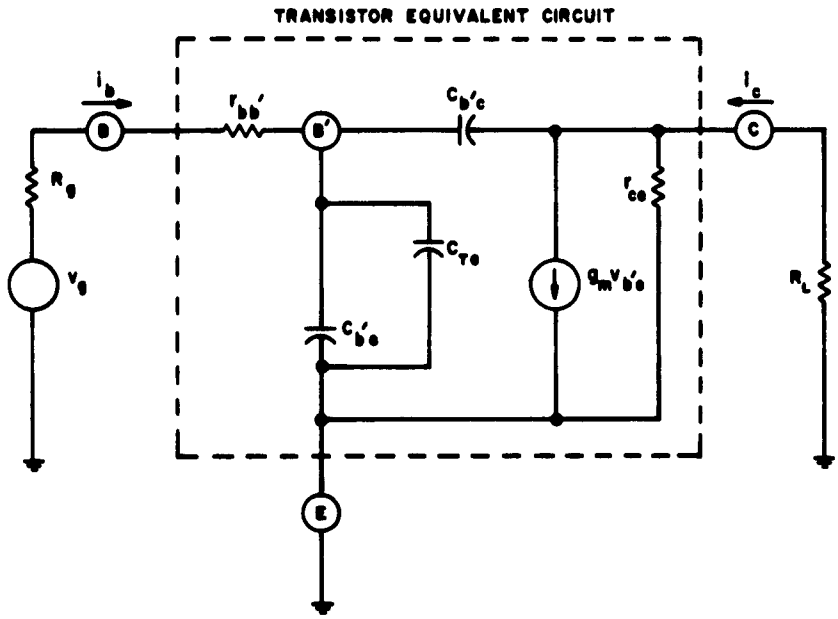

FIGURE 5-1. SIMPLIFIED EQUIVALENT CIRCUIT FOR AMPLIFIER OPERATING AT $f \gg f_\beta$

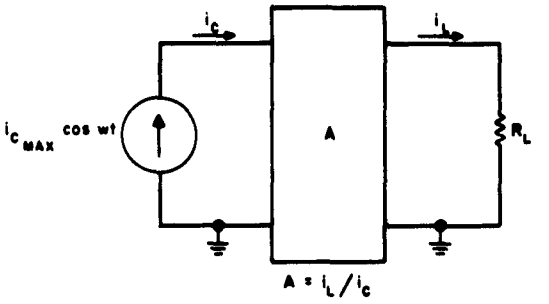

A. AMPLIFIER OUTPUT CIRCUIT FOR CALCULATING MAXIMUM OUTPUT POWER

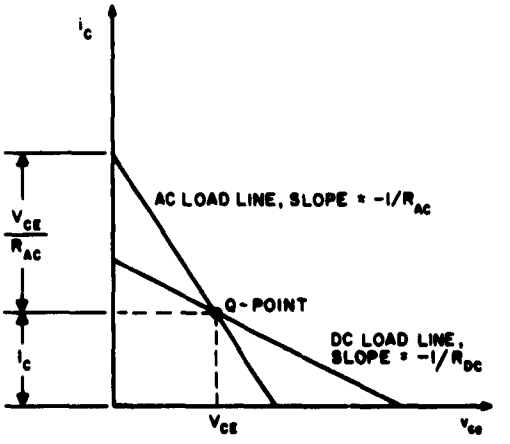

B. TYPICAL DC AND AC LOAD LINES

FIGURE 5-2. CIRCUIT USED FOR CALCULATING MAXIMUM OUTPUT POWER

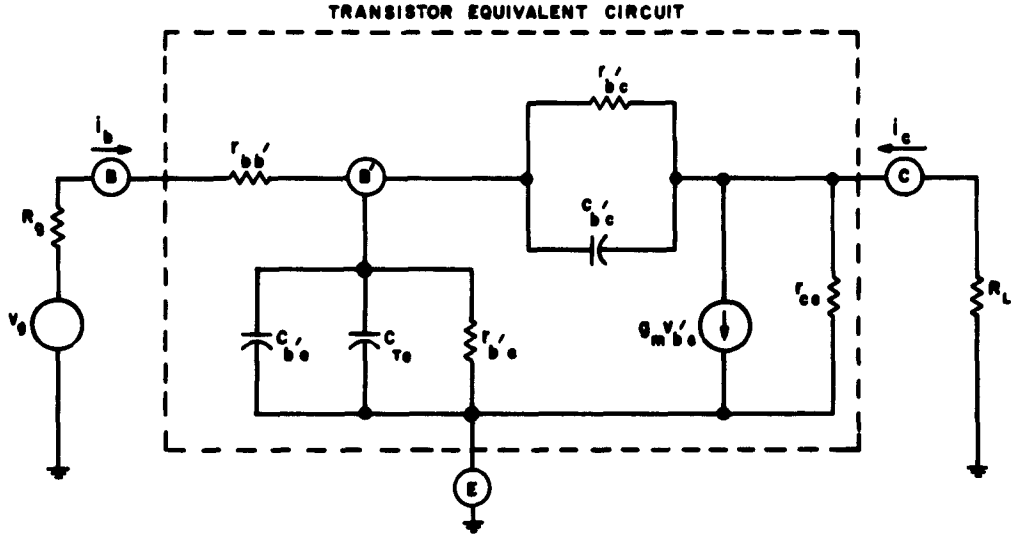

FIGURE 5-3. EQUIVALENT CIRCUIT OF COMMON-EMITTER AMPLIFIER

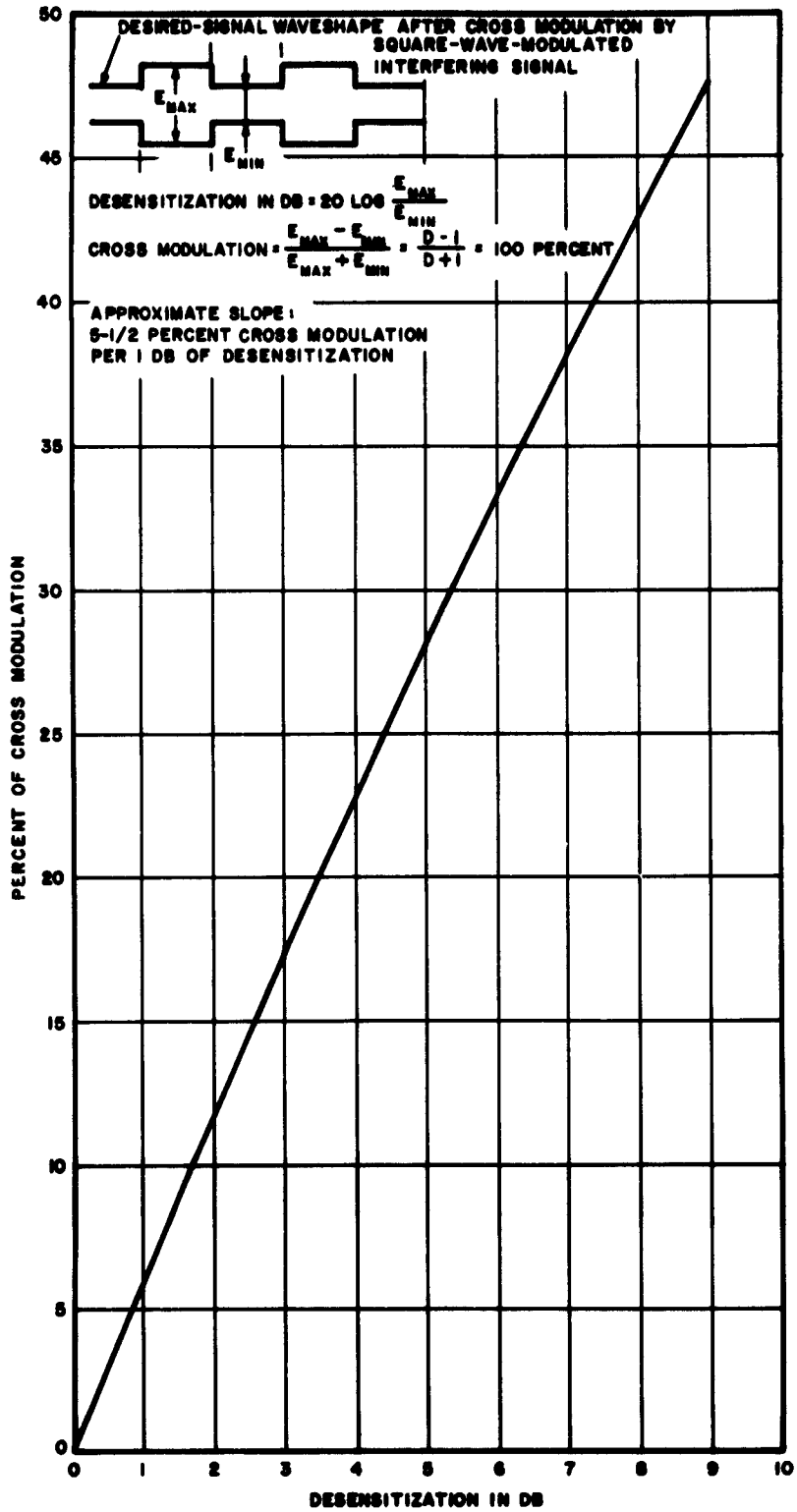

FIGURE 5-4. THEORETICAL PERCENTAGE OF CROSS MODULATION VS DESENSITIZATION

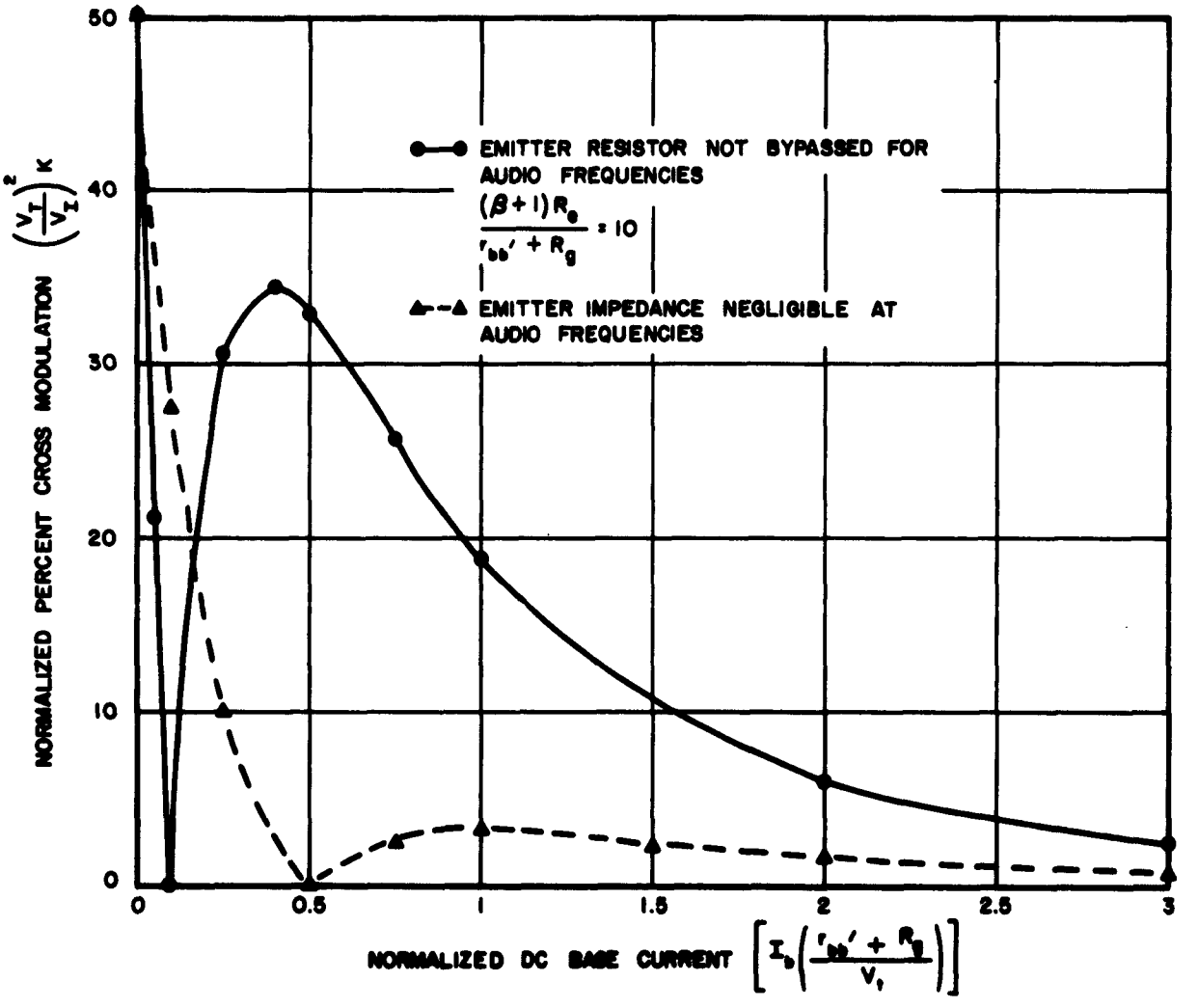

FIGURE 5-5. THEORETICAL NORMALIZED PERCENTAGE OF CROSS MODULATION VS NORMALIZED DC BASE CURRENT IN A COMMON-EMITTER TRANSISTOR AMPLIFIER

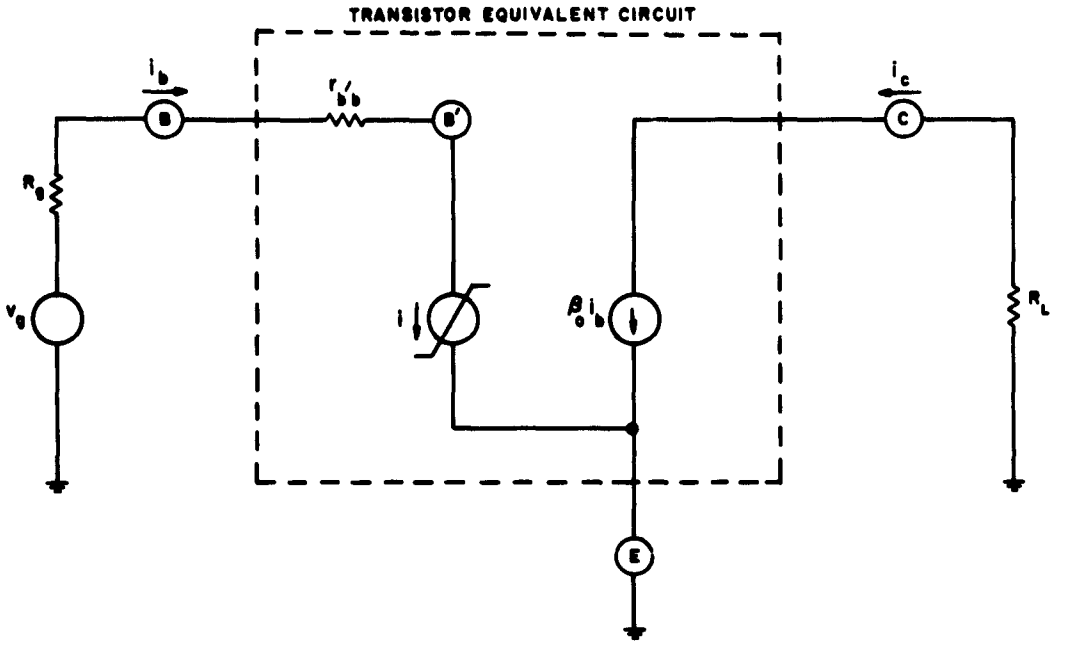

$$i_b = I_b(\exp v'_{be}/V_t - 1)$$

$$= I_b\left\{\exp\left[v_g - i_b(r_{bb'} + R_g)\right]/V_t - 1\right\}$$

$$r'_{be} = \left.\frac{d v'_{be}}{d i_b}\right|_{i_b = v'_{be} = 0}$$

FIGURE 5-6. MID-BAND EQUIVALENT CIRCUIT OF COMMON-EMITTER AMPLIFIER WITH INTERNAL NONLINEAR SOURCE

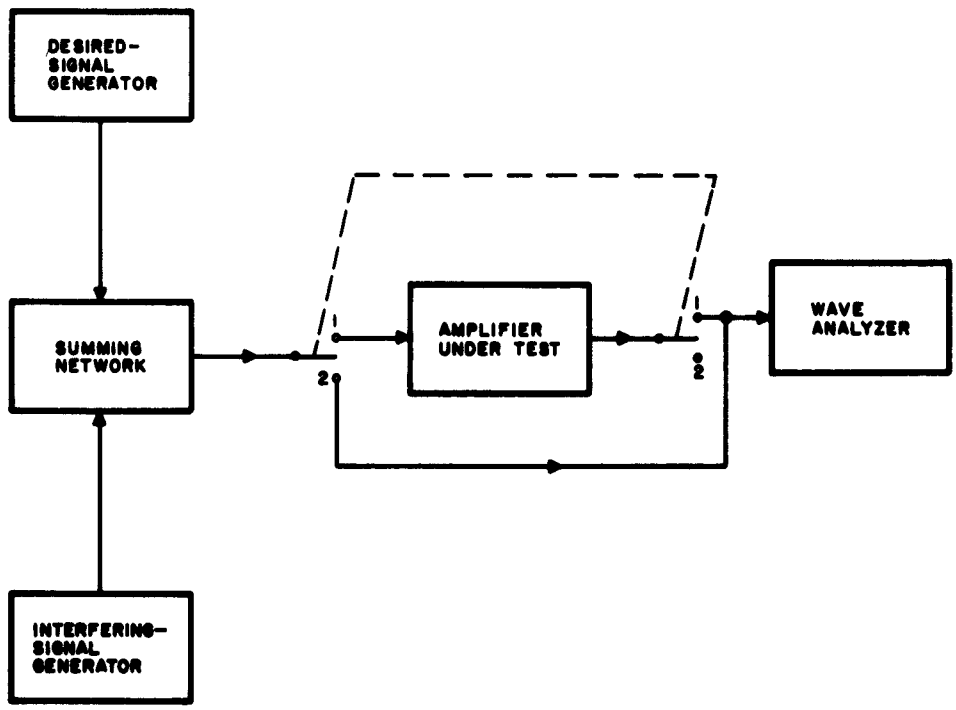

FIGURE 5-7. BLOCK DIAGRAM OF SETUP FOR MEASURING DYNAMIC RANGE, DESENSITIZATION, AND INTERMODULATION FOR LOW-FREQUENCY POWER AMPLIFIER

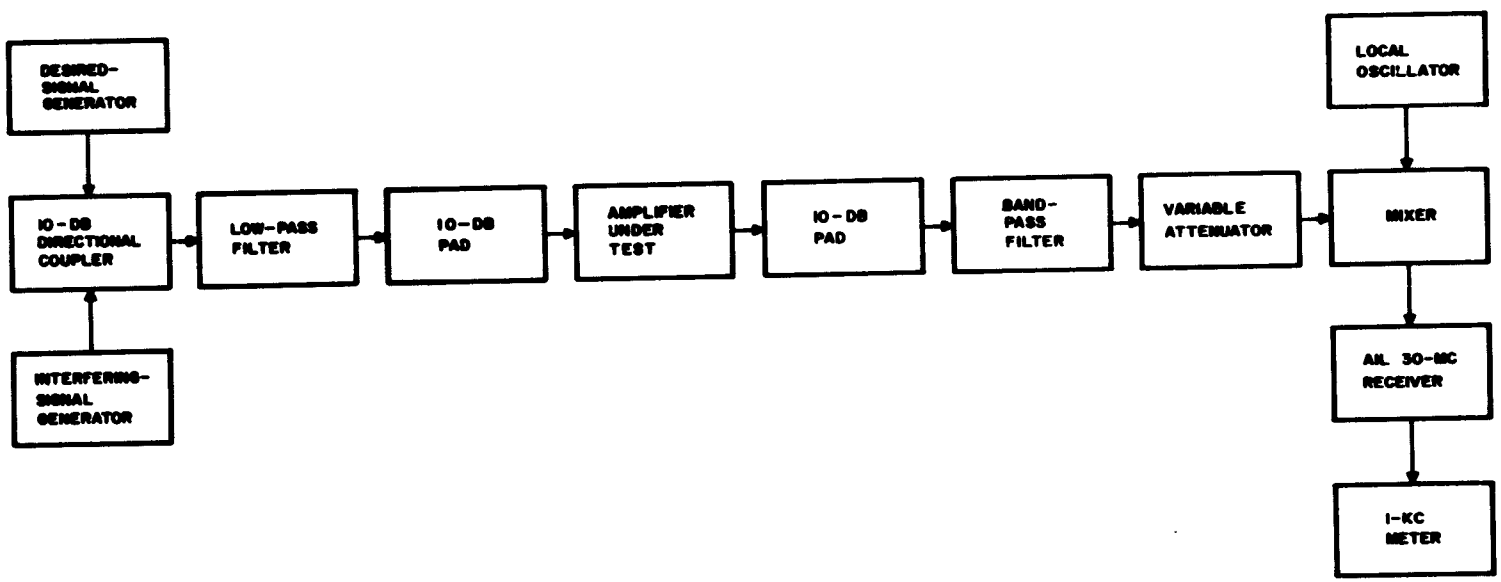

FIGURE 5-8. BLOCK DIAGRAM OF SETUP FOR MEASURING DYNAMIC RANGE, DESENSITIZATION, CROSS MODULATION, AND INTERMODULATION FOR 385-MC AMPLIFIER

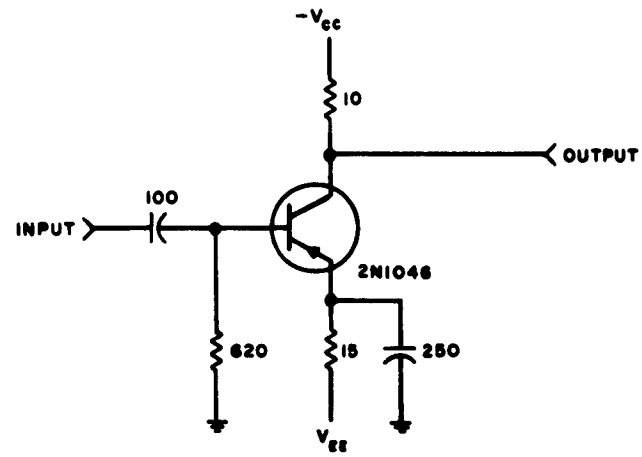

UNLESS OTHERWISE NOTED:
RESISTANCE VALUES IN OHMS
CAPACITANCE VALUES IN UF

FIGURE 5-9. LOW-FREQUENCY POWER AMPLIFIER

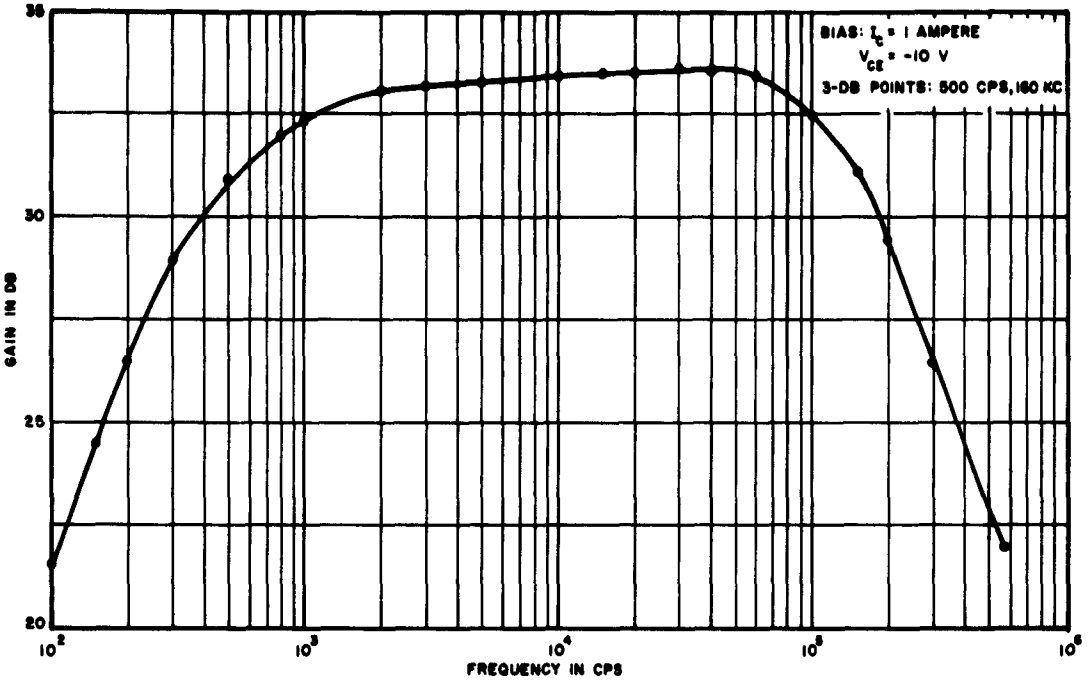

A. GAIN VERSUS FREQUENCY FOR LOW-FREQUENCY POWER AMPLIFIER

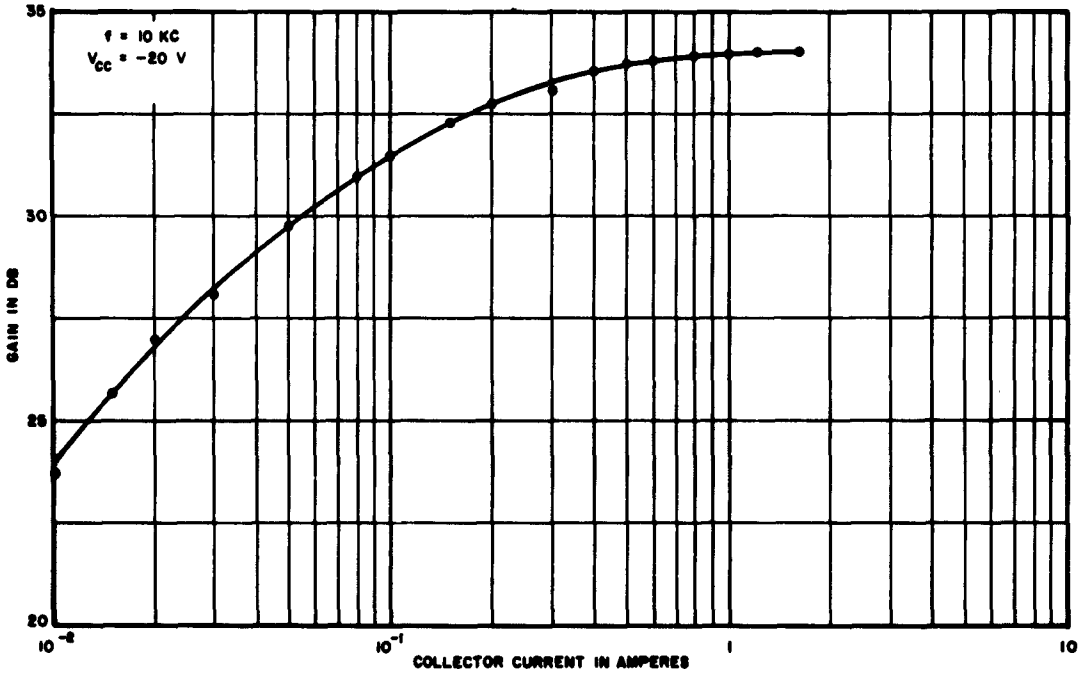

B. GAIN VERSUS BIAS CURRENT FOR LOW-FREQUENCY POWER AMPLIFIER

FIGURE 5-10. SMALL-SIGNAL CHARACTERISTICS OF LOW-FREQUENCY POWER AMPLIFIER

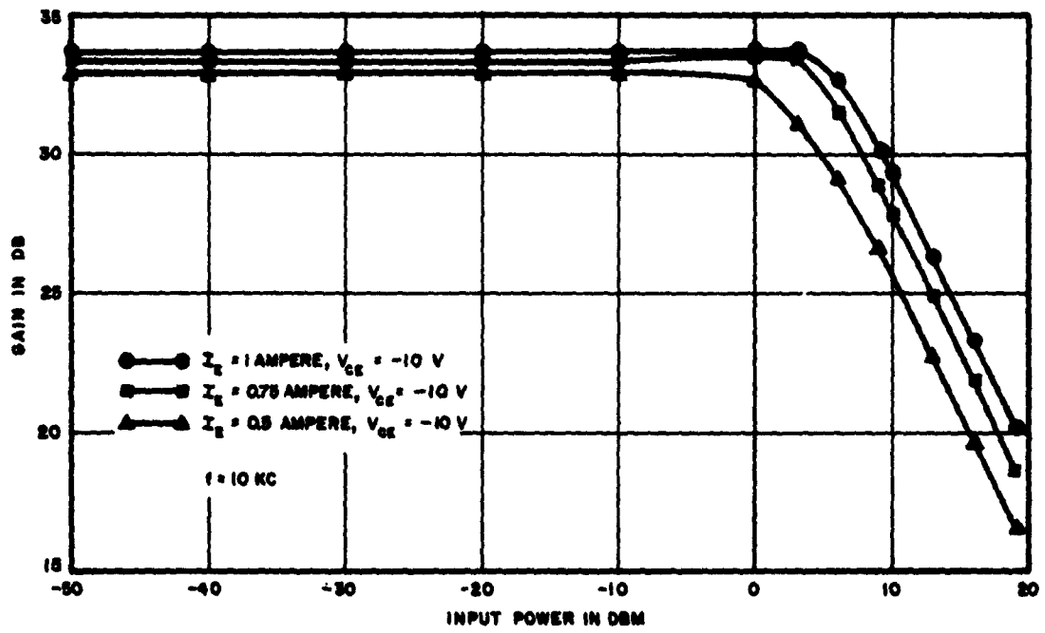

FIGURE 5-11. SATURATION CHARACTERISTICS OF LOW-FREQUENCY POWER AMPLIFIER

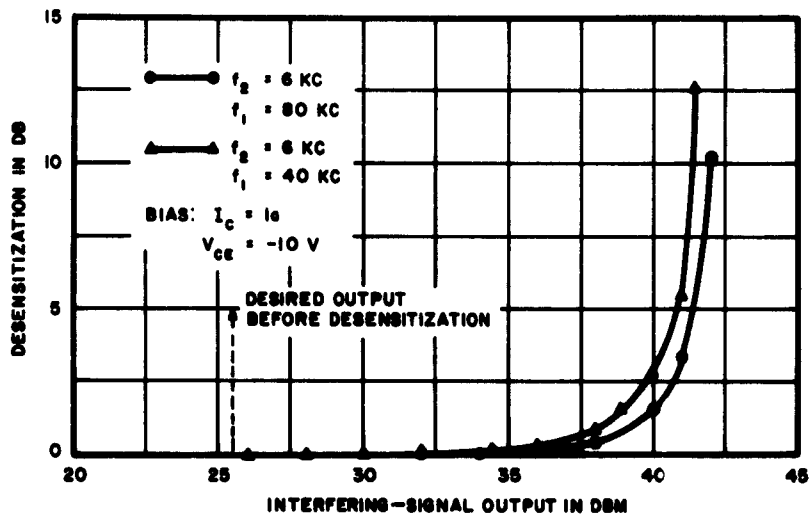

FIGURE 5-12. DESENSITIZATION VS OUTPUT POWER FOR LOW-FREQUENCY POWER AMPLIFIER

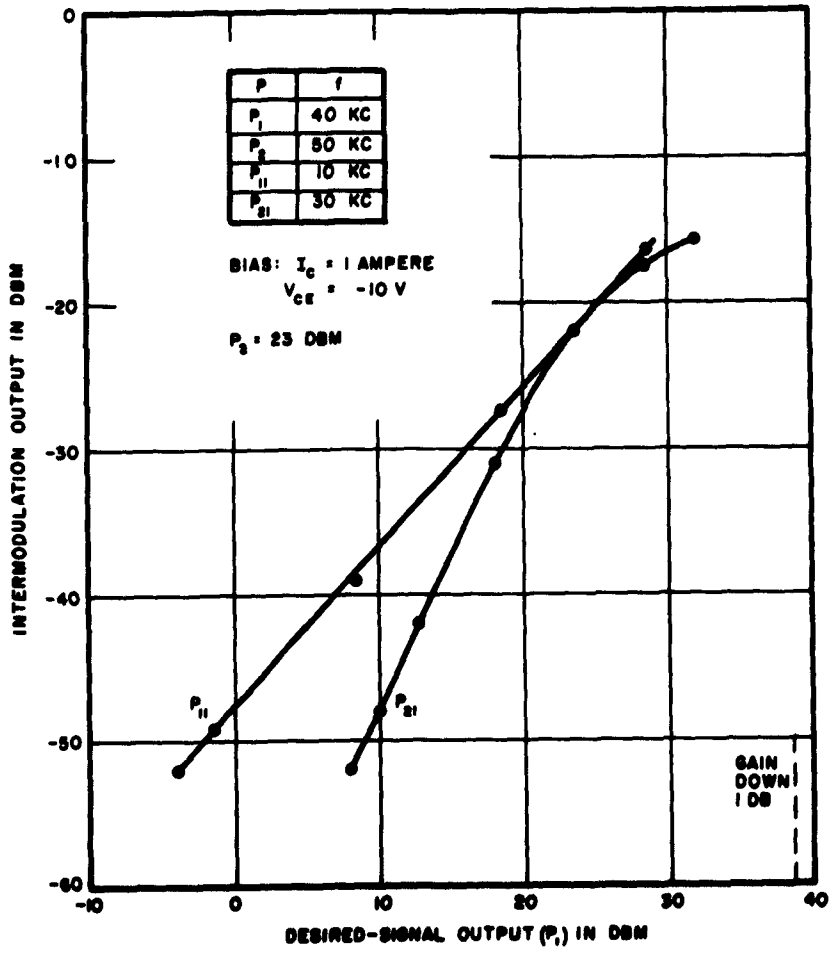

FIGURE 5-13. INTERMODULATION VS OUTPUT POWER FOR LOW-FREQUENCY POWER AMPLIFIER

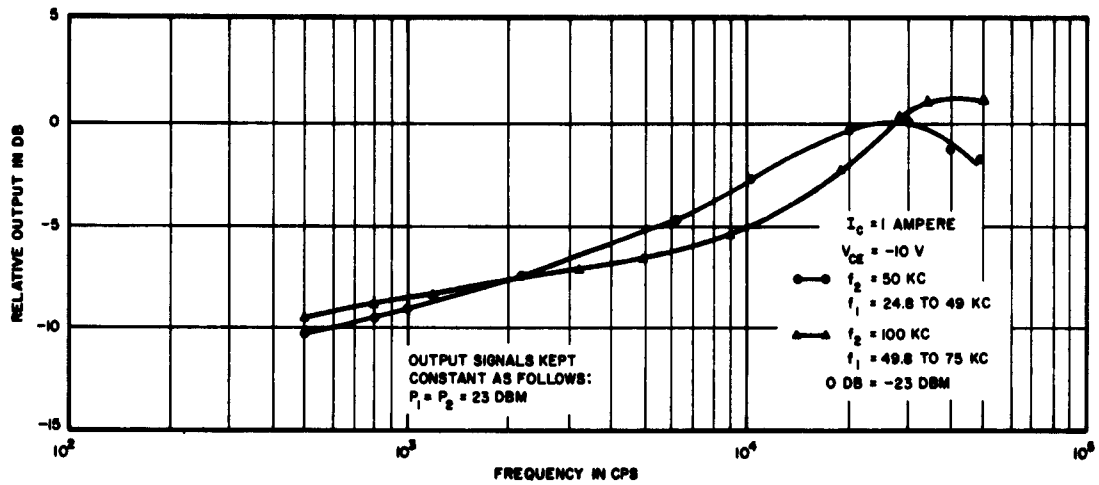

A. THIRD-ORDER INTERMODULATION OUTPUT VERSUS FREQUENCY

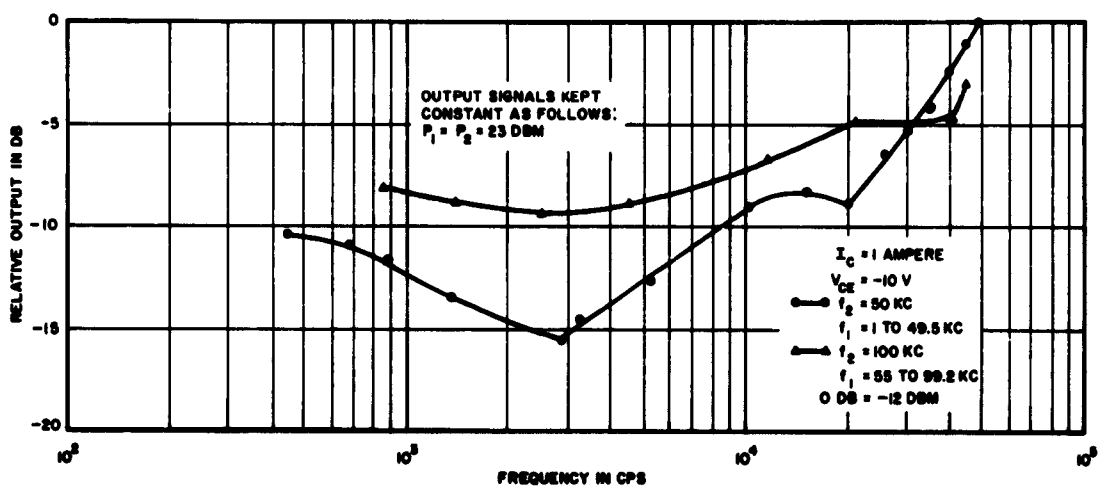

B. SECOND-ORDER INTERMODULATION OUTPUT VERSUS FREQUENCY

FIGURE 5-14. INTERMODULATION VS FREQUENCY FOR LOW-FREQUENCY POWER AMPLIFIER

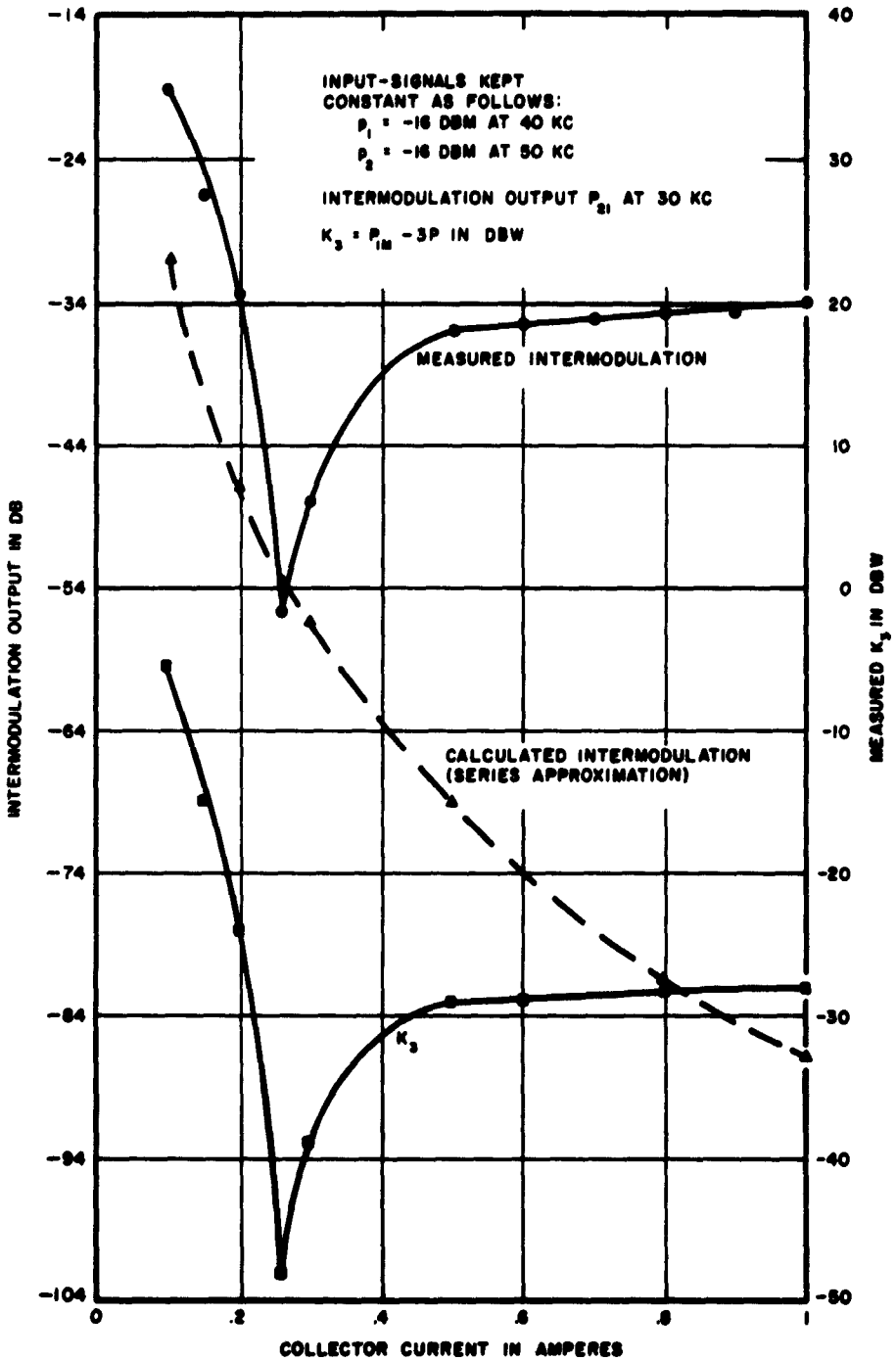

FIGURE 5-15. INTERMODULATION VS BIAS CURRENT FOR LOW-FREQUENCY POWER AMPLIFIER

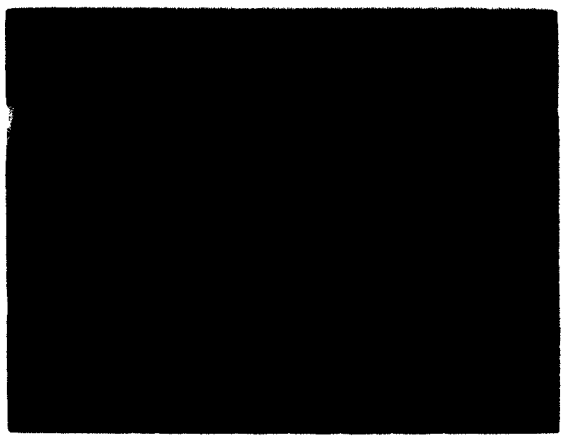

(A)

UPPER: OUTPUT PULSE FOR NEGATIVE INPUT PULSE JUST BELOW SATURATION. NO PULSE STRETCHING

MIDDLE: OUTPUT FOR INPUT PULSE 10 DB ABOVE SATURATION (10-USEC STRETCHING)

LOWER: OUTPUT FOR INPUT PULSE 16 DB ABOVE SATURATION (22-USEC STRETCHING)

VERTICAL: 5 VOLTS PER DIVISION
HORIZONTAL: 5 USEC PER DIVISION

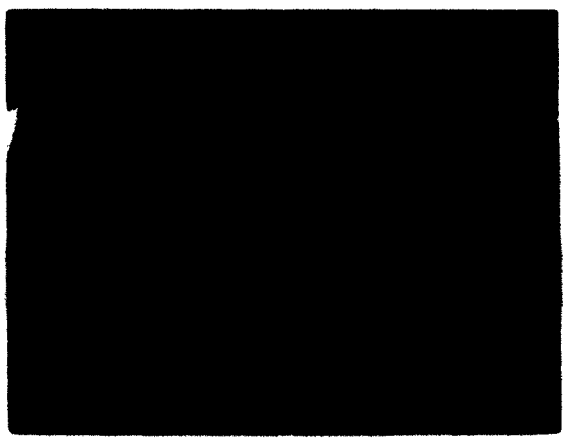

(B)

UPPER: OUTPUT FOR SUCCESSIVE NEGATIVE AND POSITIVE INPUT PULSES JUST BELOW SATURATION

MIDDLE: OUTPUT WHEN FIRST PULSE IS INCREASED 10 DB ABOVE SATURATION (PARTIAL SUPPPRESSION SECOND PULSE)

LOWER: OUTPUT WHEN FIRST PULSE IS INCREASED 16 DB ABOVE SATURATION (TOTAL SUPPRESSION OF SECOND PULSE)

FIGURE 5-16. POWER AMPLIFIER RESPONSE TO LARGE INPUT PULSES

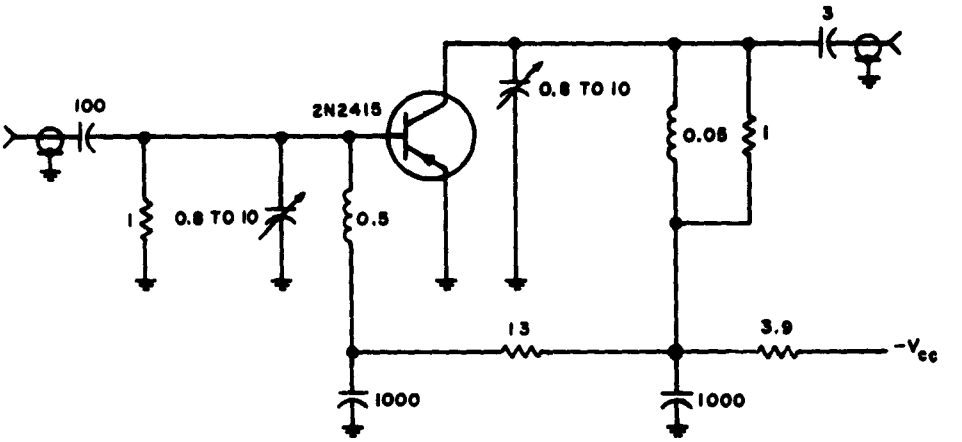

UNLESS OTHERWISE NOTED:
RESISTANCE VALUES IN KILOHMS
CAPACITANCE VALUES IN PF
INDUCTANCE VALUES IN UH

FIGURE 5-17. SINGLE-TUNED 385-MC AMPLIFIER

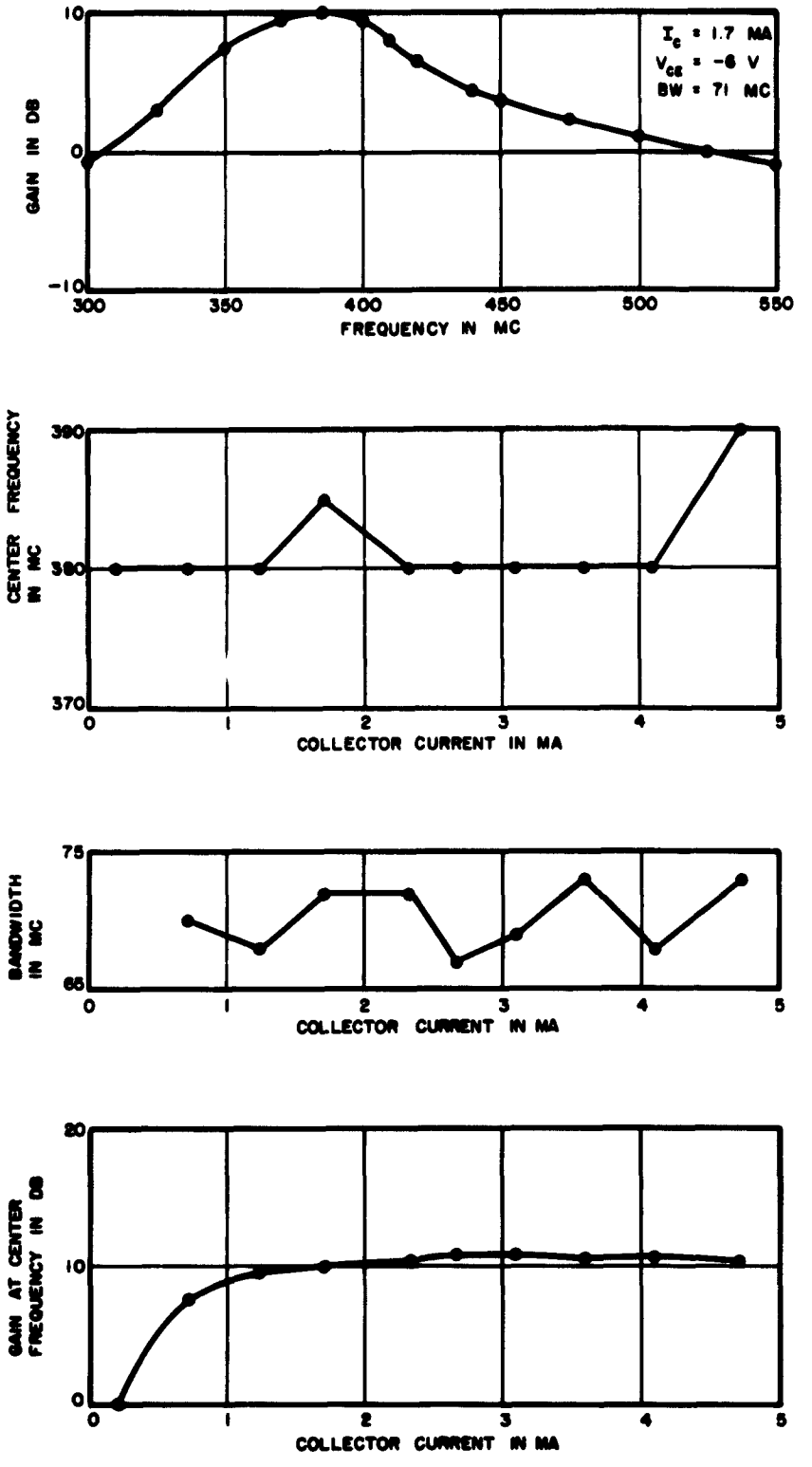

FIGURE 5-18. SMALL-SIGNAL CHARACTERISTICS OF 385-MC AMPLIFIER

I_c	1 MA	2 MA
MEASURED SATURATION OUTPUT POWER (GAIN DOWN 1 DB)	-10.3 DBM	-5.5 DBM
CALCULATED SATURATION OUTPUT POWER	-9.7 DBM, R_{OUT} (OF TRANSISTOR) = ∞ -13.7 DBM, R_{OUT} = 500 OHMS	-3.7 DBM, R_{OUT} = ∞ -9.7 DBM, R_{OUT} = 300 OHMS

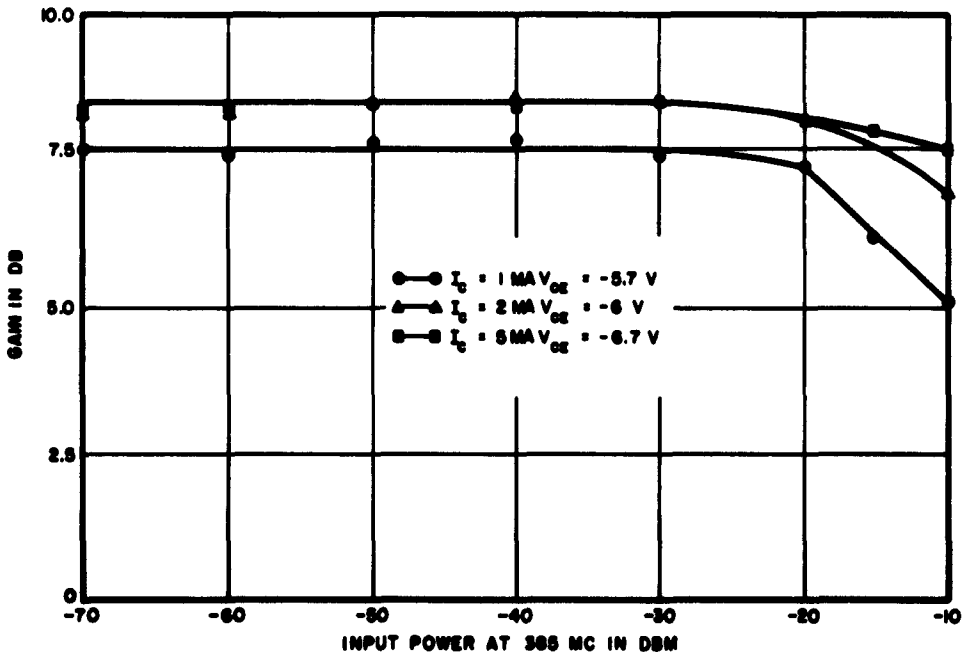

FIGURE 5-19. SATURATION CHARACTERISTICS OF 385-MC AMPLIFIER

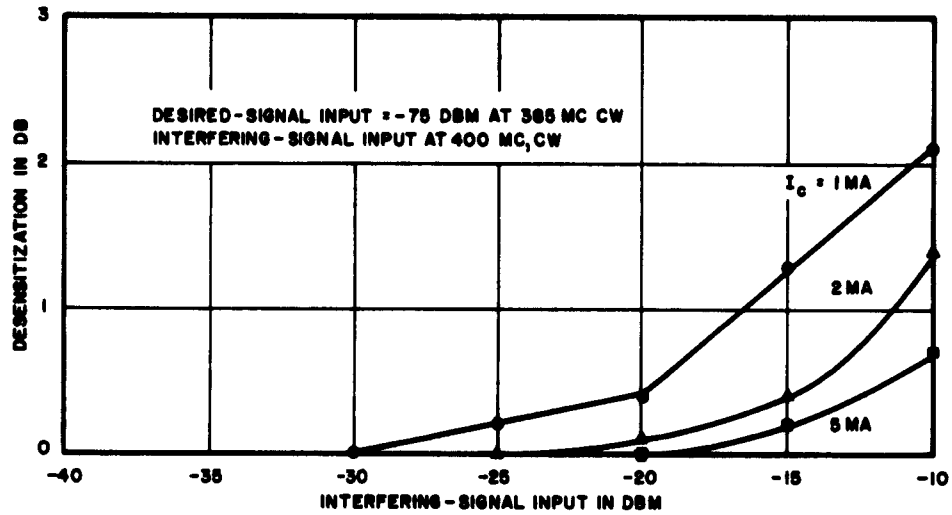

A. DESENSITIZATION FOR DIFFERENT BIAS CURRENTS

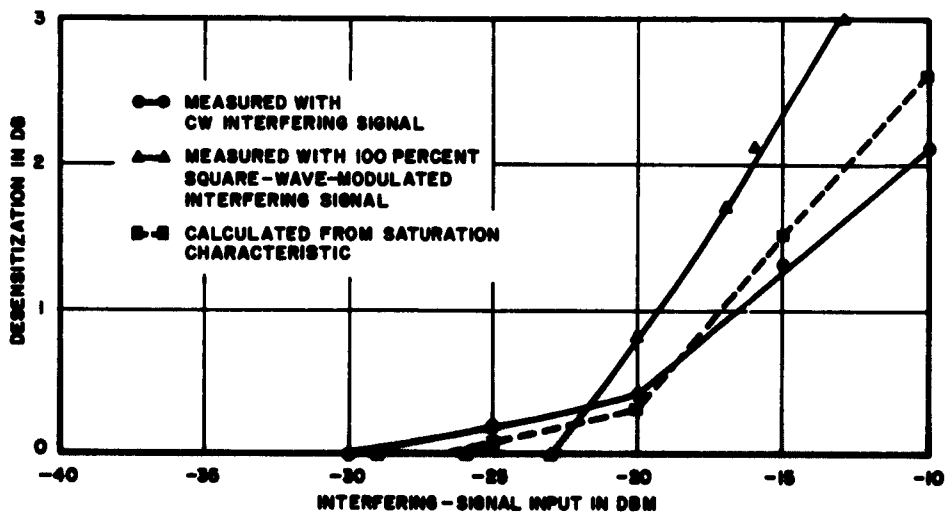

B. SMALL-SIGNAL DESENSITIZATION FOR I_c = 1 MA

FIGURE 5-20. DESENSITIZATION VS INPUT POWER FOR 385-MC AMPLIFIER

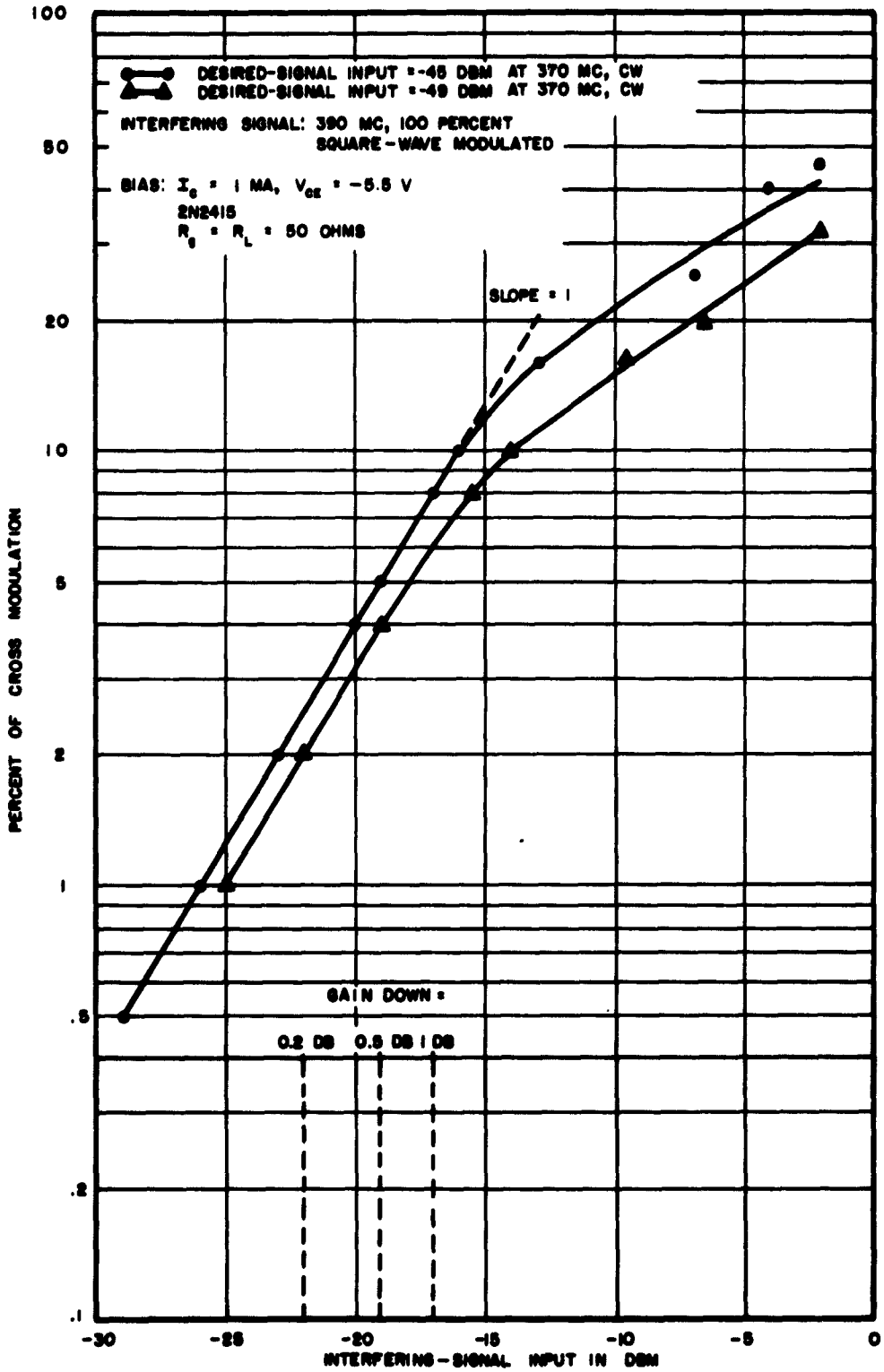

FIGURE 5-21. CROSS MODULATION VS INPUT POWER FOR 385-MC AMPLIFIER

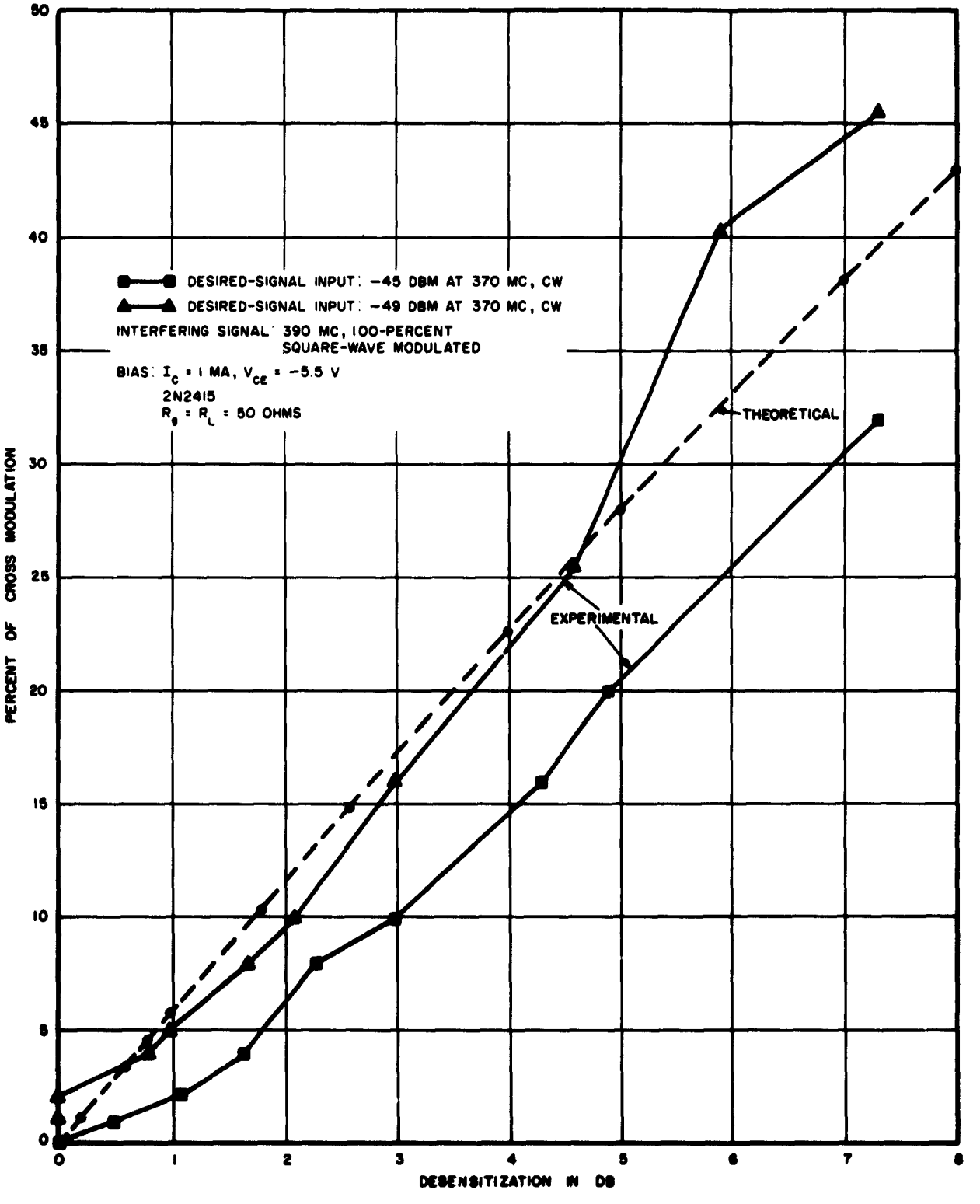

FIGURE 5-22. CROSS MODULATION VS DESENSITIZATION FOR 385-MC AMPLIFIER

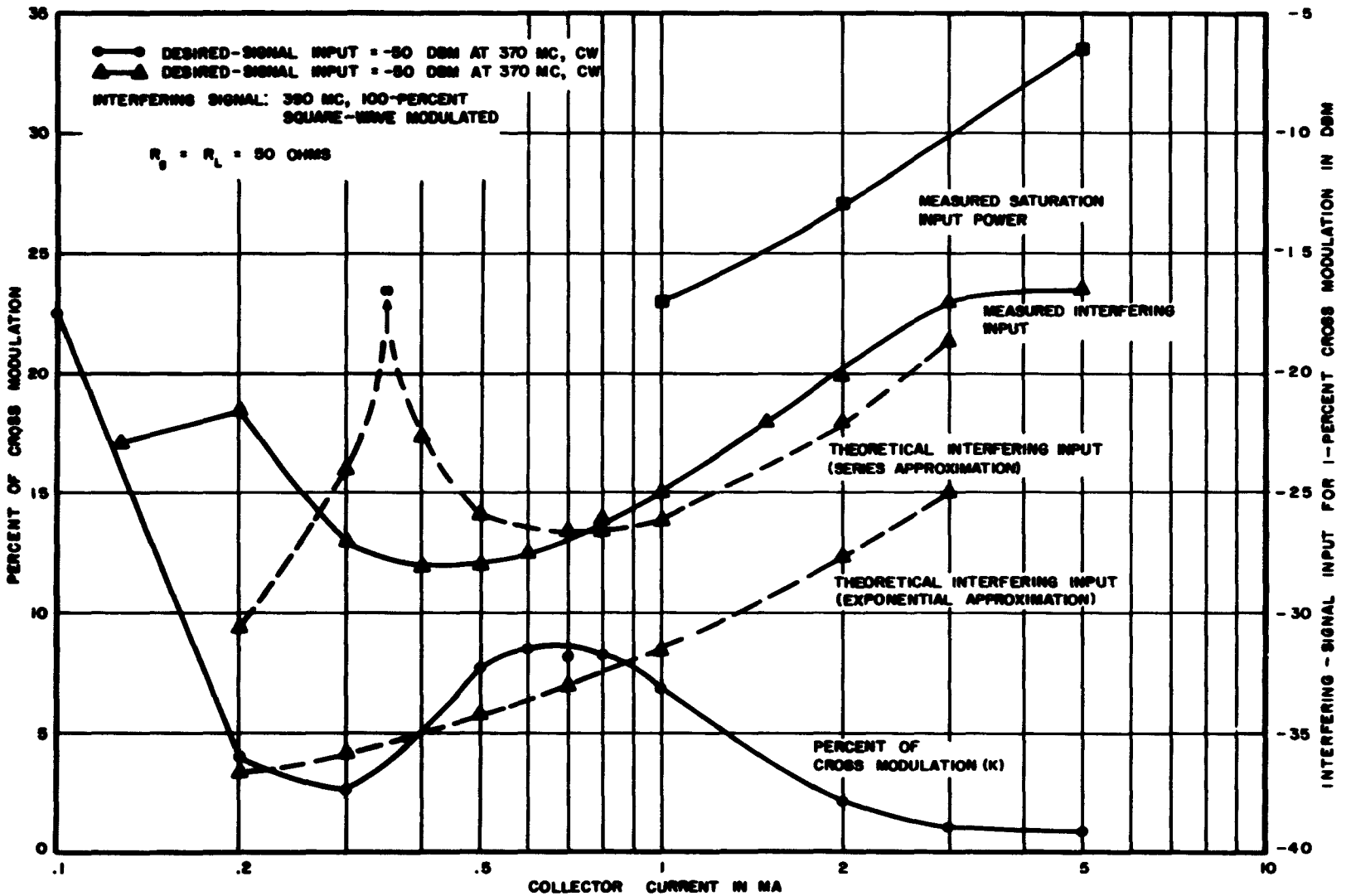

FIGURE 5-23. CROSS MODULATION VS BIAS CURRENT FOR 385-MC AMPLIFIER

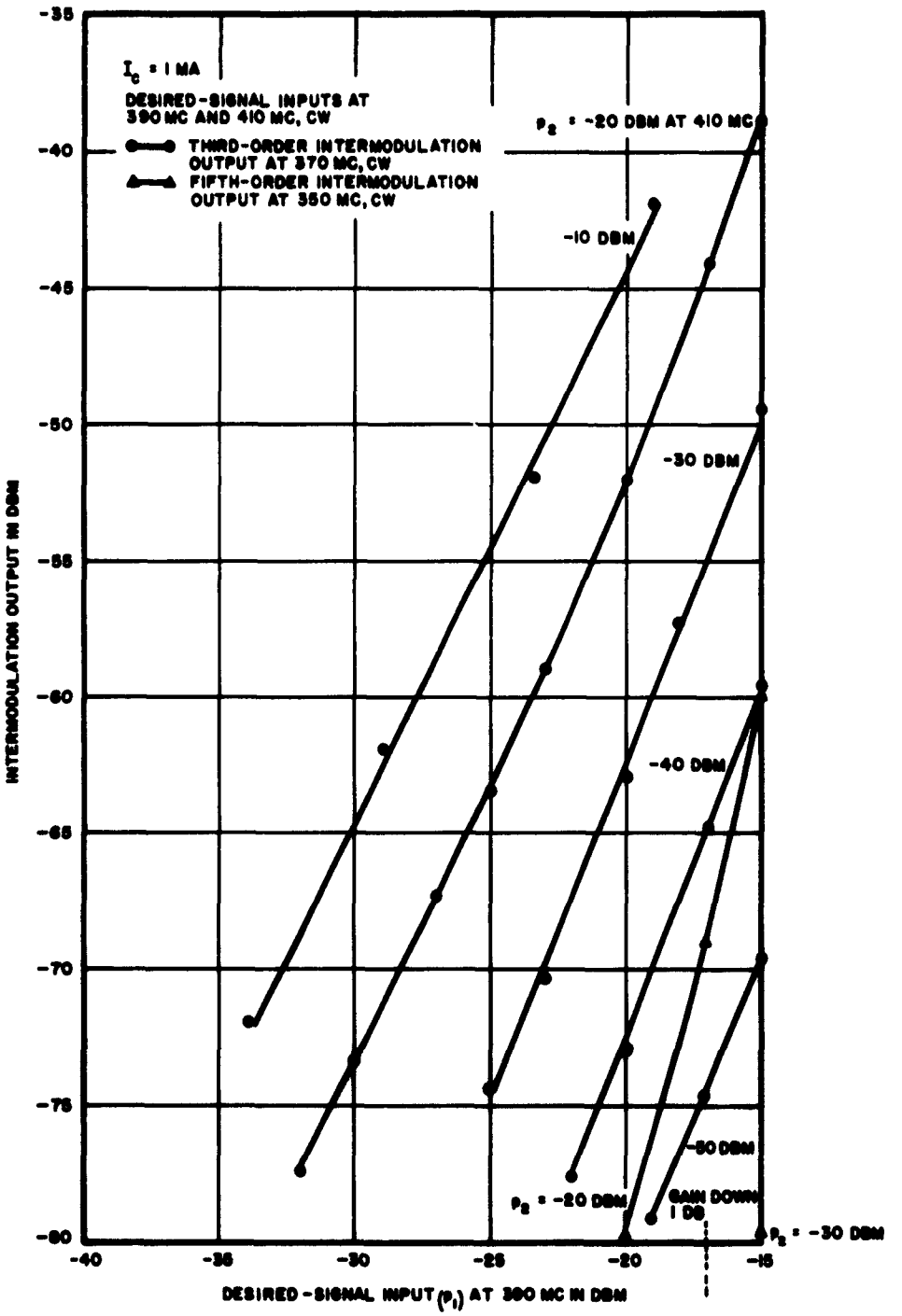

FIGURE 5-24. INTERMODULATION VS INPUT POWER FOR 385-MC AMPLIFIER

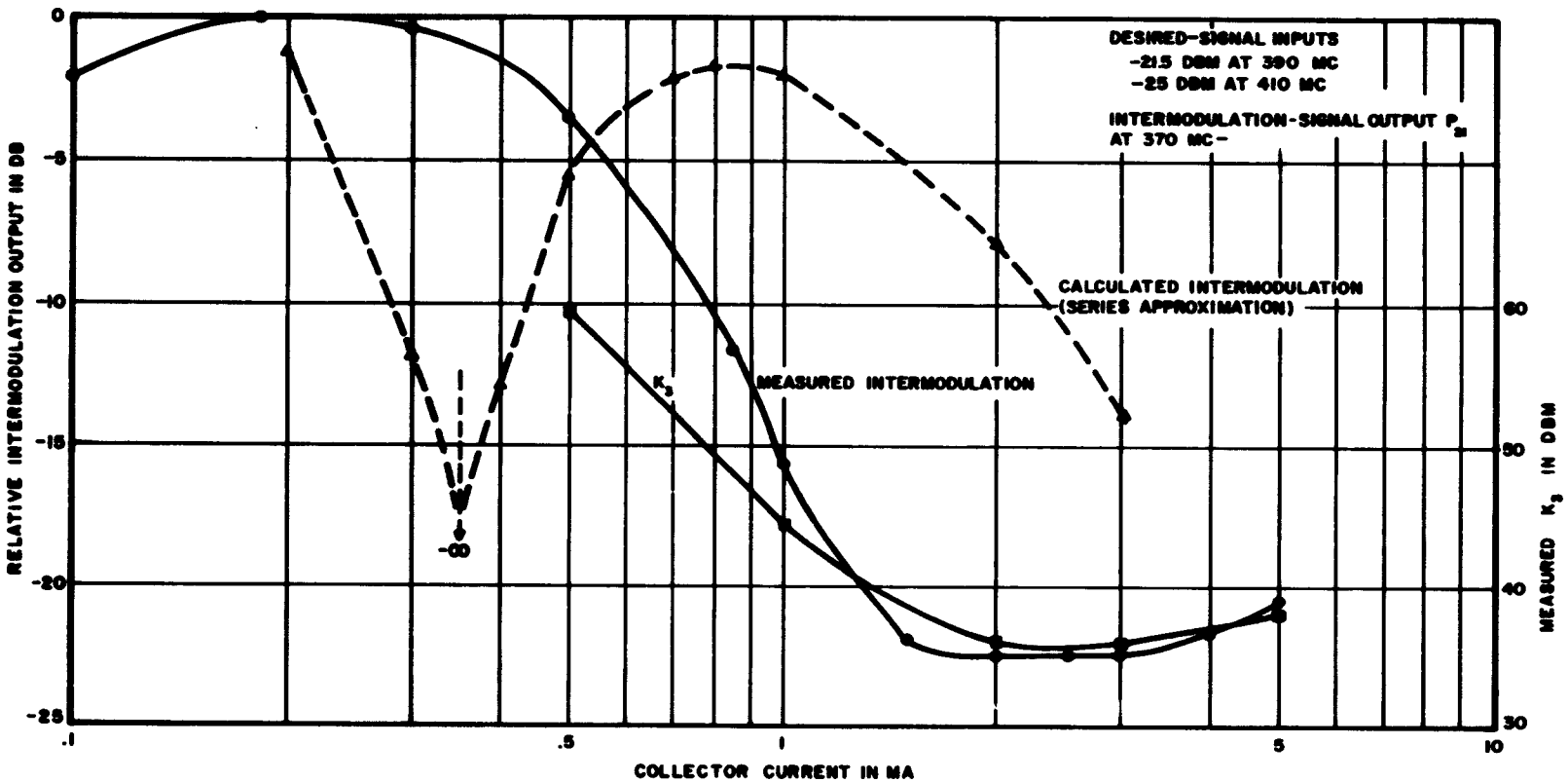

FIGURE 5-25. INTERMODULATION VS BIAS CURRENT FOR 385-MC AMPLIFIER

VI. FERRITE DEVICES

A. FILTERS

A two-element ferrite band-pass filter that has been developed by AIL has superior spurious response and residual coupling characteristics over a wide frequency range. This filter represents a recent improvement in ferrite filters. As such, its operating and interference characteristics are pertinent to this work.

This filter can be tuned from 2.4 to 4.8 kMc, and has a spurious response level of 60 to 80 db, with spot frequency spurious resonances below 44 db. It has a volume, excluding the magnet, of less than 0.25 cubic inch. The filter consists of two yttrium-Iron garnets (YIG) spheres coupled to two strip-transmission lines with a slot in the common ground plane. The slot is the coupling element between the resonators. The small size is achieved primarily by using strip-transmission-line ground-plane separations of 0.162 inch. Power is coupled from one line to the other when the YIG spheres are at their ferrimagnetic resonant frequencies. The filter has a two-pole response with a nominal 3-db bandwidth of 35 Mc. The filter is tuned by varying the field of an electromagnet about a permanent-magnet biasing field. The biasing field was set for 1140 oersteds, corresponding to a frequency of 3.2 kMc.

The filter characteristics have been evaluated between 2.4 to 4.8 Gc. Figure 6-1 shows a typical frequency response curve, and Figure 6-2 shows the characteristics of the filter over the complete tuning range. The curve in Figure 6-1 is centered at 3.8 Gc with a 34-Mc 3-db bandwidth and a 1.1-db insertion loss at the peak of the response.

It has a frequency response equivalent to a two-pole Tchebycheff filter having a 0.8-db pass-band ripple up to about 40 db of insertion loss. It then continues to a residual loss level of 83 db except for the two narrow-band responses that are 50 and 62 db down. The strongest spurious level is therefore 50 db down when the filter is tuned to 3.8 Gc. Figure 6-2A is a plot of the strongest spurious-response level in the 2.0 to 4.0 Gc range as the filter is tuned from 2.4 to 4.8 Gc. Figure 6-2B the 3-db bandwidth versus frequency, and Figure 6-2C the mid-band insertion loss. The spurious-response level is always more than 44 db down, the 3-db bandwidth averages about 35 Mc, and the mid-band insertion loss is under 2 db over most of the range. The insertion loss starts to increase slightly at the low-frequency end because the unloaded Q's of the YIG spheres are degraded. The filter is capable of tuning over the full 2.4 to 4.8 Gc range with 3 watts of power.

These data were measured after the resonant frequencies of the two garnets were very carefully aligned. The alignment, essential to low insertion loss, was achieved by rotating the axes of the garnets until they both have the same resonant frequencies. This procedure is effective because the insertion loss is only slightly higher (by 0.1 to 0.3 db) over the entire tuning range than when the filter was peaked to any specific frequency by individually tuning each sphere. Therefore, the filter can be accurately tuned by only one adjustment--the variation of the magnetic field.

In many receiver applications, the presence of the few, narrow-band, spurious-response levels appearing at any given filter center frequency does not necessarily determine the strongest spurious response of the entire receiver. By careful choice of the IF amplifier center frequency, it is often possible to reject the frew, strong, filter spurious levels present Where this is feasible, the YIG filter described would have an effective spurious response level equal to its residual level of 60 to 80 db.

B. CIRCULATORS

For power levels below the limiting level of the ferrite, circulators should perform as linear passive devices (reference 1). Thus, no interference effects should be produced in a circulator operating at normal power levels.

A standard saturation test was performed on a circulator for power levels up to 5 dbm. No deviation from linearity was found in the output versus input characteristic.

An intermodulation test was performed using the test setup shown in Figure 6-3. The 30-Mc signal generator was used to set a reference level on the AIL 30-Mc receiver. The difference between the frequencies of the two signal generators was 30 Mc. Circulators No. 1 and No. 2 were needed to isolate the two signal generators. Circulator No. 3 was the unit under test. The intermodulation power at 30 Mc was 55 db below the output power of signal generator No. 2 when signal generator No. 1 was operated at a power setting of 0 dbm. Circulator No. 3 was then removed from the circuit and the output of the hybrid was connected directly to the AIL Receiver. The intermodulation power was the same as previously recorded. Thus, no intermodulation can be attributed to the circulator. It is assumed that the intermodulation originated from residual coupling between the signal generators or from intermodulation in the receiver.

Tests of spurious responses were made on three AIL circulators (Figures 6-4, 6-5, and 6-6). Figure 6-4 shows the spurious responses of a normal narrow-band circulator; Figure 6-5 shows spurious responses for a wide-band circulator. Except for the difference in the circulator bandwidth, the two responses are about the same. Both circulators become 3-db couplers at low frequencies and have irregular responses at high frequencies. Figure 6-6 shows the spurious responses of

a special circulator that was designed for high insertion loss at high frequencies. This special circulator contains mode supressors that inhibit high-order mode propagation found at high frequencies. For frequencies above 7 Gc, isolation and insertion loss are greater than 20 db (Figure 6-6). At lower frequencies, the special circulator performs the same as the other circulators.

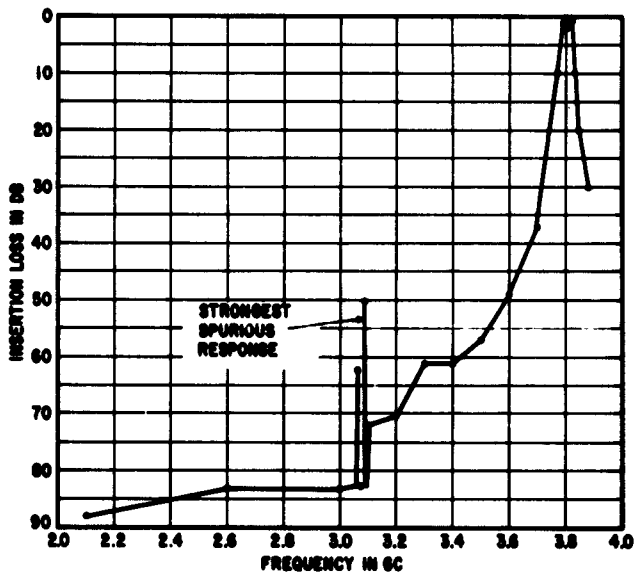

FIGURE 6-1. TYPICAL FREQUENCY RESPONSE OF FERRITE FILTER

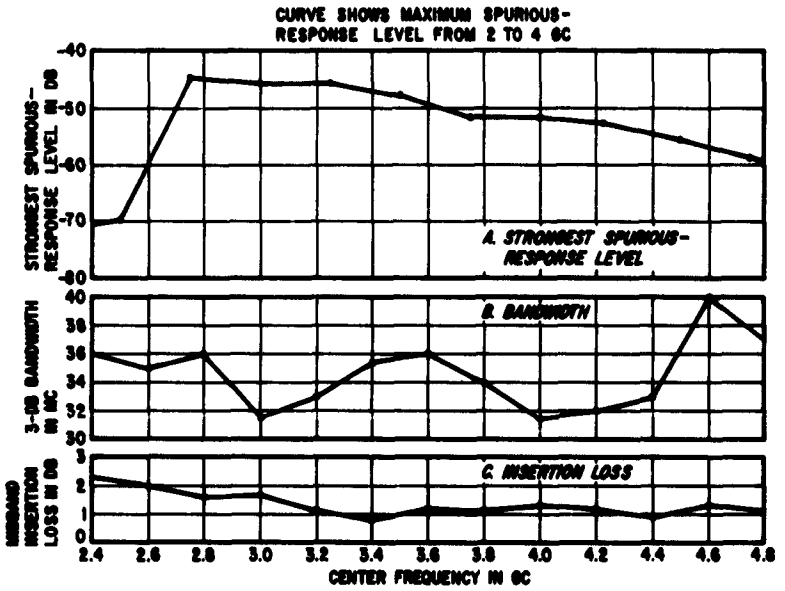

FIGURE 6-2. SPURIOUS RESPONSE, BANDWIDTH, AND INSERTION LOSS VS FREQUENCY OF FERRITE FILTER

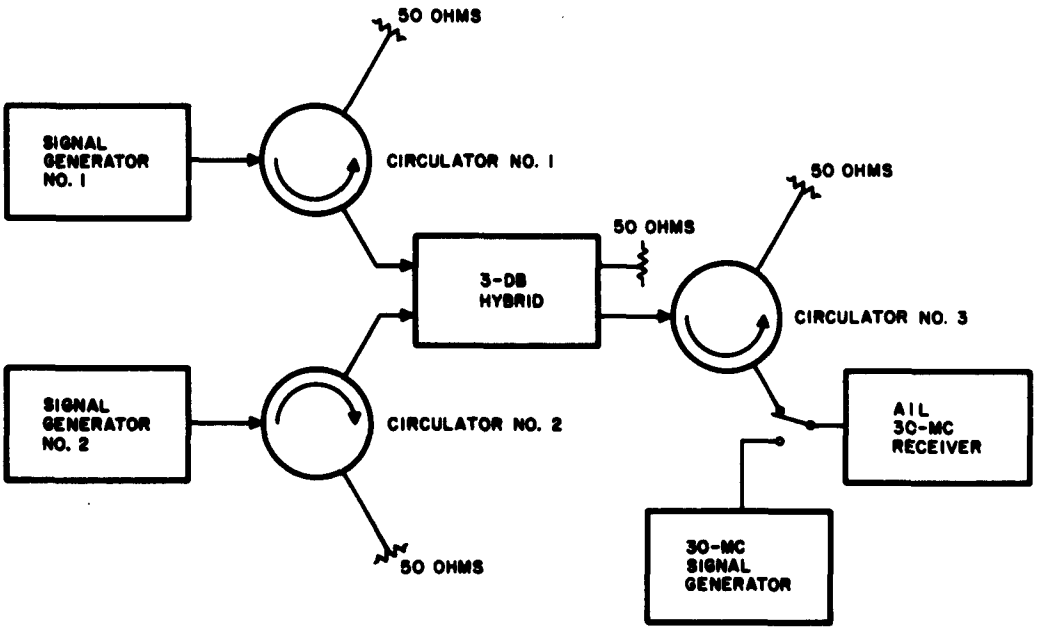

FIGURE 6-3. BLOCK DIAGRAM OF CIRCULATOR INTERMODULATION TEST SETUP

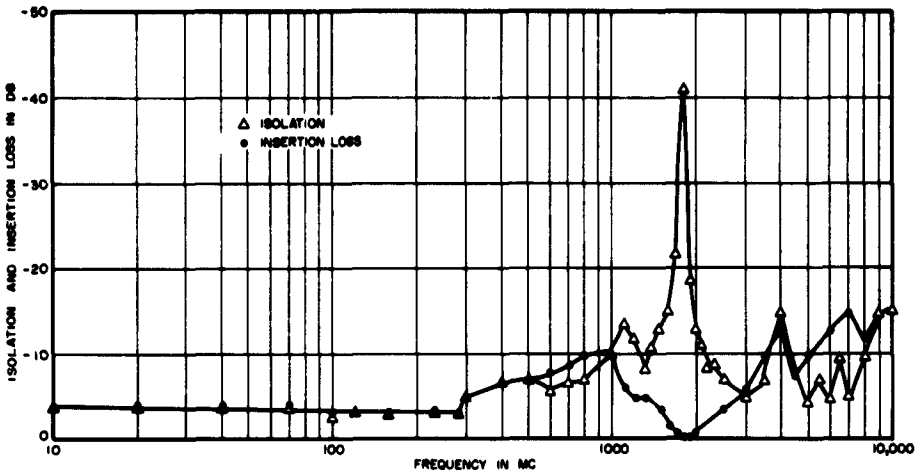

FIGURE 6-4. SPURIOUS-RESPONSE CURVE OF NARROW-BAND AIL CIRCULATOR

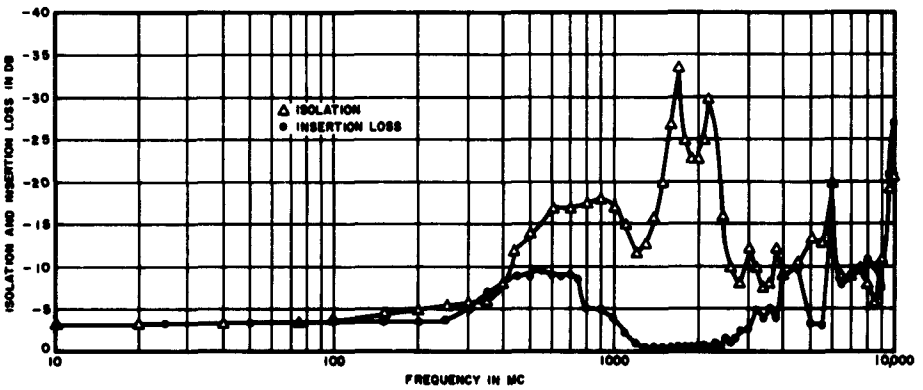

FIGURE 6-5. SPURIOUS-RESPONSE CURVE OF WIDE-BAND AIL CIRCULATOR

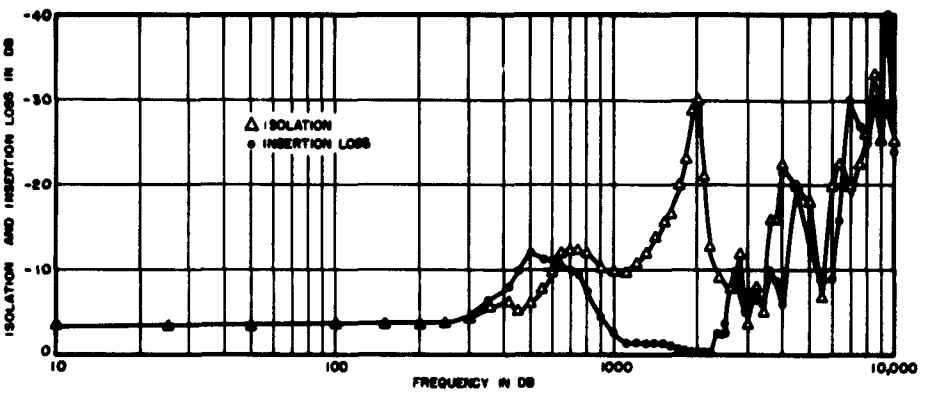

FIGURE 6-6. SPURIOUS-RESPONSE CURVE OF WIDE-BAND AIL CIRCULATOR WITH MODE SUPPRESSORS

VII. CRYSTAL MIXERS

The crystal mixer uses the nonlinear E-I characteristic of a crystal diode to produce either a sum or difference frequency output from two inputs. One input is a high-level local-oscillator voltage, and the other input is the input signal. The output, or IF, is caused by the nonlinear mixing of these inputs. The IF is usually the difference between the input-signal frequencies; however, it can also be the sum of these frequencies. The nonlinear characteristic of the crystal diode also produces intermodulation products, which are signals at difference or sum frequencies of harmonics of the inputs. The IF can usually be separated from the inputs and the intermodulation products with appropriate filtering.

A. THEORY

1. OUTPUT POWER

Assuming the diode current to be an exponential function of voltage,

$$i = i_o \left(e^{\alpha v} - 1\right) \tag{7-1}$$

where

i_o = leakage current,
α = diode constant.

The output voltage from two inputs, $A_1 \cos \omega_1 t$ and $A_2 \cos \omega_2 t$, is shown in reference 1 to be

$$E_{sb} = 2i_o \, e^{\alpha v_o} R_o \, I_s(\alpha A_1) \, I_b(\alpha A_2) \times \omega_2 \, (s\omega_1 \pm b\omega_2)t \quad (7\text{-}2)$$

where

v_o = DC bias voltage,
R_o = average diode resistance,
s = harmonic of ω_1 (input signal),
b = harmonic of ω_2 (local oscillator)

$I_s\ (\alpha A_1)$ and $I_b\ (\alpha A_2)$ are modified Bessel functions of the first kind of orders s and b, respectively. For the main response, $s = b = 1$; for a low-level input, the modified Bessel function $I_s\ (\alpha A_1)$ can be approximated by its first term. From equation 7-2,

$$E_{11} = 2i_o \, e^{\alpha v_o} R_o \, \frac{\alpha A_1}{2} \, I_1(\alpha A_2) \cos\ (\omega_1 \pm \omega_2)t \quad (7\text{-}3)$$

The average output power is expressed as,

$$P_{11} = \frac{\overline{\left[E_{11}\right]^2}}{R_o}$$

where $\overline{\left[E_{11}\right]^2}$ is the mean-square value of E_{11}. Using equation 7-3 and averaging either the sum or difference frequency gives:

$$P_{11} = \frac{2}{R_o} \left(i_o \, e^{\alpha v_o} R_o\right)^2 \frac{\alpha^2 A_1{}^2}{4} \left[I_1\left(\alpha A_2\right)\right]^2 \quad (7\text{-}4)$$

The input power is $p_1 = \frac{A_1^2}{2R_o}$. Substituting this relationship into equation 7-4 and rearranging terms results in:

$$P_{11} = \left[\alpha i_o R_o e^{\alpha v_o} I_1 \left(\alpha A_2\right)\right]^2 p_1 \qquad (7\text{-}5)$$

Thus, for low-level signals, the output power, P_{11}, is a linear function of input power, p_1.

2. SATURATION

The output voltage for large input-signal voltages can be found from equation 7-2. The output of the desired response (IF) is obtained by setting the variables s and b equal to one. For small signals, the output is linearly proportional to the input, and for large signals, the output increases at a greater rate than the input. Apparently, an increase in gain is predicted by equation 7-2 rather than the decrease that is expected. The increase in gain is predicted because the value of the Bessel function, $I_1(\alpha A_1)$, tends toward an exponential increase for large arguments, whereas the value of the Bessel function is linear for small arguments. However, for large signals the operating point of the diode changes, thereby causing a decrease in the value of α. The value of α can be thought of as representing the degree of departure from linearity of the diode. When the diode is biased at higher voltage levels, the E-I curve becomes nearly linear. The increase in linearity is reflected by a corresponding decrease in α. Calculation of α (reference 1) should be at an input voltage equal to the sum of the peaks of the signal and oscillator voltages.

3. DESENSITIZATION AND CROSS MODULATION

Generalizing equation 7-2 to include two input signals and a local-oscillator voltage (Appendix III) yields the following expression for the desired response:

$$E_{11} = 2i_o \, e^{\alpha v_o} R_o \, I_1(\alpha A_1) \, I_1(\alpha A_2) \, I_0(\alpha A_1') \qquad (7\text{-}6)$$

where

A_1' = peak voltage of interfering signal voltage,

$I_0(\alpha A_1')$ = zero-order modified Bessel function of argument αA_1.

$I_o(\alpha A_1')$ is equal to one for small signal levels and increases for large values of A_1'. As in saturation, the change in α caused by a shift in operating point must be calculated to determine the actual effect of the interfering signal.

The amount of cross modulation can be found from the desensitization effect using equation 1-5.

4. INTERMODULATION

As shown in Appendix III, equation III-7, the generalization for the intermodulation output for two input signals and a local oscillator is given by:

$$E_{svb} = 2i_o \, e^{\alpha v_o} R_o \, I_s(\alpha A_1) \, I_v(\alpha A_1') \, I_b(\alpha A_2) \qquad (7\text{-}7)$$

$$\cos\,(s\omega_1 \pm v\omega_1' \pm b\omega_2)$$

where s, v, and b are the first-signal harmonic, the second-signal harmonic, and the local-oscillator harmonic, respec-

tively. Assuming low-level signals and solving for the output power in terms of input signal powers, equation III-8 (Appendix III), gives:

$$P_{svb} = \left[2\alpha^{s+v} i_o R_o e^{\alpha v_o} I_b(\alpha A_2)\right]^2 \left(\frac{R_o}{2}\right)^{s+v-1} (p_1)^s (p_1')^v \tag{7-8}$$

All intermodulation products can be found by using this expression.

Methods of determining all the constants except i_o are shown in reference 1. The value of i_o can be found from a measurement of the small-signal insertion loss of the desired signal. For the desired signal s = 1, v = o and b = 1. The small-signal insertion loss is $\frac{P_{101}}{p_1}$. From equation 7-8

$$P_{101} = \left[2\alpha i_o R_o e^{\alpha v_o} I_b(\alpha A_2)\right]^2 p_1 \tag{7-9}$$

Solving for i_o,

$$i_o = \frac{\sqrt{\frac{P_{101}}{p_1}}}{2\alpha R_o e^{\alpha v_o} I_b(\alpha A_2)} \tag{7-10}$$

B. EXPERIMENT

Measurements of saturation, desensitization, and intermodulation were taken using the general setup shown in Figure 7-1. Two signal generators, each followed by a band-

pass filter, were used. The signals were added through a 20-db coupler and the resultant sum sent to the input of a single-ended crystal-diode mixer. A local oscillator was also connected to the mixer through a 700-Mc low-pass filter. The filter suppressed any harmonics originating in the local oscillator. The output of the mixer was sent to a 60-Mc tuned preamplifier and then to an AIL precision test receiver. The meter on the receiver was the output indicator. A 60-Mc signal generator was used to set a reference level on the receiver, and a bias meter was used to record DC bias current through the mixer diode.

1. SATURATION

The local oscillator was set at a frequency of 500 Mc, and the output was adjusted to give the desired bias current. Signal generator No. 1 and band-pass filter No. 1 were set at a frequency of 560 Mc. Signal generator No. 2 was not used. Relative output versus input was measured for input signal levels to -8 dbm, for three levels of bias current--0.1, 0.5, and 0.9 ma (Figure 7-2). From this figure, it can be seen that the higher the bias current the lower the amount of saturation. For example, for an input signal power of -8 dbm, the gain change is -8.8, -5.2, and -2.0 db for bias currents of 0.2, 0.5, and 0.9 ma, respectively.

No attempt was made to predict the saturation curve. To make such a prediction it would first be necessary to calculate a value of α for each input signal level and then determine the output using the α from equation 7-2. Since the equation which determines α is not an explicit function, an iterative process is necessary for each value. It is more practical to measure the saturation level than to calculate it.

2. DESENSITIZATION

For desensitization measurements, the local oscillator and signal generator No. 1 were kept at the same frequencies (500- and 560- Mc). The output of signal generator No. 1 provided an input signal of -40 dbm from which a reference output was set on the AIL receiver. The DC bias current of the mixer was set by the local-oscillator input power. Signal generator No. 2 was set at a frequency of 610 Mc. Data on the relative output of the desired response as a function of interfering signal input power was taken for several values of the DC bias current of the mixer. The results are shown in Figure 7-3. The current given for each curve is the bias current with no interfering signal present. Desensitization is shown to be dependent upon bias current; the desensitization at the largest bias is least affected by interfering signal. For low bias currents, the interfering signals at certain power levels decrease the insertion loss of the desired response.

3. INTERMODULATION

Intermodulation responses were measured using the test setup shown in Figure 7-1 as follows:

1. The 60-Mc reference signal source was connected to the 60-Mc preamplifier. For a given input power, a reference was established on the meter of the AIL precision test receiver.
2. The mixer was connected to the 60-Mc preamplifier, and the signal and local oscillator frequencies were adjusted to obtain a 60-Mc output for a given intermodulation product ($sf_1 \pm vf_1 \pm bf_2$).
3. The local oscillator level was set for a bias current of 0.5 ma.

4. The input power versus output power was measured by using the power settings of the signal generators as the input powers. The attenuator setting on the AIL receiver, which was necessary to give the reference output, was used to find the output power.

5. Steps 2 to 4 were repeated for various intermodulation products up to the sixth order.

The results of these measurements are shown in Figures 7-4 through 7-8. The solid lines in these figures represent the experimental results and the dashed lines represent those values predicted by using equation 7-8. For intermodulation between one input signal and the local oscillator, the theoretical predictions and the experimental results agreed very well--the predicted signal input was accurate within 6 db for a given intermodulation output. When two signals and the local oscillator were involved in the intermodulation product, the accuracy degraded as much as 33 db between theory and experiment. In these cases, only the general shape of the curve was predicted accurately.

In all cases, a conservative prediction of intermodulation power output levels was used. Thus, in any design, the intermodulation will be less than the value found by using equation 7-8.

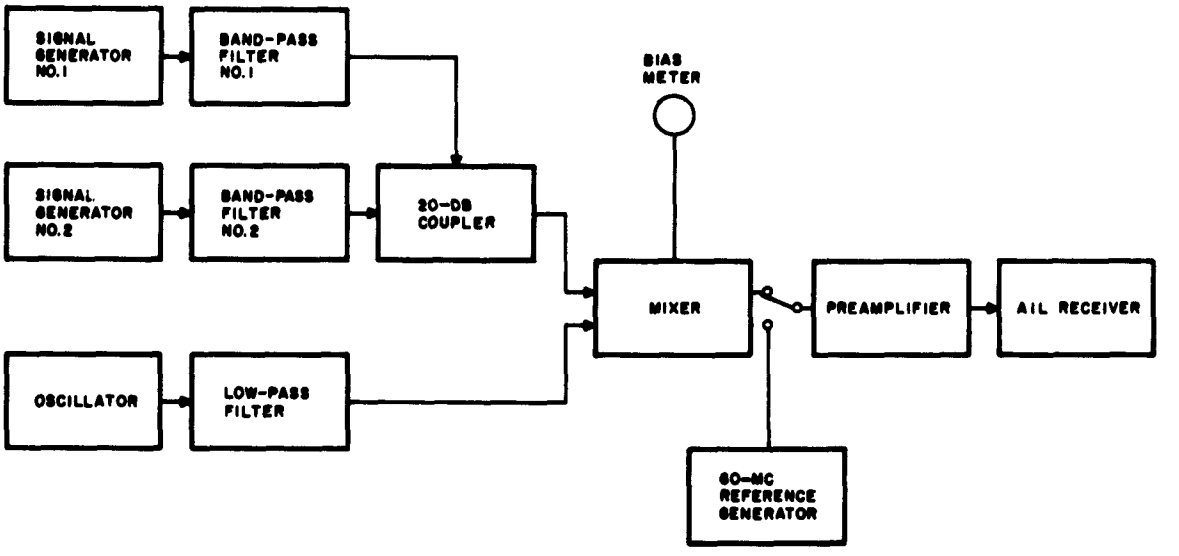

FIGURE 7-1. BLOCK DIAGRAM OF CRYSTAL MIXER TEST SETUP

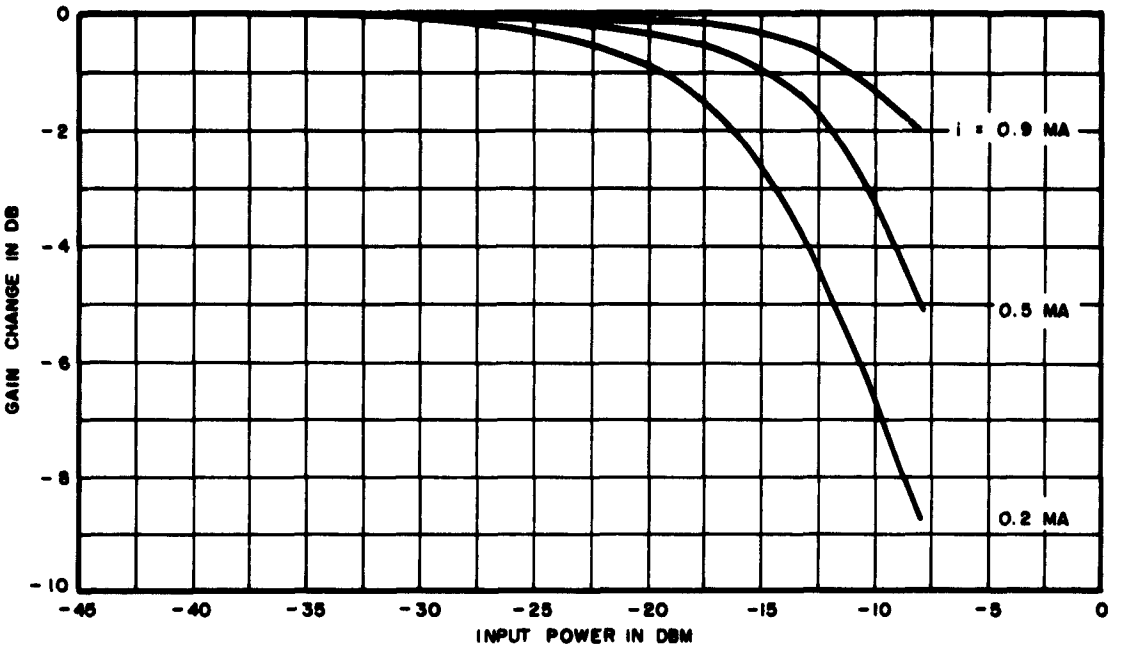

FIGURE 7-2. SATURATION VS INPUT POWER FOR CRYSTAL MIXER

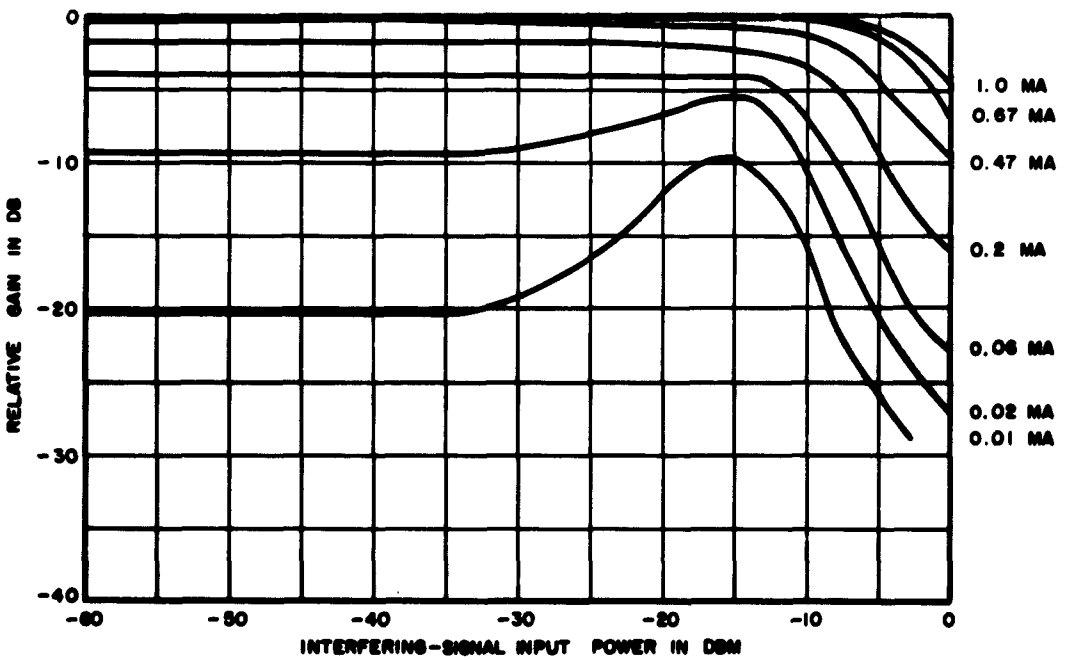

FIGURE 7-3. GAIN VS INTERFERING INPUT POWER FOR CRYSTAL MIXER

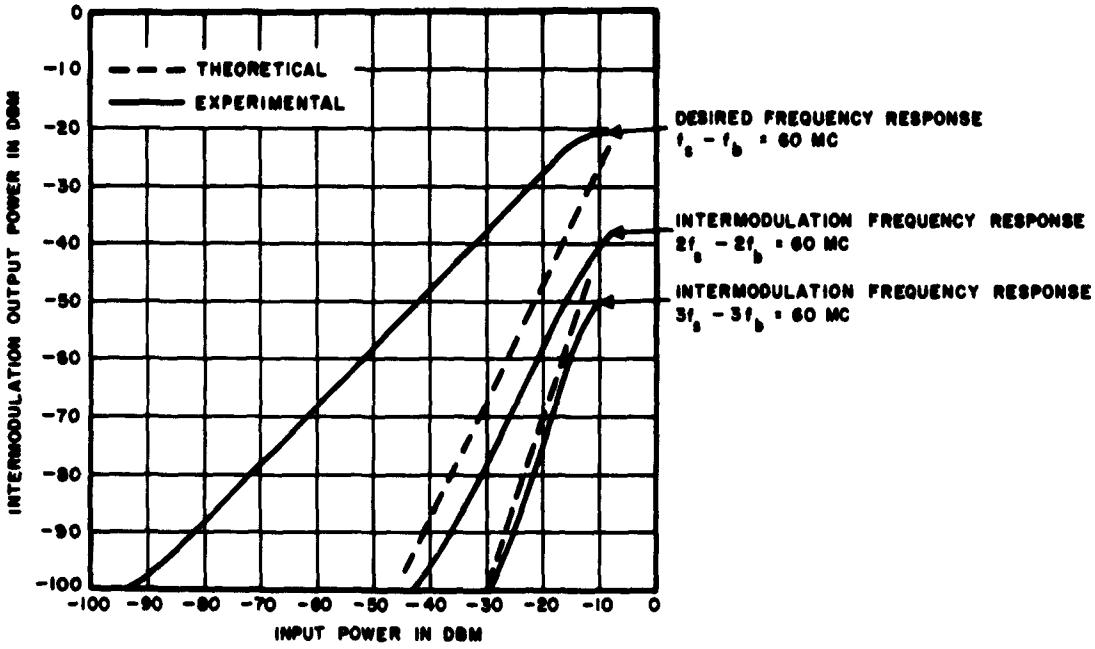

FIGURE 7-4. DESIRED RESPONSE AND EVEN-ORDER INTERMODULATION PRODUCTS BETWEEN SIGNAL AND LOCAL OSCILLATOR VS INPUT POWER FOR CRYSTAL MIXER

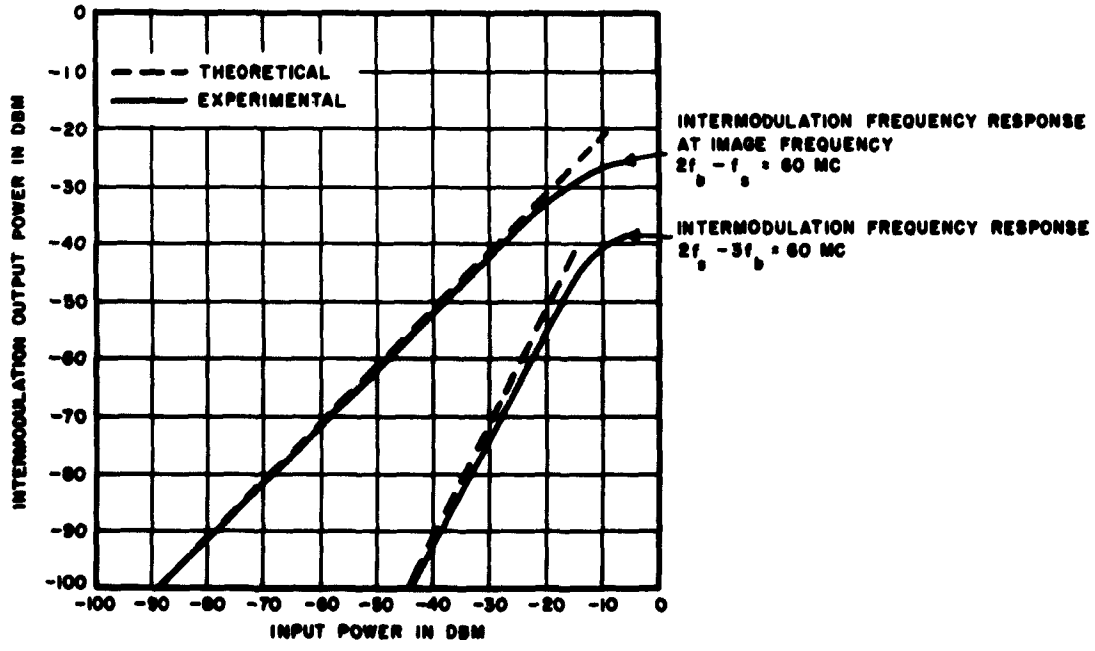

FIGURE 7-5. ODD-ORDER INTERMODULATION PRODUCTS BETWEEN SIGNAL AND LOCAL OSCILLATOR VS INPUT POWER FOR CRYSTAL MIXER

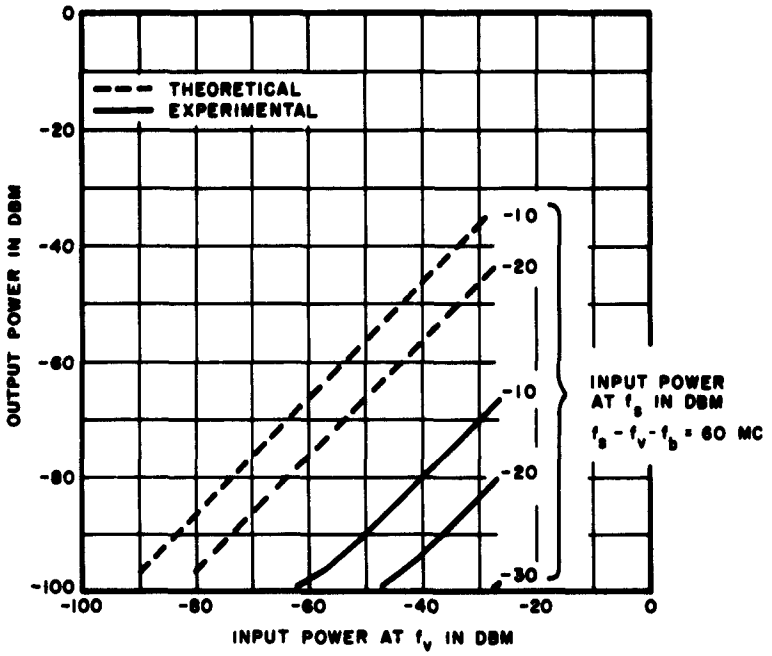

FIGURE 7-6. THIRD-ORDER INTERMODULATION BETWEEN TWO SIGNALS AND LOCAL OSCILLATOR VS INPUT POWER FOR CRYSTAL MIXER

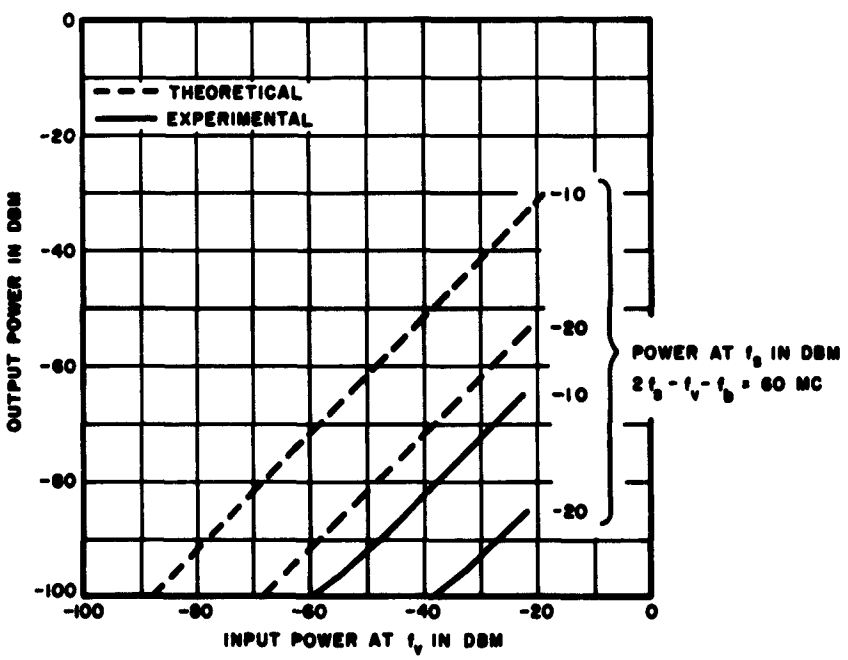

FIGURE 7-7. FOURTH-ORDER INTERMODULATION BETWEEN TWO SIGNALS AND LOCAL OSCILLATOR VS INPUT POWER FOR CRYSTAL MIXER

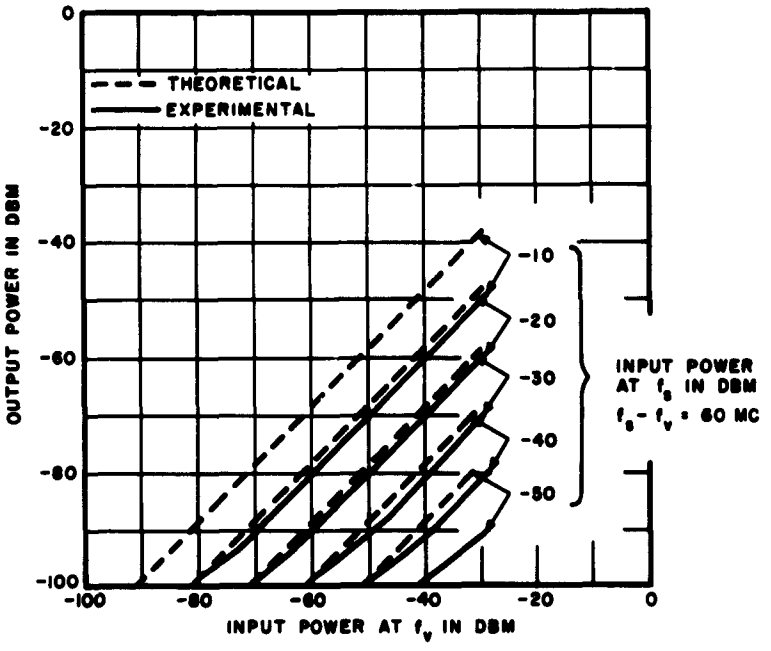

FIGURE 7-8. SECOND-ORDER INTERMODULATION BETWEEN TWO SIGNALS VS INPUT POWER FOR CRYSTAL MIXER

VIII. CONCLUSIONS

A. MASERS

The multiple time constants found in the TWM gain recovery can be readily explained by the cross relaxation mechanism. The reduced recovery time occurs when the duration of the saturating signal is short with respect to the cross-relaxation time constant. For saturating signals of greater duration than this time constant, the maser will recover in the spin-lattice relaxation time.

B. PARAMETRIC AMPLIFIERS

The prediction of nonlinear behavior of one-port and two-port parametric amplifiers is extremely complex. Even if the values of the transfer functions, voltages, and admittances were substituted into the equations, errors in the known values of the quantities would cause large errors in the prediction of nonlinear behavior. A comparison of intermodulation in one-port and two-port amplifiers indicates that the two-port amplifier is no less susceptible to interfering signals than the one-port amplifier.

The balanced parametric amplifier is inherently a broader-band amplifier than a single-diode amplifier because each diode of the balanced pair, operative at its self resonant frequency, acts as the tuned idler circuit for the other. Thus, the idler circuit generally has a broader bandwidth than the single-resonant circuit normally used. The saturation level and therefore the dynamic range of the balanced amplifier are expected to be greater than that of the single-diode amplifier.

Desensitization and cross-modulation measurements taken in the balanced amplifier show that the amplifier is most sensitive to desensitization and cross modulation for interfering signals that are near the frequency at which maximum gain occurs in the amplifier. Measurements also indicate that the balanced amplifier produces intermodulation products whose amplitudes are functionally dependent on the input signals, much the same as in the single-diode amplifier. In addition, the balanced amplifier can operate over a wide range of ambient temperatures when bias and pump power are adjusted accordingly.

The gain-recovery time of a parametric amplifier is highly dependent upon the time constant of the DC bias circuit. To ensure short recovery time, this time constant should be reduced to a minimum.

C. TUNNEL DIODES

The measurements of gain, saturation, desnsitization, and intermodulation in the hybrid-coupled tunnel-diode amplifier agreed very closely with theoretical predictions. The tunnel-diode equivalent circuit was assumed to have a simple negative resistance, and the i-v characteristic is expressed mathematically in equation 4-5. The differences between the theoretical i-v characteristic and the measured characteristic are mainly in the peak and valley areas (Figure 4-4). Therefore, some inaccuracies in predictions at high signal levels are to be expected. The theoretical saturation and desensitization levels were very close to the measured results, though the predicted intermodulation coefficient K was somewhat lower than measured. The theoretical noise figure is lower than measured; the difference is probably due to the assumptions of matched output and ideal hybrid action. In the measurement of noise figure

for the hybrid-coupled amplifier, it becomes apparent that mismatches at the hybrid input adversely affect noise figure. The theoretical noise figure, taking into account input mismatch is lower than measured; the difference is probably caused by the assumptions of matched output and ideal hybrid action.

The measurements of gain, saturation, and desensitization of the balanced tunnel-diode amplifier agreed closely with the theoretical predictions. When investigating the theory of the dynamic range of the balanced tunnel-diode configuration, it was discovered that the theory predicted an increase in 3 db of the dynamic range, which would be the same for two diodes in parallel. Therefore, the supposed increase in dynamic range due to the balanced configuration as reported in reference 9 does not occur as was supported by the measurements. However, an increase in the dynamic range is obtained when biasing the diodes in the low-noise region of the i-v characteristic compared to biasing at the inflection point. Figure 4-18 shows that the theoretical gain characteristic of a tunnel diode biased at the low-noise point has a 3 db greater saturation level compared to a tunnel diode biased at the inflection point. Here, saturation is defined as a 3 db loss of gain.

The increase in dynamic range of the balanced tunnel-diode amplifier, biased at the low-noise point, is thus attributed to the bias point rather than the balanced configuration. However, the balanced configuration reduces even-order harmonics and intermodulation products.

There is a fairly large difference between the measured third-order intermodulation coefficient (C = 52 dbm) and the theoretical prediction (C = 84 dbm) for a bias of 93 mv. A possible explanation is the prediction of a null in the third-order intermodulation products when the bias

is equal to 82.5 mv. The intermodulation product is a sensitive function of bias in this region and any inaccuracy in measuring the bias point would produce a large error in the intermodulation coefficient.

D. TRANSISTORS

The basic interference properties of two different transistor amplifiers were analyzed and measurements were made to verify predicted results.

The dynamic range for both the low-frequency power amplifier and the high-frequency tuned amplifier is predicted to within 3 db. The dynamic range of the high-frequency amplifier is approximately proportional to the square of the bias current.

The desensitization for both amplifiers is approximately equal to the loss of gain due to saturation. The desensitization for a given interfering input-signal level decreases as the bias current increases because of the corresponding increase of dynamic range.

The cross-modulation output of the high-frequency amplifier is predicted within 2 db by a power series approximation of the transfer characteristic. Cross modulation, predicted by an exponential approximation, was found to be within 8 db. The variation of cross modulation with bias current and interfering power agrees closely with the predicted variation. For low cross-modulation output, it is desirable to bias the transistor with relatively high current.

The intermodulation output as a function of input power for both amplifiers follows the predicted relationships for power levels below saturation. For the low-frequency amplifier, the calculated and measured values of K_3 (using the power-series approximation) agree to within 13 db for

relatively low values of bias current ($I_c \leq 0.3$ ampere). For $I_c > 0.3$ ampere, the measured values are much greater than the theoretical values. The deviation may be caused by nonlinear effects generated by the electrolytic capacitors in the circuit. For the high-frequency amplifier, the measured and calculated values of K_3 agree to within 15 db over the current range in which the transistor is usually biased. The fifth-order intermodulation output in the pass band of the high-frequency amplifier is at least 26 db below the third-order intermodulation.

The measured third-order intermodulation constant K_3 for the low-frequency amplifier is much lower than for the high-frequency amplifier and the other amplifiers investigated (reference 1). For example, for the low-frequency power amplifier, $K_3 = -29$ dbw at $I_c = 0.5$ ampere. For the high-frequency amplifier, $K_3 = 36$ dbw at $I_c = 2$ ma. Thus, for applications where it is necessary to minimize intermodulation output, it is desirable to use a power transistor instead of a small-signal transistor if possible. However, when a power transistor is used to obtain lower intermodulation, the efficiency is lowered because the power transistor would be biased at a current much higher than that required by the dynamic range of the amplifier.

Gain-recovery time effects are measured for the low frequency amplifier. The basic observed effect is pulse stretching at the output. Pulse stretching for this amplifier is not proportional to large signal input level.

Lack of better agreement between theory and measurement is caused by the simplifying assumptions made in the theory. These approximations are:

1. The transfer characteristic in the active region is approximated by a linearized exponential (power-series approximation) or a pure exponential.

2. Voltage dependent nonlinear effects a e neglected.

3. Frequency dependence of nonlinearities is not treated rigorously.

4. The current-amplification factor of the transistor is assumed to be a constant.

E. FERRITE DEVICES

Tunable ferrite filters can now be built with the following specifications:

1. Insertion loss less than 2 db,
2. All spurious responses down more than 40 db,
3. Residual spurious level down from 60 to 80 db,
4. Bandwidth constant over entire tuning range,
5. Single adjustment tuning requiring 3 watts.

Ferrite circulators act as linear passive devices at low power levels. No saturation or intermodulation contributions can be detected.

Ferrite circulators exhibit spurious responses at all input frequencies. At low frequencies, a circulator acts similarly to a 3-db power divider. At high frequencies, insertion loss and isolation vary irregularly. At high frequencies, insertion loss and isolation can be increased by using mode suppressors to inhibit propagation of high-order modes.

F. CRYSTAL MIXERS

The degree to which a crystal mixer is susceptible to saturation and desensitization depends upon the amount of bias current provided by the local oscillator--the higher the bias current, the lower the saturation and desensitization for a given input power. Thus, for maximum dynamic range and the least amount of desensitization, the mixer should be operated at the maximum local oscillator power that is consistent with the low insertion loss of the desired response.

Intermodulation between a signal input and the local oscillator can be accurately predicted using equation 7-8. Experimental evidence shows that the accuracy is within 6 db for input-signal levels below saturation.

For intermodulation products involving two input signals and the local oscillator, the prediction is less accurate. Only the shape of the intermodulation curve is predictable. The predicted output power levels are always above the measured values of output power. Thus, equation 7-8 can be used to determine the upper limit of the intermodulation output power.

G. COMPARATIVE RESULTS

To decide which device is best for a particular application, the interference properties of all devices must be known. The most important interference properties are saturation, desensitization, cross modulation, and intermodulation. As shown in Section I, desensitization and cross modulation are closely related to the saturation characteristic. Thus, only saturation and intermodulation have to be found to describe each device adequately. In this report these two quantities were studied for two tunnel-diode amplifiers, a balanced parametric amplifier, a crystal mixer, a high frequency transistor amplifier, and a power transistor amplifier.

The input power needed to cause 1 db of saturation was measured in each device. The comparative input powers are shown in Figure 8-1. The power for 1 db of saturation varies from -28 dbm for the tunnel diode amplifiers (both tunnel diode amplifiers performed about the same) to +5.5 dbm for the transistor power amplifier.

Third-order intermodulation between two input signals was measured in all the devices studied. However, due to the different characteristics of each device, there were

differences in the type of intermodulation measurement. In all cases the intermodulation followed the equation $P_{IM} = P_1 + 2P_2 + K$ but the power measurements in some cases refer to output powers and in other cases to input powers. To give a fair comparison of all devices it was necessary to refer all power levels to the output. Thus, P_1 and P_2 are taken as the output powers of the two signals and the quantity P_{IM} is the output power at the intermodulation frequency. The comparative results are shown in Figure 8-2. The values of K are given in dbw. The intermodulation K varies from +92 dbw for the tunnel diode amplifiers to -31 dbw for the power transistor amplifier.

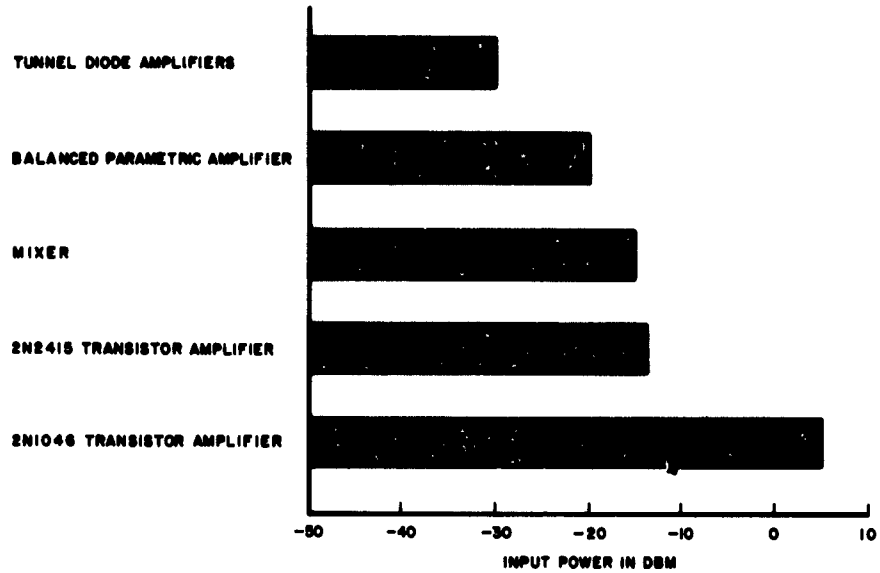

FIGURE 8-1. COMPARATIVE SATURATION LEVELS OF SOLID-STATE DEVICES

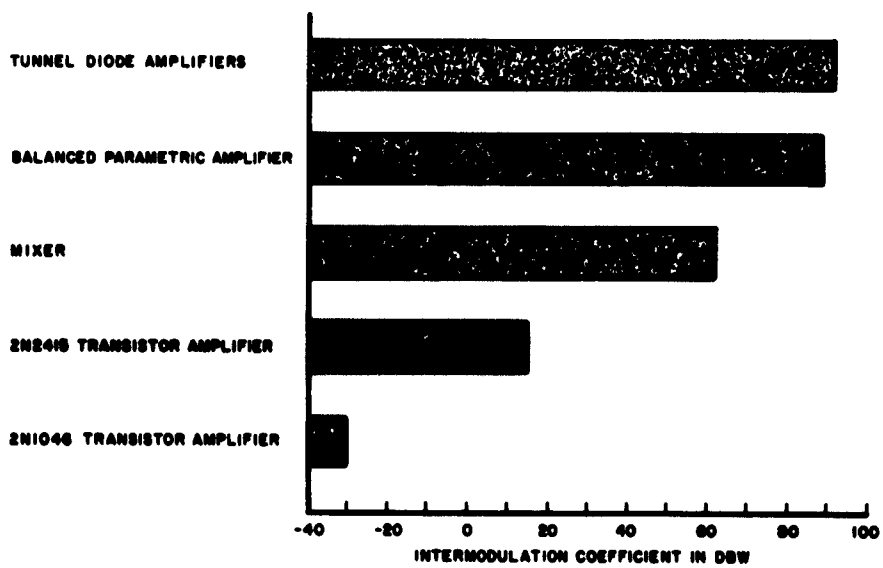

FIGURE 8-2. COMPARATIVE INTERMODULATION COEFFICIENTS OF SOLID-STATE DEVICES

IX. REFERENCES

1. S. Becker et al., "Final Report on Interference Analysis of New Components and Circuit Techniques, RADC-TDR-62-221, May 1962.
2. N. Bloembergen et al., "Cross-Relaxation in Spin Systems," Physical Review, Vol 114, No. 2, p 445-459, April 1959.
3. G. S. Boyle, "Cross Relaxation Masers," Proc IRE, Vol 49, No. 3, p 573-590, March 1961.
4. S. Okwit and J. G. Smith, "Packaged Electronically Tunable S-Band Traveling Wave Maser System," Proc IRE, Vol 50, No. 6, p 1470-1483, June 1962.
5. W. B. Muins and J. D. McGee, "Cross-Relaxation in Ruby," Physical Review, Vol 119, No. 4, p 1233-1237, August 1960.
6. D. Fleri and H. Bayet, "Investigation of Traveling Wave Parametric and Hybrid-Coupled Tunnel-Diode Amplifiers," RADC-TR-61-231, July 1961.
7. F. H. Mitchell, "Deriving The Tunnel-Diode Curve," Electronic Industries, October 1961.
8. F. B. Hildebrand, "Advanced Calculus for Engineers," Prentice-Hall, 1949.
9. L. E. Dickens, "Push-Pull Tunnel Diodes," PGMTT Transactions, p 361, July 1961.
10. J. J. Moll, "Large Signal Transient Response of Junction Transistors," Proc IRE, Vol 42, p 1773-1784, 1954.
11. J. Lindmayer and C. Y. Wrigley, "Beta Cutoff Frequencies of Junction Transistors," Proc IRE, Vol 50, p 194-198, February 1962.
12. C. T. Kirk, Jr., "A Theory of Transistor Cutoff Frequency Falloff at High Current Densities," IRE Transactions on Electron Devices, p 164-174, March 1962.
13. J. R. A. Beale and A. F. Beer, "The Study of Large-Signal High-Frequency Effects in Junction Transistors Using Analog Techniques," Proc IRE, p 66-77, January 1962.
14. E. A. Guillemin, "The Mathematics of Circuit Analysis," John Wiley & Sons, 1949.

APPENDIX I

FIRST-ORDER OPERATION OF A TWO-PORT PARAMETRIC AMPLIFIER

Using the frequency spectrum and the diode matrix equations derived in reference 1, a pair of equations that describe the two-port amplifier can be written as:

$$I_2 = Y_{22}\, v_2 + Y_{27}\, v_7^* = I_o - Y_{x2}\, v_2 \qquad \text{(I-1)}$$

$$I_7^* = Y_{77}^*\, v_7^* + Y_{72}^*\, v_2 = -Y_{x7}^*\, v_7^* \qquad \text{(I-2)}$$

Substituting equation (I-1) into equation (I-2)

$$I_7^* = Y_{77}^*\, v_7^* + \frac{Y_{72}^* \left(I_o - Y_{27}\, v_7^*\right)}{Y_{t2}} \qquad \text{(I-3)}$$

The two-port gain is:

$$K_{72} = \frac{v_7^*}{v_{o2}}$$

with $I_o = v_{o2}\, Y_{x2}$,

$$K_{72} = \frac{-Y_{72}^*}{Y_{t7}^*} \left(\frac{Y_{x2}}{Y_{t2} - \dfrac{Y_{72}\, Y_{27}}{Y_{t7}}} \right) \qquad \text{(I-4)}$$

The expression in parenthesis in equation (I-4) is equal to the one-port gain, K_{22}, thus:

$$K_{72} = \frac{-Y_{72}^*}{Y_{t7}^*} K_{22} \qquad \text{(I-5)}$$

Substituting from the original diode matrix equations from reference 1,

$$K_{72} = \frac{j\omega_7 b v_9^*}{G_{x7}} K_{22} \qquad \text{(I-6)}$$

where G_{x7} is the external conductance at ω_7.

APPENDIX II

DERIVATION OF NONLINEAR OUTPUT FOR CLASS A TRANSISTOR AMPLIFIER BASED ON EXPONENTIAL APPROXIMATION OF TRANSFER CHARACTERISTIC

This derivation is calculated for the common-emitter transistor equivalent circuit shown in Figure 5-5. The signal current i_b flowing in the input circuit is given by:

$$i_b = I_B\left(\exp v_{b'e}/V_T - 1\right) \qquad \text{(II-1)}$$

where

I_B = base DC current,

$V_T = \frac{KT}{q}$, thermal junction voltage (about 25 mv at room temperature),

$v_{b'e}$ = signal voltage across intrinsic base emitter junction.

It is assumed that $v_{b'e}$ is proportional to the input voltage v_g, though the Fourier spectrum of $v_{b'e}$ actually consists of all the input frequencies plus all the harmonics and intermodulation products of the input frequencies. However, all generated nonlinear components are assumed to be small in relation to the fundamental output. Furthermore, the current amplification factor β_o is assumed to be independent of bias.

The nonlinear output is derived for the voltage $v_{b'e}$, which consists of the sum of two continuous waves, as follows:

$$v_{b'e} = V_1 \cos \omega_1 t + V_2 \cos \omega_2 t \qquad \text{(II-2)}$$

Substituting equation II-2 into equation II-1:

$$1 + \frac{i_b}{I_B} = \exp\left[(V_1/V_T)\cos\omega_1 t\right]\exp\left[(V_2/V_T)\cos\omega_2 t\right] \qquad \text{(II-3)}$$

Equation II-3 represents a function that is periodic for each of its two independent variables $\omega_1 t$ and $\omega_2 t$ and therefore can be expanded into a Fourier series as follows (reference 14):

$$1 + \frac{i_b}{I_B} = \sum_{m=-\infty}^{\infty} \sum_{n=-\infty}^{\infty} c_{mn}\, e^{j(m\omega_1 t + n\omega_2 t)} \qquad \text{(II-4)}$$

where

$$c_{mn} = \frac{1}{2\pi}\int_0^{2\pi} e^{(V_1/V_T)\cos\omega_1 t}\, e^{-jm\omega_1 t}\, d(\omega_1 t)$$

$$\frac{1}{2\pi}\int_0^{2\pi} e^{(V_2/V_T)\cos\omega_2 t}\, e^{-jn\omega_2 t}\, d(\omega_2 t) \qquad \text{(II-5)}$$

$$= I_m(V_1/V_T)\, I_n(V_2/V_T)$$

Substituting equation II-5 into equation II-4 and combining:

$$\begin{aligned}
i_b = {} & I_B\left[I_o(V_1/V_T)\, I_o(V_2/V_T) - 1\right] + && \text{(DC term)} \\
& 2I_B I_o(V_2/V_T) \sum_{m=1}^{\infty} I_m(V_1/V_T)\cos m\omega_1 t + && \text{(harmonics of } \omega_1\text{)} \qquad \text{(II-6)} \\
& 2I_B I_o(V_1/V_T) \sum_{n=1}^{\infty} I_n(V_2/V_T)\cos n\omega_2 t + && \text{(harmonics of } \omega_2\text{)} \\
& 4I_B \sum_{m=1}^{\infty}\sum_{n=1}^{\infty} I_m(V_1/V_T)\, I_n(V_2/V_T)\cos m\omega_1 t\cos n\omega_2 t && \text{(intermodulation products)}
\end{aligned}$$

The I-functions are modified Bessel functions of the first kind. The expression for the intermodulation current at either of the frequencies $\omega = m\omega_1 t \pm n\omega_2 t$ is given by:

$$i_{b_{mn}} = 2I_B I_m(V_1/V_T)\ I_n(V_2/V_T)\ \cos\ (m\omega_1 t \pm n\omega_2 t) \qquad \text{(II-7)}$$

For small input signals $V_1/V_T << 1$ and $V_2/V_T << 1$, the I-functions can be approximated by the first term of their series expansion given by:

$$I_n(x) \approx \frac{(x/2)^n}{n!} \qquad \text{(II-8)}$$

Substituting in equation II-7 yields:

$$i_{b_{mn}} \approx \frac{2I_B}{m!n!\ (2V_T)^{m+n}}\ V_1^m\ V_2^n \qquad \text{(II-9)}$$

The amplitudes V_1 and V_2 are proportional to the input amplitudes V_{g_1} and V_{g_2}. Thus,

$$V_1 = \delta V_{g_1}$$

$$V_2 = \delta V_{g_2} \qquad \text{(II-10)}$$

where

$$\delta = \frac{r_{b'e}}{r_{b'e} + r_{bb'} + R_g}$$

$$r_{b'e} = V_T/I_B = \beta_o\ V_T/I_c$$

The available input powers are given by:

$$p_1 = V_{g_1}^2/8R_g$$

$$p_2 = V_{g_2}^2/8R_g \qquad \text{(II-11)}$$

The intermodulation output P_{mn} is given by:

$$P_{mn} = i_{c_{mn}}^2 R_L = \left(\beta_o \, i_{b_{mn}}\right)^2 R_L \qquad \text{(II-12)}$$

Combining equations II-9, II-10, II-11, and II-12 yields,

$$P_{mn} \approx R_L \left[\frac{2I_c}{m!n!} \left(\frac{\delta\sqrt{2R_g}}{V_T} \right)^{m+n} \right]^2 p_1^m \, p_2^n \qquad \text{(II-13)}$$

or in terms of the output powers P_1 and P_2,

$$P_{mn} \approx R_L \left[\frac{2I_c}{m!n!} \left(\frac{\delta}{V_T}\sqrt{\frac{2R_g}{G}} \right)^{m+n} \right]^2 P_1^m \, P_2^n$$

$$= K_{mn} \, P_1^m \, P_2^n \qquad \text{(II-14)}$$

where

$$P_1^m = (p_1 G)^m$$

$$P_2^n = (p_2 G)^n$$

From equation II-14, K_{mn} is given by

$$K_{mn} = R_L \left[\frac{2I_c}{m!n!} \left(\frac{\delta}{V_T} \sqrt{\frac{2R_g}{G}} \right)^{m+n} \right]^2 \qquad \text{(II-15)}$$

The current desensitization D_i is defined as the ratio of the amplitude of the fundamental of i_b in the presence of the second signal to the amplitude of the fundamental of i_b with the second signal set to zero. From equation II-6:

$$D_i \Big|_{\text{for } f_1} = I_o(V_2/V_T)$$

$$D_i \Big|_{\text{for } f_2} = I_o(V_1/V_T) \qquad \text{(II-16)}$$

For $(V/V_T) \leq 1.5$, $I_o(V/V_T)$ can be approximated by the first two terms of its series expansion with less than 6 percent error. Substituting this approximation in equation II-16:

$$D_i \Big|_{\text{for } f_1} \approx 1 + 2R_g \left(\frac{\delta}{V_T}\right)^2 p_2$$

$$D_i \Big|_{\text{for } f_2} \approx 1 + 2R_g \left(\frac{\delta}{V_T}\right)^2 p_1 \qquad \text{(II-17)}$$

Current saturation S_i is defined as the ratio of the amplitude of the fundamental of i_b at relatively high levels of input to the amplitude of the fundamental of i_b at low levels of input. The amplitude of the second signal is assumed to be zero. Thus $v_b{}'_e = V \cos \omega t$. For $(V/V_T) \leq 2$,

$I_1(V/V_T)$ can be approximated by the first two terms of its series expansion with less than a 6-percent error. Using this approximation in equation II-6:

$$S_1 \approx 1 + \frac{(V/V_T)^2}{8}$$

$$\approx 1 + R_g \left(\frac{\delta}{V_T}\right)^2 p \qquad \text{(II-18)}$$

D_1 (equation II-17) and S_1 (equation II-18) are always larger than 1. Therefore, the amplitude of the fundamental of i_b actually increases at high input levels and in the presence of a second input signal. However, in practice, saturation and desensitization effects generally result in a decrease of fundamental output. This discrepancy can be attributed to the fact that D_1 and S_1 are derived by assuming that the transfer characteristic is exponential and setting no upper limit on DC current I_B and signal $v_{b'e}$ at which the approximation degrades. Actually, the exponential function is a poor approximation for large values of I_B. It is an incorrect approximation for input signals that drive the transistor into the saturation region. Thus equations II-15, II-17, and II-18 should be used for calculating nonlinear parameters only in the active region of the amplifier.

APPENDIX III

ANALYSIS OF INTERMODULATION IN A CRYSTAL FOR TWO INPUT SIGNALS

A diode can be assumed to have an exponential current-voltage characteristic:

$$i = i_o \left(e^{\alpha v} - 1\right) \qquad \text{(III-1)}$$

where

i_o = leakage current,
α = diode constant,

with an input voltage consisting of three sinusoidal inputs and a DC component,

$$v = v_o + A_1 \cos \omega_1 t + A_1 \cos \omega_1 t + A_2 \cos \omega_2 t \qquad \text{(III-2)}$$

where v_o is the DC bias voltage. Combining these two equations results in:

$$i = i_o e^{\alpha v_o} \left(e^{\alpha A_1 \cos \omega_1 t}\right) \left(e^{\alpha A_1' \cos \omega_1' t}\right) \left(e^{\alpha A_2 \cos \omega_2 t}\right) - i_o$$

$$i + i_o = i_o e^{\alpha v_o} \sum_{m=o}^{\infty} \left(\frac{\alpha A_1}{m!}\right)^m \cos^m \omega_1 t \sum_{n=o}^{\infty} \left(\frac{\alpha A_1'}{n!}\right)^n \cos^n \left(\omega_1' t\right) \sum_{p=o}^{\infty} \left(\frac{\alpha A_2}{p!}\right)^p \cos^p \omega_2 t \qquad \text{(III-3)}$$

From reference 1,

$$\cos^k x = \left(\frac{1}{2}\right)^{k-1} \sum_{y=o}^{Y} \frac{k!}{(k-y)!\ y!} \cos\ (k - 2y)\ x$$

where $Y = \frac{k}{2}$ for k even, and $Y = \frac{k-1}{2}$ for k odd.

Substituting this expression into equation III-3 gives:

$$(i + i_o) = i_o\, e^{\alpha v_o} \sum_{m=o}^{\infty} \sum_{n=o}^{\infty} \sum_{p=o}^{\infty} \sum_{c=o}^{C} \sum_{d=o}^{D} \sum_{f=o}^{F}$$

$$\frac{(\alpha A_1)^m \quad (\alpha A_1')^n \quad (\alpha A_2)^p}{(m-1)!\ 1!\ (n-d)!\ d!\ (p-f)!\ f!\ 2^{m+n+p-3}} \times$$

$$\cos\ (m - 2c)\omega_1 t\ \cos\ (n - 2d)\omega_1 t\ \cos\ (p - 2f)\omega_2 t$$

Substituting $m - 2c = s$, $n - 2d = v$ and $p - 2f = b$

where

$s = \omega_1$ harmonic of the local oscillator,
$b = \omega_2$ harmonic of the signal.

and solving for particular harmonics of the three inputs gives

$$i_{svb} = e^{\alpha v_o} i_o \sum_{m=s}^{\infty} \sum_{n=v}^{\infty} \sum_{p=b}^{\infty}$$

$$\frac{\left(\frac{1}{2}\right)^{m+n+p-1} (\alpha A_1)^m (\alpha A_1')^n (\alpha A_2)^p}{\left(\frac{m+s}{2}\right)! \left(\frac{m-s}{2}\right)! \left(\frac{n+v}{2}\right)! \left(\frac{n-v}{2}\right)! \left(\frac{p+b}{2}\right)! \left(\frac{p-b}{2}\right)!} \times \qquad \text{(III-4)}$$

$$\cos\,(s\omega_1 \pm v\omega_1' \pm \omega_2)t$$

where the summations are taken over every other integer.

Substituting $g = \frac{m-s}{2}$, $h = \frac{n-t}{2}$, and $k = \frac{p-b}{2}$, and rearranging terms gives

$$E_{svb} = i_{svb} R_o = 2i_o e^{\alpha v_o} R_o \sum_{g=o}^{\infty} \left(\frac{\alpha A_1}{2}\right)^{2g+s} \frac{1}{(g+s)!\ g!}$$

$$\sum_{h=o}^{\infty} \left(\frac{\alpha A_1'}{2}\right)^{2k+v} \frac{1}{(k+v)!\ k!} \sum_{k=o}^{\infty} \left(\frac{\alpha A_2}{2}\right)^{2k+b} \frac{1}{(k+b)!\ k!} \times \qquad \text{(III-5)}$$

$$\cos\,(s\omega_1 \pm v\omega_1' \pm b\omega_2)t$$

where

E_{svb} = output voltage,
R_o = output resistance.

Since the summations are modified Bessel functions of the first kind, $I_s(\alpha A_1)$, $I_v(\alpha A_1')$, and $I_b(\alpha A_2)$:

$$E_{svb} = 2i_o R_o e^{\alpha v_o} I_s(\alpha A_1)\ I_v(\alpha A_1')\ I_b(\alpha A_2)$$
$$\cos\ (s\omega_1 \pm v\omega_1 \pm b\omega_2)t \qquad \text{(III-6)}$$

Assuming small signals, $\alpha A_1 << 1$ and $\alpha A_1' << 1$, gives:

$$E_{svb} = 2i_o R_o e^{\alpha v_o} \left(\frac{\alpha A_1}{2}\right)^s \frac{1}{s!} \left(\frac{\alpha A_1'}{2}\right)^v \frac{1}{v!} \left(\frac{\alpha A_2}{2}\right)^b \frac{1}{b!} \times$$
$$\cos\ (s\omega_1 \pm v\omega_1' \pm b\omega_2)t \qquad \text{(III-7)}$$

Lettering $P_{svb} = \dfrac{\overline{(E_{svb})^2}}{R_o}$, $p_1 = \dfrac{\overline{A_1^2}}{R_o}$, $p_1' = \dfrac{\overline{(A_1')^2}}{R_o}$

where $\overline{(E)^2}$ is the mean-square average of voltage (E). Using equation III-7, squaring E_{svb}, averaging, and substituting the expressions for power gives the following expression:

$$P_{svb} = \left[\frac{2\alpha^{s+v}\ i_o R_o e^{\alpha v_o}\ I_b(\alpha A_2)}{s!\ v!}\right]^2 \left(\frac{R_o}{2}\right)^{s+v-1} (p_1)^s\ (p_1')^v \qquad \text{(III-8)}$$

Using the above expression, any output can be solved for low-level input signals. Some important outputs follow:

The main response:

$$P_{101} = P_{11} = \left[2\alpha\ i_o R_o e^{\alpha v_o}\ I_1\left(\alpha A_2\right)\right]^2 p_1 \qquad \text{(III-9)}$$

The intermodulation response at the image frequency:

$$P_{102} = P_{12} = \left[2\alpha\ i_o R_o e^{\alpha v_o}\ I_2\left(\alpha A_2\right)\right]^2 p_1 \qquad \text{(III-10)}$$

Intermodulation between two signals and the local oscillator:

$$P_{121} = \left[\alpha^3\ i_o R_o e^{\alpha v_o}\ I_1\left(\alpha A_2\right)\right]^2 \left(\frac{R_o}{2}\right)^2 \left(p_1\right)\left(p_1\right)^2 \qquad \text{(III-11)}$$

where

$s = 1,$
$v = 2,$
$b = 1.$

Intermodulation between one signal and the local oscillator:

$$P_{202} = P_{22} = \left[\alpha^2\ i_o R_o e^{\alpha v_o}\ I_2\left(\alpha A_2\right)\right]^2 \left(\frac{R_o}{2}\right)\left(p_1\right)^2 \qquad \text{(III-12)}$$

where

$s = 2,$
$v = o,$
$b = 2.$

DISTRIBUTION LIST FOR REPORT NO. 1760-TN-1

Copy No.	Address	No. of Copies
1-3	*RADC (RAUMI, Captain R. E. Fitts) Griffiss Air Force Base, New York	3
4	*RADC (RAAPT) Griffiss Air Force Base, New York	1
5	*RADC (RAALD) Griffiss Air Force Base, New York	1
6	*GEEIA (ROZMCAT) Griffiss Air Force Base, New York	1
7	*RADC (RAIS, Mr. Malloy) Griffiss Air Force Base, New York	1
8	*Signal Corps Liaison Officer RADC (RAOL, Major Norton) Griffiss Air Force Base, New York	1
9	*AUL (3T) Maxwell Air Force Base, Alabama	1
10	ASD (ASAPRD) Wright-Patterson Air Force Base, Ohio	1
11	Chief, Naval Research Lab ATTN: Code 2027 Washington 25, D. C.	1
12	Air Force Field Representative Naval Research Lab ATTN: Code 1010 Washington 25, D. C.	1
13	Commanding Officer USASRDL ATTN: SIGRA/SL-ADT Fort Monmouth, New Jersey	1
14	NASA Langley Research Center (LIB) Langley Station Hampton, Virginia	1
15	AFSC (SCSE) Andrews Air Force Base Washington 25, D. C.	1

* Mandatory.

Copy No.	Address	No. of Copies
16	Commanding General U. S. Army Electronic Proving Ground ATTN: Technical Documents Library Fort Huachuca, Arizona	1
17-26	*Armed Services Technical Information Agency (TISIA-2) Arlington Hall Station Arlington 12, Virginia	10
27	Commander U. S. Naval Air Dev Cen (NADC Lib) Johnsville, Pennsylvania	1
28	Commander U. S. Naval Ordnance Lab (Tech Lib) White Oak, Silver Springs, Maryland	1
29	Director U. S. Army Engineer R&D Labs Technical Documents Center Fort Belvoir, Virginia	1
30	Commanding Officer and Director U. S. Navy Electronics Lab (Lib) San Diego 52, California	1
31	NASA George C. Marshall Space Laboratory ATTN: Mr. Grady Saunders Redstone Arsenal, Alabama	1
32	Commanding Officer U. S. Army Rocket and Guided Missile Agency ATTN: Interference Analysis Group Redstone Arsenal, Alabama	1
33	Army Ballistic Missile Agency Guidance Control and Aero Ballistics ATTN: Mr. J. B. Huff, Jr. 876-1551 and Dr. A. Rudolph 876-4711 Redstone Arsenal, Alabama	1
34	NASA ATTN: Dr. C. Carroll P. O. Box 4007 Patrick Air Force Base, Florida	1
35	Lockheed Aircraft Corp ATTN: X-N Development Division P. O. Box 504 962 W. El Camino Real Sunnyvale, California	1

* Mandatory

Copy No.	Address	No. of Copies
36	BSD (BSMCF, Major W. Birks) Air Force Unit Post Office Los Angeles 45, California	1
37	Area Frequency Coordinator Pacific Missile Range ATTN: Commander R. Langland or Mr. J. McClanahan Point Mugu, California	1
38	Area Frequency Coordinator White Sands Signal Missile Support Agency ATTN: SIGWS, Mr. H. W. Wingate White Sands Missile Range, New Mexico	1
39	ESD (ESRDV, Mr. Dix) L. G. Hanscom Fld Bedford, Massachusetts	1
40	National Security Agency ATTN: Mr. J. C. McKinney (R-312) Fort Meade, Maryland	1
41	Southwest Research Institute ATTN: Mr. A. Schrader 8500 Culebra Road San Antonio 6, Texas	1
42	AFSC Scientific/Technical Liaison Office Lewis Research Center (NASA) 21000 Brookpark Road ATTN: L/C D. J. Iddins Cleveland 35, Ohio	1
43	Naval Missile Center ATTN: L/C O. L. Moontz Point Mugu, California	1
44	Dept of Electrical Engineering University of Hawaii ATTN: Paul C. Yuen, Chairman Honolulu 14, Hawaii	1
45	ASD (ASNPRE-1, Mr. Skolnik) Wright-Patterson Air Force Base, Ohio	1
46	ASD (ASNDCD, Mr. Brewster) Wright-Patterson Air Force Base, Ohio	1
47	ASD (ASNSSP, Mr. Tyzzer) Wright-Patterson Air Force Base, Ohio	1
48-49	AFSC (SCRC) Bolling Air Force Base Washington 25, D. C.	2

Copy No.	Address	No. of Copies
50	NASA Goddard Space Flight Center ATTN: Code 621, Bldg T-5, Mr. J. Berliner Greenbelt, Maryland	1
51	NASA Goddard Space Flight Center ATTN: Code 523, Mr. V. R. Simas Greenbelt, Maryland	1
52	ASD (ASRNCS-2, Mr. H. Bartman) Wright-Patterson Air Force Base, Ohio	1
53-54	Electromagnetic Compatibility Analysis Center ATTN: Mr. B. Lindeman U. S. Naval Engineering Experimental Station Annapolis, Maryland	2
55	RADC (RAUMM, Mr. Porter) Griffiss Air Force Base, New York	1
56	Navy Air Navigation Electronic Project Weapons System Test Division (Mr. O. D. Stewart) Naval Air Test Center Patuxent River, Maryland	1
57	Radio Corporation of America ATTN: Mr. A. Matheson P. O. Box 588 Burlington, Massachusetts	1
58	Radiation, Inc. ATTN: Mr. W. F. Quinlivan P. O. Box 37 Melbourne, Florida	1
59	Melpar, Inc. ATTN: Mr. W. Myers Falls Church, Virginia	1
60	Bendix Corporation Bendix Radio Division ATTN: Mr. A. E. F. Grempler Towson, Maryland	1
61	Jansky & Bailey ATTN: Mr. K. G. Heisler, Jr. 1339 Wisconsin Avenue, N. W. Washington 25, D. C.	1

Copy No.	Address	No. of Copies
62	Georgia Institute of Technology ATTN: Mr. Bruce Warren Atlanta 13, Georgia	1
63	American Electronics Laboratories, Inc. ATTN: Mr. C. J. Fowler Richardson Road Colmar, Pennsylvania	1
64	University of Pennsylvania ATTN: Prof O. D. Salati 34 Walnut Street Philadelphia 4, Pennsylvania	1
65	USASRDL ATTN: Mr. S. Weitz Fort Monmouth, New Jersey	1
66	Sylvania Electronic Products ATTN: Mr. J. Whittman 1100 Wherle Drive Buffalo 9, New York	1
67	Electro-Mechanics Co. ATTN: Dr. F. J. Morris P. O. Box 802 Austin 64, Texas	1
68	Westinghouse Electric Corp. ATTN: Mr. J. Carter P. O. Box 1897 Baltimore, Maryland	1
69	GEEIA (ROZMWT, Mr. D. Clark) Griffiss Air Force Base, New York	1
70	Armour Research Foundation ATTN: Mr. B. Ebstein 10 West 35th Street Chicago, Illinois	1
71	White Electromagnetics, Inc. ATTN: J. E. McShulskis 4903 Auburn Avenue Bethesda 14, Maryland	1
72	U. S. Department of Commerce National Bureau of Standards Boulder Laboratories ATTN: A. V. Cottny Boulder, Colorado	1